



# Development of Nanomaterials for Environmental monitoring

**Flavio Pino**

Thesis to apply for the PhD in Biotechnology

Department of Genetic and Microbiology

Autonomous University of Barcelona

## **Directors**

**Prof. Arben Merkoçi and Carmen Mayorga Martinez**

*Nanobioelectronics and Biosensors Group*

*Institut Català de Nanociència Nanotecnologia (ICN2)*

## **Tutor**

**Antonio Villaverde Corrales**

**2015**

---



---

The present thesis titled “Development of nanomaterials for environmental monitoring” presented by Flavio Pino has been performed at the laboratories of the Nanobioelectronics and Biosensor Group at the *Institut Catalá de NanoCiència y Nanotecnologia (ICN2)*, under the supervision of Prof. Arben Merkoçi and Dr Carmen Mayorga Martinez.

### Directors

---

Prof. Arben Merkoçi

ICREA Research Professor

*Nanobioelectronics & Biosensors group*

*Instituto Catalá de Nanociència i  
Nanotecnologia (ICN2)*

---

Dr. Carmen Mayorga Martinez

Senior Researcher

*Nanobioelectronics & Biosensors group*

*Instituto Catalá de Nanociència i  
Nanotecnologia (ICN2)*

### Tutor

---

Prof. Antoni Villaverde Corrales

Autonomous University of Barcelona

---

Flavio Pino

*Nanobioelectronics & Biosensors group*

*Instituto Catalá de Nanociència i Nanotecnologia (ICN2)*



---

## Acknowledgement for the financing support



## “Detection of PTHrP using magnetic immunoassay”

Work done by ICN group as a contribution to the project:

*“Evaluation of the calcium sensing receptor as a potential gene and therapeutic target in neuroblas*



The development of simple biosensing platforms for environmental monitoring has increasing their relevance not only in the research field but also in the market industry. This is due to their advantages such as simple use, the decrease of sample amount in addition to their cost efficiency while being also disposable.

Moreover the recent advances in nanoscience and nanotechnology increase the emerging of new nanomaterials with interesting electrical properties such as their capacity to improve the electrode conductivity has particular interest in the development of electrochemical biosensing systems.

The combination of nanomaterials with electrochemical biosensing platforms can build up powerful analytical tool for the environmental monitoring. This represents the main objective of this PhD Thesis, that divided in six chapters describes the development and application of three new biosensing platforms for environmental monitoring using nanomaterials.

**Chapter one** gives a general introduction on environmental monitoring of pesticides and phenolic compounds that also offers a brief description and classification of these compounds.

This chapter also gives an overview of the relevance of the use of nanomaterial in biosensing systems for environmental monitoring with a detailed review of the last published works describing also their innovation aspects and also the possible drawbacks .

The **Chapter 2** presents the main objectives of this PhD Thesis.

In the **Chapter 3** entitled “Electrochemical detection of pesticide using boron doped diamond” a new enzymatic biosensor using boron doped diamond for detection of the pesticide chlorpyrifos is described.

The developed system uses magnetic beads and acetylcholinesterase enzyme over Boron Doped Diamond Electrode. It is based on acetylcholinesterase enzyme inhibition.

Moreover through the use of magnetic beads and the surface characteristics of the electrode this platform will be used as multi use system with high reproducibility.

As a first BDDE enzymatic platform a complete study over the detection of the enzyme product was performed obtaining interesting results. Finally the efficiency of this biosensor is studied not only analyzing standard sample but also measuring the pesticide in real sample ( from Yokoama river in Japan).

In the **Chapter 4** entitled “Electrochemical detection of phenol compound and pesticide using IrOx nanoparticles” an enzymatic biosensor for dual different pollutants detection, catechol (a phenol derivative) and chlorpyrifos (an organophosphate pesticide) is evaluated. Such sensing is achieved through a SPCE modified with IrOx NPs and tyrosinase. The proposed biosensor reports improvement in the sensitivity for catechol compared to previously reported biosensors. This biosensor shows also a high sensitivity for chlorpyrifos while being used in a tyrosinase inhibition mode operation. Finally the efficiency of this biosensor for real applications in chlorpyrifos detection in river and tap water is also explored showing great possibilities for future application as a low cost platform for pesticide detection. A dual biosensor for environmental monitoring using IrOx nanoparticle also is evaluated.

In the **Chapter 5** entitled “CuO nanoparticles based system for free enzymatic detection of phenols compounds and diuron pesticide” a free enzymatic bio-sensing system based on the CuO nanoparticles is proposed.

Such sensing is achieved through a SPCE where CuO NPs create stable complex with phenolic compounds that are measured through electrochemical reaction at electrode surface.

Therefore the CuO NPs have the function to mimic the active centre of tyrosinase able to detect diuron (high toxic herbicide) and phenolic compounds ( catechol, phenol 4-chlorophenol ). The obtained results are comparable with other enzymatic platforms and can be used for real samples due to the fact that the detection limit is within the requested levels of monitoring established by the legislation for those pollutants .

In the **Chapter 6** the general conclusions and the future prospective are discussed.





<b>Chapter 1: Introduction</b> .....	1
<b>1.1 Pesticides and phenolic compounds</b> .....	3
<b>1.2 Biosensing systems for environmental monitoring</b> .....	6
<b>1.3 Electrochemical biosensors</b> .....	7
1.3.1 Electrochemical-based Immunosensors .....	9
1.3.2 Enzyme-Based Electrochemical Systems.....	14
1.3.3 MIPs and Other Host–Guest-Like Systems .....	21
1.3.4 Other Electrochemical Strategies.....	24
<b>1.4 Conclusions</b> .....	25
<b>1.5 Bibliography</b> .....	28
<b>Chapter 2 : Objectives</b> .....	¡Error! Marcador no definido.
<b>2.1 General Objectives</b> .....	¡Error! Marcador no definido.
<b>Chapter 3: Magnetic enzymatic platform for organophosphate pesticide detection using Boron-doped Diamond Electrodes</b> .....	37
<b>3.1 INTRODUCTION</b> .....	39
<b>3.2 Experimental section</b> .....	40
3.2.1 Reagent and Solution .....	40
3.2.2 Electrode preparation.....	41
3.2.3 Methods and Procedure.....	41
3.2.4 Electrochemical measurements .....	42
3.2.5 Enzymatic Assay.....	42
<b>3.3 RESULTS AND DISCUSSION</b> .....	43
3.3.1 Electrochemical Characteristic of Thiocholine at BDD electrodes .....	43
3.3.2 Modification of magnetic beads with AChE.....	48
3.3.3 Application of AChE-modified magnetic beads in Chlorpyrifos Sensors .....	49
3.3.4 Analysis of chlorpyrifos in tap water.....	51
<b>3.4 Conclusion</b> .....	53
<b>3.5 Bibliography</b> .....	54
<b>Chapter 4 : Electrochemical detection of phenol compound and pesticide using IrOx nanoparticles</b> .....	¡Error! Marcador no definido.
<b>4.1 Introduction</b> .....	¡Error! Marcador no definido.
<b>4.2 Experimental section</b> .....	¡Error! Marcador no definido.

4.2.1 Apparatus and electrodes .....	¡Error! Marcador no definido.
4.2.2 Reagents and solutions .....	¡Error! Marcador no definido.
4.2.3 Synthesis of iridium oxide nanoparticles .....	¡Error! Marcador no definido.
4.2.4 Preparation and modification of Screen Printed Electrodes .....	¡Error! Marcador no definido.
<b>4.3 Results and discussion</b> .....	¡Error! Marcador no definido.
4.3.1 Morphological studies .....	¡Error! Marcador no definido.
4.3.2 Analytical measurements .....	¡Error! Marcador no definido.
<b>4.4 Conclusion</b> .....	¡Error! Marcador no definido.
<b>4.5 Bibliography</b> .....	¡Error! Marcador no definido.
<b>Chapter 5: CuO nanoparticles based system for free enzymatic detection of phenolic compounds and pesticide</b> .....	¡Error! Marcador no definido.
<b>5.1 INTRODUCTION</b> .....	¡Error! Marcador no definido.
<b>5.2 Experimental section</b> .....	¡Error! Marcador no definido.
5.2.1 Instruments and Methods .....	¡Error! Marcador no definido.
5.2.2. Reagents .....	¡Error! Marcador no definido.
5.2.3 Synthesis of Copper oxide nanoparticles .....	¡Error! Marcador no definido.
5.2.4 Methods .....	¡Error! Marcador no definido.
<b>5.3 Results and discussion</b> .....	¡Error! Marcador no definido.
5.3.1 Morphological studies .....	¡Error! Marcador no definido.
5.3.2 Electrochemical behavior of the CuO NPs .....	¡Error! Marcador no definido.
5.3.3 Phenolics Compounds detection.....	¡Error! Marcador no definido.
<b>5.4 Conclusion</b> .....	¡Error! Marcador no definido.
<b>5.5 Bibliography</b> .....	88
<b>Chapter 6: General conclusions and future perspectives</b> .....	91
<b>6.1 General conclusions</b> .....	93
<b>6.2 Future Perspectives</b> .....	94
<b>Annex A Publications</b> .....	97



# Chapter 1

## Introduction

### Related publication

---

Gemma Aragay, Flavio Pino, Arben Merkoçi. *Chemical Reviews* **2012**, 112, 5317-5338.

---



---

## Introduction

### 1.1 Pesticides and phenolic compounds

The environment pollution is one of the main threats and challenges that humanity faces today.<sup>1,2</sup> Public concern and legislation are nowadays demanding better environmental control. Although a lot of efforts have been put to prevent the contamination of the environment monitoring is still a fundamental key for the health of the ecosystem and human being, able in fact to understanding and managing possible future risks.

Different toxic compounds released every day in the air, soil and water from agriculture and industrial activities are impossible to be eliminated through normal biodegradation processes. The World Health Organization (WHO) informed in fact that in 2012 around 7 million people died as a result of air pollution exposure.<sup>3</sup>

Between the various toxic compounds present or released in the environment, pesticides and phenolic compounds, have a great interest to be monitored and have been the focus of the projects that have supported this PhD thesis.

Pesticides are toxic compounds that deter, incapacitate, kill, or otherwise discourage pests worldwide used in the agriculture for improving the field production. Despite their benefits, the drawbacks of these compounds are their potential toxicity to humans and other species.

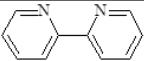
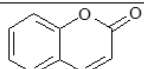
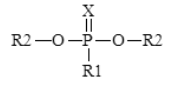
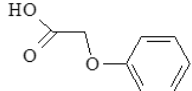
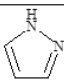
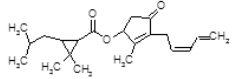
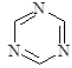
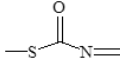
Even though these hazard compounds are well known and classified, their detection or degradation is still a complicated process considering for example the different possible matrix (water, soil, and ground) where these elements have to be analyzed. The European Community (EC) in the directive 98/93/EC establishes the low limit for this pollutant in water of human consumption at 0.1 $\mu$ g/l for individual and 0.5  $\mu$ g/l for total pesticides.<sup>4</sup>

Table 1 gives the classification through the chemical structure and commercial names of the pesticides as well as the symptoms that can appear once these hazard compounds enter into the human body.<sup>5-8</sup> Particularly it is shown that the most toxic compounds such

---

as carbamates and organophosphate effect the nervous system inhibiting key enzymes or irritating the skin.

**Table 1** Pesticides classification and symptoms appearing to humans.

Chemical Class	Chemical Formula	Commercial Group	Symptoms
Arsenic compounds	$\text{AsO}_4^{3-}$	Fungicide Insecticide Herbicide	Stomachache, nausea, vomiting, and diarrhea
Bipyridylum derivatives		Herbicide	Neurologic effects, irritation
Carbamates	$(-\text{OCONHCH}_3)$	Acaricide Fungicide	Central nervous system effects
Coumarin derivatives		Rodenticide	Internal hemorrhage
Copper compounds	$\text{CuO}, \text{CuS}, \text{Cu}(\text{OH})_2$	Algaecide Fungicide Insecticide	Skin and respiratory irritation
Mercury compounds	Inorganic and Organic mercury	Fungicide	Neurological effects
Organochlorine compounds	$-\text{CH}_2\text{Cl}$	Fungicide Insecticide	Gastrointestinal and neurological effects
Organophosphorous compounds		Acaricide Fungicide Rodenticide	Central nervous system effects
Organotin compounds	$\text{R}_4\text{Sn}, \text{R}_3\text{SnX}, \text{R}_2\text{SnX}_2, \text{RSnX}_3$	Fungicide Herbicide	Gastrointestinal irritation
Phenoxyacetic acid derivatives		Herbicide	Eye and dermal irritation
Pyrazole derivatives		Insecticide	Cytotoxic and mutagenic effects
Pyrethroids		Acaricide Insecticide	Respiratory irritation
Triazine derivatives		Herbicide	Nausea, vomiting, diarrhea and abdominal pain
Thiocarbamates		Acaricide Fungicide	Irritation effects



Phenolic compounds have been used as deterrents for pests like pentachlorophenol (PCP) or dinoseb<sup>9</sup> but also in the production of dyes, polymers, drugs and other related organic substances. Phenols and their derivatives may appear in the environment in different forms. Table 2 shows the classification and identification of the most important ones.

**Table 2** Classification of phenolic compounds.

<b>Structure</b>	<b>Class</b>
$C_6$	Simple Phenolics
$C_6-C_1$	Phenolic acid and related compounds
$C_6-C_2$	Acetophenones and phenylacetic acids
$C_6-C_3$	Cinnamic acid, cinnamyl aldehydes, cinnamyl alcohols
$C_6-C_3$	Coumarins, isocoumarins and chromes
$C_{15}$	Chalcones, aurones, dihydrochalcones
$C_{15}$	Flavans
$C_{15}$	Flavones
$C_{15}$	Flavanones
$C_{15}$	Flavanonols
$C_{15}$	Anthocyanidins
$C_{15}$	Antocyanins
$C_{30}$	Biflavonyls
$C_6-C_1-C_6$ , $C_6-C_2-C_6$	Benzophenones, xanthenes, stilbenes
$C_6-C_{10}-C_{14}$	Quinones
$C_{18}$	Betacyanins
Lignans-neolignans	Dimers or oligomers
Lignin	Polymers
Tannins	Oligomers, or polymers
Phlobaphenes	Polymers

Phenolic compounds also are highly toxic for human beings, animals and the ecosystem. Their toxicity has been attributed to the hydrophobicity of the compounds and the

formation of free toxic radical.<sup>10</sup> Their toxic process starts with their penetration into the cells undergoing damaging of DNA or enzymes.<sup>11</sup>

Given the high toxicity of pesticides and phenolic compounds there is a huge demand for biosensing systems that are cost effective, robust and easy to be used.

## 1.2 Biosensing systems for environmental monitoring

Federal agencies such as the United States Environmental Protection Agency (US EPA) and National Institute for Occupational Safety and Health routinely use GC-MS and HPLC methods in their protocols for environmental analytical techniques.<sup>12,13</sup> These methods use to be complex in terms of the need for different steps such as sampling, sample transportation and sample preparation before analysis. In addition these methods are related to rather sophisticated instruments, require well prepared professional for their use and are not suitable for *in situ* and simple screening procedures.

In this context there is a need to develop simple (bio)sensing platforms as alternative (or complementary one) to these existing conventional techniques. Recent developments of microfabrication, bioengineering and in particular nanotechnology are bringing new opportunities for the design and application of new analytical platforms for environmental monitoring such as biosensors.

According to a recently proposed IUPAC definition “A biosensor is a self-contained integrated device which is capable to providing specific quantitative or semi-quantitative analytical information using a biological recognition element (biochemical receptor) which is in direct spatial contact with a transducer element.”<sup>14</sup>

As written above the biosensor is constituted of three fundamental parts: a biological recognition element (enzyme, DNA, antibodies, whole-cells etc.), a transducer (optical, electrical, mass etc) and an electronic device that associates the signal to a countable value easy to be understood even by nonexpert users.<sup>15</sup>

In agreement to the signal transduction or to the bio-recognition principles biosensors can be categorized in different ways. Figure 1 is a general schematic of a biosensor and its components.

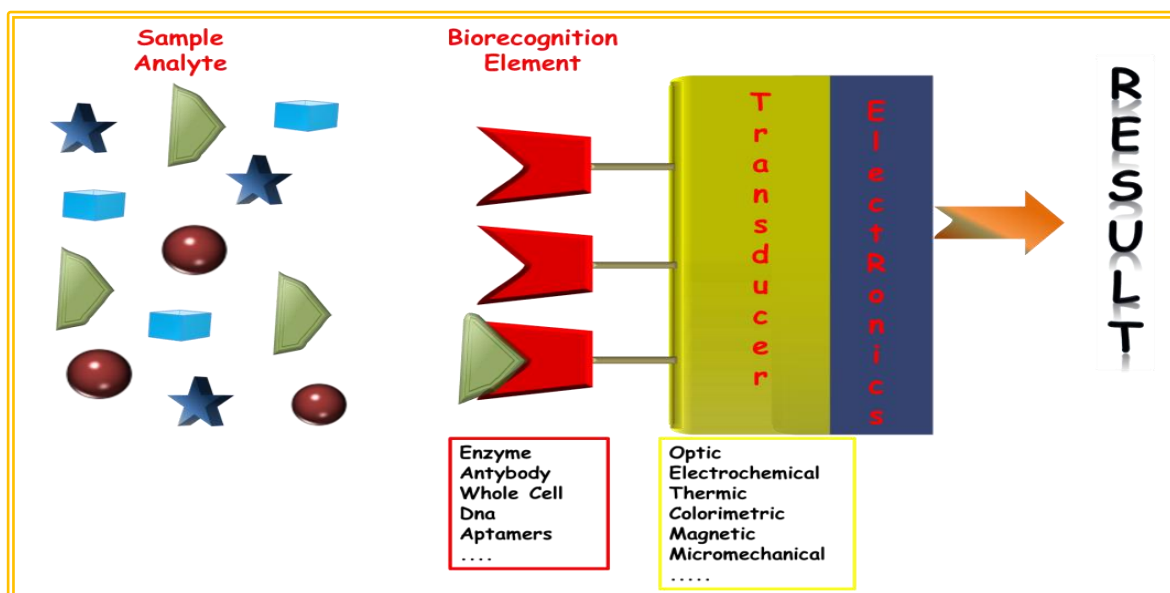


**Figure 1** Schematic representation of a biosensor, its components and possible classification.

In the following part some more descriptions on electrochemical biosensors, being the technology used in this PhD thesis, will be given.

### 1.3 Electrochemical biosensors

The main parameters that must be considered for development of electrochemical biosensors - especially those for pesticide and phenol compounds detection are reproducibility, selectivity, sensitivity, long-term stability, portability, ease of use, and cost-effectiveness. Driven by these needs, great efforts have been made in the design, fabrication, and application of nanomaterials for electrochemical sensing devices. Table 3 provides an overview of technological and analytical performance data for the nanomaterial-based electrochemical pesticide and phenols compound sensors reported in the literature.

**Table 3** Examples of biosensing systems based on electrochemical detection strategies for pesticide and phenols compounds detection.

Recognition Principle	Pesticide	Electrochemical Platform / Label	Recognition element	D.L	Detection Technique	Sample Matrix	Ref
Immunoassay	Picloram	Chitosan-AuNPs membrane	Anti Picloram Ab	5.0 ng/mL	Chronoamperometry	Rice, lettuce and paddy field water	[25]
	Picloram	3D-Au nanoclusters	Anti Picloram Ab	0.5 ng/mL	Chronoamperometry	Peach samples	[26]
	Atrazine	AuNPs labeled Ab	Anti Atrazine Ab	0.034 µg/L	Conductivity	Red wine Samples	[27]
	Diuron	PB-AuNPs film	Alkaline phosphatase rabbit anti-IgG Ab	1.0 ppt	SWV	--	[28]
	Paraoxon	CdS@ZnS QDs labeled Ab	Antiphospherine pAb	0.15 ng/mL	SWV	Plasma samples	[29]
	Paraoxon	ZrO <sub>2</sub> NPs coated SPE / QDs labeled Ab	ZrO <sub>2</sub> NPs	8.0 pM	SWV	Spiked human plasma samples	[30]
Enzymatic	Paraoxon	AChE-AuNPs into scaffolds gel	AChE inhibition	6 pM	Chronoamperometry	River water samples	[31]
	DDV/Carbofuran	MWCNT-AChE/PB/MWCNT	AChE inhibition	0.04/0.1 ppb	Amperometry	Spiked beverage samples	[33]
	Paraoxon	AuNPs-MWCNTs-based electrode	AChE inhibition	0.1 nM	Amperometry	--	[34]
	Methyl parathion	AuNPs-MWCNTs-CdTeQDs-MPDE	MPDE hydrolysis	1.0 ng/mL	Amperometry	Spiked garlic samples	[36]
	Methyl parathion	AuNP-SP-MWCNT-MPDE	MPDE catalytic hydrolysis	0.3 ng/mL	SWV	Spiked garlic samples	[38]
	Paraoxon	AuNPs/cr-Gs hybrid	AChE inhibition	0.1 pM	Chronoamperometry	--	[44]
	Paraoxon	AChE - Fe <sub>3</sub> O <sub>4</sub> NPs- silica shell SPE	AChE inhibition	5.0 · 10 <sup>-9</sup> M	Chronoamperometry	--	[46]
	Catechol/Phenol	BiNPhs/Tyr	Tyr hydrolyxation	26/ 62 nM	Amperometry	-	[48]
	Catechol/Bisphenol	Graphene-silkpeptide/Tyr	Tyr hydrolyxation	0,23/0,75nM	Amperometry	Plastic drinking bottle water	[49]
	Catechol	Graphene oxide PdCu NCs/Laccase	Laccase oxidation	2µM	Amperometry	Tea	[50]
Immunoassay/ Enzymatic	Organophosphates	CdS@ZnS QDs labeled Ab	Anti BChE Ab/ BChE inhibition	0.5 nM	SWV	Spiked human plasma samples	[47]
Host-Guest	Chlorpyrifos	PATP-AuNPs -GCE	Molecular imprinted PATP	3.3 · 10 <sup>-7</sup> M	CV	Spiked tap water samples	[51]
	Dimethoate	AgNPs-PoPD	Molecular imprinted PoPD	0.5 ng/mL	CV	--	[52]
	4-nonyl-phenol	Graphene Nanoribbons	Molecular Imprinted	8nM	CV	Water sample	[53]
Other methods	Paraoxon	RGON hybrid based electrodes	--	1.37 · 10 <sup>-7</sup> M	Chronoamperometry	--	[42]
	Dichlofenthion	TiO <sub>2</sub> NPs SPE	--	2.0 nmol/L	DPASV	Green vegetable samples	[54]
	Cypermethrin/ Permethrin	Chitosan - Fe <sub>3</sub> O <sub>4</sub> nanobiocomposite	Binding of pesticides to ssCT-DNA	0.0025 ppm/ 1 ppm	DPV	--	[55]
	Methyl parathion	CNT-web-based electrode	--	1.0 nM	DPV	--	[56]

---

### 1.3.1 Electrochemical-based Immunosensors

Immunoassays have been used for many years in clinical chemistry as reliable and sensitive strategies to determine low concentrations of analytes in different matrices.<sup>16</sup> The use of immunoassays for sensing is advantageous in terms of speed, simplicity, reliability, cost-effectiveness, and other factors. Immunoassays for various targets, including pesticides, have been adapted for field measurements. Indeed, reports indicate an increasing number of successful studies on immunoassay systems for pesticide monitoring.<sup>17-21</sup> Immunoassays exploit the strong, specific interaction between an antibody (Ab) and its corresponding specific antigen (Ag).

Antibodies are specifically generated by the immune system to defend against foreign substances (antigens). Substances with molecular weights lower than 1 000 Da (e.g., most pesticides) do not provoke an immunogenic reaction alone but can do so upon binding to larger molecules (e.g., albumin).

Such low-molecular-weight substances are called haptens. Although the production of haptens and their corresponding antibodies is fairly tedious, many kinds of immunoassay formats have been developed. Competitive immunoassays are the most frequently used type for pesticide sensing using optical detection.

A schematic of a conventional competitive immunoassay for pesticide detection is shown in Figure 2. These immunoassays typically take one of two formats: they feature an immobilized antibody coupled to an antigen (hapten) label (Figure 2A) or vice versa (Figure 2B). Nonetheless, novel formats are being designed to avoid nonspecific reactions.

Different types of nanomaterials, including metal nanoparticles (e.g., gold nanoparticles (AuNP's)) and semiconductor nanoparticles (e.g., quantum dots (QDs)), have been widely used as versatile labels in immunoassays and enable superior signal amplification compared to traditional labels (e.g., organic dyes).

---

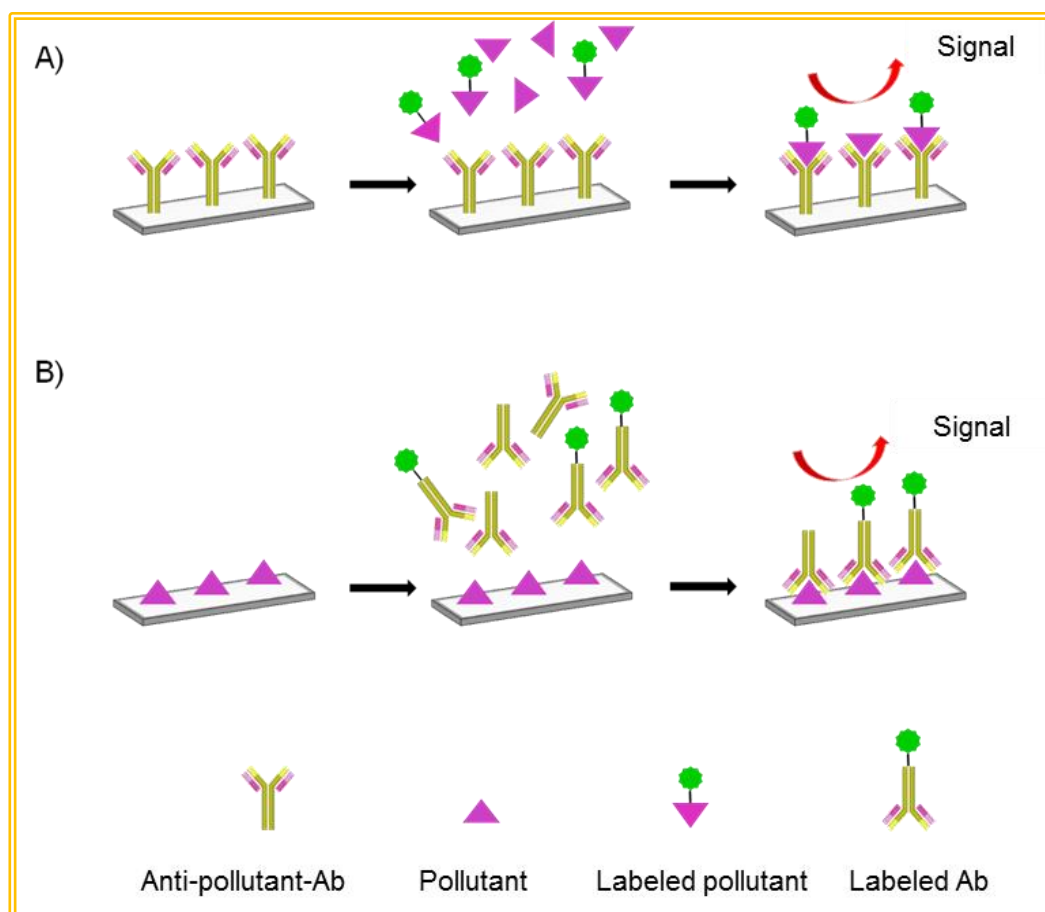


**Figure 2** Schematic of traditional competitive immunoassay formats for pollutant detection. The concentration of analyte to be monitored is correlated with the amount of labelled antigen (A) or antibody (B) to the corresponding ligand coated on the transducer surface.

Therefore electrochemical immunosensors have attracted considerable interest for many years because of their high sensitivity, low cost, and inherent miniaturization.<sup>22,23</sup>

Emerging nanomaterials, ranging from nanoparticles to graphene, are opening new doors for electrochemical immunoassays, in terms of improved electrochemical properties of the transducers and better conjugation with biological compounds and acting in some cases as electrochemical labels.

In this field, colloidal gold has been extensively used in pesticide electrochemical immunoassays because of its intrinsic electrochemical characteristics.<sup>24</sup>

Tang et al. described a system based on a chitosan/AuNP composite membrane for the electrochemical detection of picloram, a widely used chlorinated herbicide.<sup>25</sup> The antipicloram antibody was embedded in the composite membrane, to which horseradish peroxidase (HRP)-labelled secondary antibody was then attached; pesticide quantification was tracked using this secondary antibody. Enzymatic electrocatalytic hydrolysis of quinone (by HRP) was used for the electrochemical response. In this work, nanoparticles shuttle the electron transfer between the HRP and the electrode surface. A detection limit of 21 nM of picloram was achieved using cyclic voltammetry with good precision and storage stability.

Chen et al. recently published a similar picloram-detection system to that previously described.<sup>26</sup> Their system deals with ordered three-dimensional (3D) gold (Au) nanoclusters.

Enzymatic electrocatalytic hydrolysis of quinone (by HRP) was used here also. The authors highlight that compared to the chitosan/AuNP composite system devised by Tang et al.<sup>24</sup> (see above), their AuNP 3D network offers significantly greater specific surface area for molecular bioconjugation and better electron-exchange capability, thereby enabling lower detection limits.

Although the aforementioned systems have good responses and low detection limits, the fact that they require additional substrates (in these two cases, HRP) to generate the analytical response is not very desirable. Around the same time as the Chen group reported its work, Valera et al. reported the use of interdigitated  $\mu$ -electrodes (ID $\mu$ Es) combined with AuNP's and specific antibodies to detect atrazine in wine samples by conductometric measurements.<sup>27</sup>

The detection principle is based on the conductometric change, which occurs when secondary antibodies labelled with AuNP's are deposited onto the electrode gaps after the immunoassay. Gold nanoparticle inclusions reduce the gap between ID $\mu$ Es and increase the electric field between them, generating an analytical readout signal.

Among the main advantages of the ID $\mu$ E system is the potential for relatively high throughput (48 samples in 5 h) without the need for sample pretreatment.

Sharma et al. recently reported an electrochemical immunosensor for diuron herbicide involving the use of laser-ablated gold electrodes modified with a Prussian Blue-gold nanoparticle (PB-AuNP) film.<sup>28</sup> The available antipesticide antibodies were bound to the PB-AuNP film using alkaline phosphatase rabbit anti-IgGAb and 1-naphthyl phosphate substrate for the electrochemical analytical response by square wave voltammetry (SWV). The authors of the work state that PB-AuNP film has the advantage of a large surface-to-volume ratio, strong adhesion, and high surface activity, all of which give the assay greater sensitivity relative to the case of unmodified electrodes. The system is highly specific for diuron, with a sensitivity of 4 pM to 0.4  $\mu$ M.

In addition to AuNP's, other nanomaterials, such as QDs or ZrO<sub>2</sub> nanoparticles, have been used for electrochemical pesticide immunoassays. Wang et al. employed QDs in a new tool for biomonitoring exposure to organophosphates (OPs) by direct detection of organophosphorylated acetylcholinesterase.<sup>29</sup> The system combines magnetic separation for preconcentration purpose and the sensitive square wave voltammetric technique for QD label detection.

Antiphosphoserine polyclonal antibodies were immobilized onto magnetic nanoparticles (MNPs) to capture phosphorylated acetylcholinesterase (AChE-OP). In addition, antihuman AChE monoclonal antibodies were labelled with CdS@ZnS QDs to selectively recognize the captured AChE-OP. The group was able to quantify organophosphorous compounds based on CdS@ZnS QDs stripping signals in square-wave voltammetry.

Phosphorylated AChE has been used in other works. For example, Liu et al. reported an electrochemical immunoassay based on the use of zirconia nanoparticles, for the selective binding of OP-AChE adduct, and QDs, as tags for labeling anti-AChE-Ab to quantify the immunorecognition event (see Figure 3A).<sup>30</sup>

Typical electrochemical responses for increasing amounts of phosphorylated AChE (coming from increasing amounts of paraoxon) are shown in Figure 3B. Well-defined stripping peaks are observed across the concentration range. The resulting calibration plot of current versus known concentration of AChE-OP (inset Figure 3B) is linear from 10 pM to 4 nM, which is suitable for the quantitative working range.



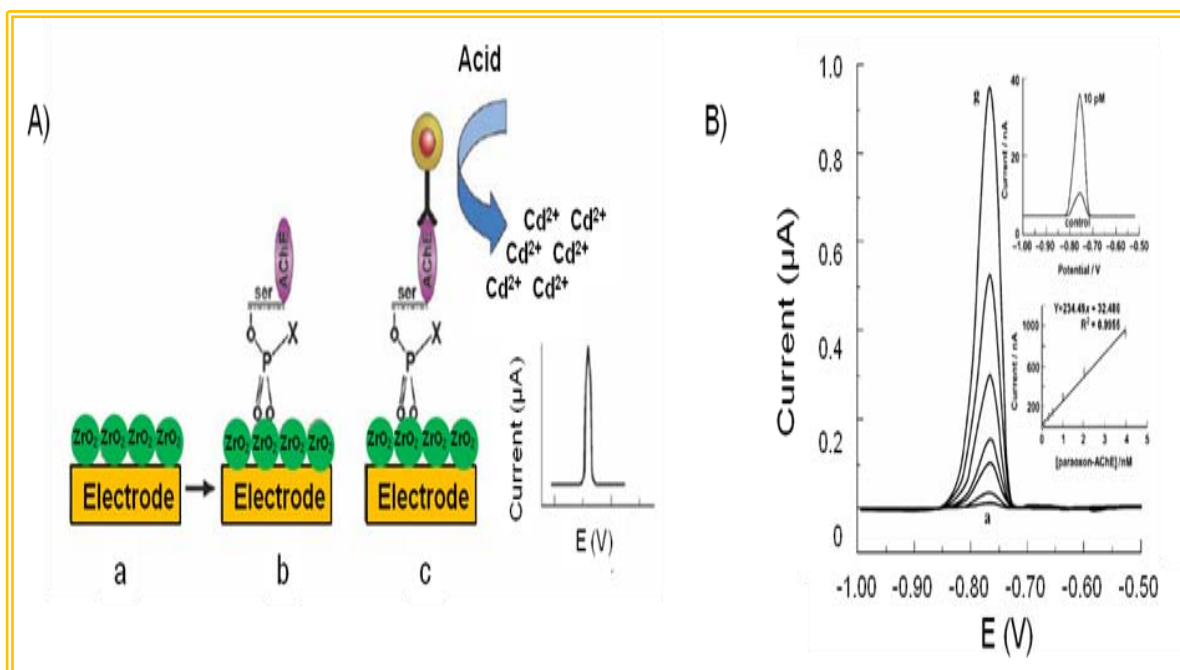


**Figure 3** A) A.1) The principle of electrochemical immunosensing of phosphorylated AChE, (a.  $ZrO_2$  NPs modified SPE; b. Selective capturing phosphorylated AChE adducts; c. Immunoreaction between bound phosphorylated AChE adducts and QD-labeled anti-AChE antibody; d. Dissolution of nanoparticle with acid following an electrochemical stripping analysis. AChE: purple,  $ZnO_2$  : green, electrode: yellow; A.2) Typical electrochemical responses of the immunosensor with the increasing phosphorylated AChE concentration (0.01, 0.05, 0.3, 0.5, 1.0, 2.0, 4 nM from 'a' to 'g'). The insets show the resulting calibration plot (bottom) and the electrochemical responses of 10 pM and 0 pM (top) paraoxon-AChE.

The main advantage of these two last presented works is that they provide a general response to OPs, an entire pesticide chemical group, rather than to one single pesticide, thus providing a broader response of interest for real sample analysis. In terms of electrochemical immunosensor systems for pesticide monitoring, efforts must be focused on the development of multiple electrochemical detection systems for different pesticides, as most of the developments in this field involve single detection only.

One potentially interesting alternative would be the use of different QDs with different electrochemical fingerprints coated with antibodies specific for different pesticides. However, generation of antibodies against small molecules is a very tedious and expensive task; therefore, other recognition molecules are desirable.

---

## 1.3.2 Enzyme-Based Electrochemical Systems

Enzyme –based electrochemical systems for detection of pollutants compounds are normally based in a process of inhibition. In particularly different inhibition biosensor systems based on the use of AChE immobilized onto different nanostructured electrochemical transducers have been proposed for pollutants compounds screening.

The most widely applied nanomaterials in this field have been AuNP's and carbon nanostructure-based platforms, including combinations of these two materials.

Lu et al. recently reported a work involving immobilization of AuNP-AChE conjugates for paraoxon electrochemical biosensing.<sup>31</sup> The authors highlight the use of gel scaffolds to provide essentially the same local aqueous microenvironment as in biological medium, giving rise to a favorable host matrix that isolates the AuNP-AChE conjugates, thereby protecting them from aggregation and leaching. The system enables direct measurements of OPs in real environmental samples, with impressive detection limits (6 pM for paraoxon).

Regarding carbon nanomaterials, multiwalled carbon nanotubes (MWCNTs) have attracted much attention not only due to their unique electronic properties but also due to the high surface area that they offer when used as electrodes and to their ability to enhance enzymatic activity.<sup>32</sup>

In this field, Chen et al. reported a system comprising MWCNTs coupled to Prussian blue (as redox mediator for the electrochemical oxidation of the enzymatic product thiocholine) and AChE, whereby inhibition of AChE by pesticides generates an electrochemical signal that is amplified by the MWCNTs.<sup>33</sup>

The combination of MWCNTs and AuNP's has also been studied for pesticide-monitoring systems.

For example, Jha et al.<sup>34</sup> modified a glassy carbon electrode (GCE) with AuNP's and MWCNTs to achieve strong electron transfer and large immobilization sites for the

---

bioenzyme (AChE), exploiting the strong electrocatalytic activity of the MWCNTs. Without using any redox mediator, they reached a very high sensitivity of 0.1 nM for the model analyte paraoxon.

Du et al. performed similar work<sup>35</sup> combining AuNP-MWCNT-based electrodes with CdTe QDs as carriers to load a large amount of enzyme. Their use of methyl parathion degrading enzyme (MPDE) further set their work apart from that of Jha et al.<sup>34</sup> The authors highlight that, unlike cholinesterase-based biosensors, the MPDE-based biosensor can be potentially reused and is suitable for continuous monitoring. They reported the system to be selective toward pesticides containing P–S bonds, which obviates any interference coming from carbamates or OP pesticides.

Methyl parathion hydrolase (MPDE) was also used by Chen et al. to develop a nanocomposite biosensor based on the mixture of silica particles SP@AuNP and MWCNTs placed on the surface of a glassy carbon electrode (GCE).<sup>36</sup> The biosensor is selective for methyl parathion over its analogues. The authors used SWV to obtain the analytical signal.

The response for this specific system comes from the electrochemical activity of 4-nitrophenol, which is provided by the hydrolysis of methyl parathion (MP). Figure 4A.1 depicts the working principle of the MPDE biosensor for the determination of MP, as proposed by the authors. Figure 3A.2 displays the SWV responses for the designed MPDE/SP@AuNP's/MWCNT/GCE biosensor to different concentrations of methyl parathion as well as the linear relationship between peak currents and MP concentration (inset Figure 4A.2).

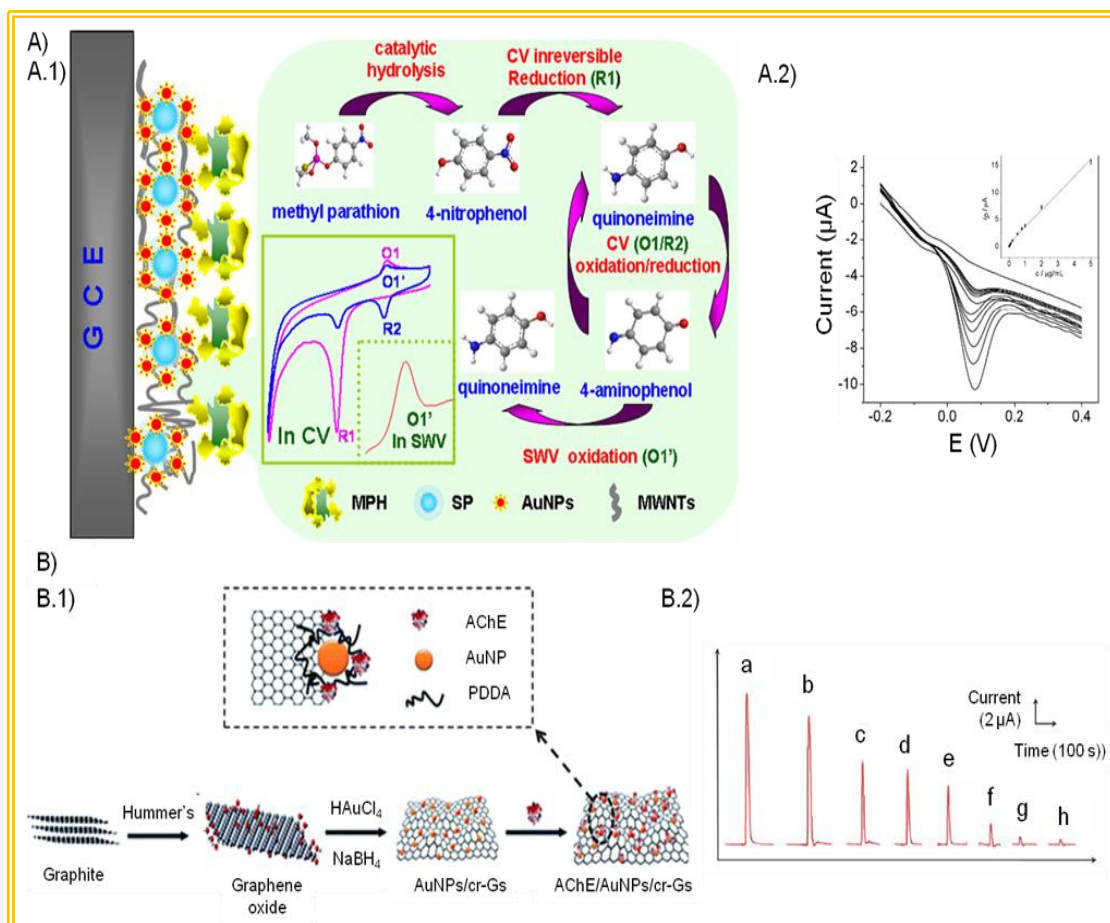


**Figure 4.** A) Working principle of MPH biosensor for determination of methyl parathion. B) SWV responses of the MPH/SP@AuNPs/MWNTs/GCE biosensor for varying concentrations. Inset: linear relationship between peak currents and methyl parathion concentrations. B) B.1) Schematic illustration of Au NP/cr-Gs hybrid synthesis and AChE/Au NP/cr-Gs nanoassembly generation by using PDDA; B.2) Typical amperometric responses of AChE/Au NP/cr-Gs based SPEs to paraoxon by using FIA system. Signal (a) is from 2 mM ATCh, signals from (b to h) are from 2 mM ATCh after the AChE/Au NPs/cr-Gs based SPEs were incubated with paraoxon for 15 min with different concentrations.

Beyond MWCNTs, other carbon nanomaterials are being employed for pesticide sensors. For example, owing to its remarkable electrochemical properties, graphene shows fascinating advantages in electrochemical biosensors. Compared to CNTs, graphene, which was experimentally discovered only 7 years ago,<sup>37</sup> is reported to offer more advanced properties and is likely to exhibit fewer weaknesses.<sup>38</sup>

Graphene is an excellent electrical conductor. Heterogeneous electron transfer occurs at the edges of the graphene or at defects in the basal plane. Thus, the high surface area of graphene translates to numerous defects and, consequently, to many electroactive sites.

Wang et al. described a strategy for depositing AuNP's and AChE onto chemically reduced graphene nanosheets (cr-Gs) with a long-chain polyelectrolyte (poly(diallyldimethylammonium chloride), PDDA), which acts as a stabilizer and dispersible medium for the other materials (see Figure 4B.1).<sup>39</sup> Figure 4B.2 shows typical amperometric responses of the AChE/Au NP/cr-Gs-based screen-printed electrodes (SPEs) to paraoxon, obtained using a flow-injection analysis system. The novel device gave lower detection limits compared to other systems for paraoxon detection.<sup>40,41</sup>

Despite having been designed for pesticide detection, the nanoassembly could be outfitted with other immobilized materials, such as antibodies or even host–guest recognition molecules, for analysis of other compounds (e.g., toxins or nerve agents). The optical properties of graphene are also being studied extensively; simultaneously exploiting its electrochemical and optical properties may yield interesting applications.

Choi et al. have demonstrated a proof-of-concept system using graphene-based electrodes for pesticide detection.<sup>42</sup> They used free-standing, conductive, reduced graphene oxide/Nafion (RGON) nanohybrids to create an electrochemical biosensor platform that contains organophosphorus hydrolase as an enzyme for the hydrolysis of OPs. Functionalization by Nafion provided highly stable dispersibility of RGOs and mechanical integrity of the hybrid material, due to its intrinsic molecular structures and functionality. A detection limit of  $1.37 \times 10^{-7}$  M of paraoxon was obtained.

Liu et al. have described a nanocomposite modified electrode system based on RGO, AuNP's, and AChE, which they used to detect organophosphorous and carbamate pesticides via enzyme inhibition.<sup>43</sup>

Other nanostructures besides AuNP's and carbon nanomaterials have been applied in electrochemical pesticide-detection tools involving inhibition of AChE.<sup>44,45</sup> For instance,

Won et al.<sup>46</sup> devised a model system for nanomolar detection of paraoxon incorporating biomagnetic glass platforms based on Fe<sub>3</sub>O<sub>4</sub>–silica NPs and AChE. They immobilized the core–shell NPs by simple physical adsorption onto a carbon–SPE that they used as a working electrode for the amperometric measurements, which could imply problems with stability. The authors did not exploit the magnetism of the Fe<sub>3</sub>O<sub>4</sub> silica NPs to preconcentrate the sample on the working electrode, which would have enabled a stronger response.

Enzyme activity assays and immunoassay strategies based on electrochemical detection of pesticides can be combined for further improvements. Du et al. recently reported a system involving both strategies for biomonitoring of exposure to OPs.<sup>47</sup>

As shown in Figure 5A, they used antibodies to selectively capture enzyme for the enzyme activity assay (Figure 5A.1), while simultaneously using an immunoassay to quantify total enzyme levels (Figure 5A.2).

The values obtained from the difference between the total amount and the active butylcholinesterase (BChE) are used to estimate the amount of OP–BChE adducts in serum. Additionally, magnetic beads are used to capture the analyte from the biological matrix. The analytical signal comes from thiocholine oxidation (for the immunodetection of enzyme activity) and from antibodies labeled with CdS@ZnS QDs (for the total BChE determination).

Square wave voltammetry responses for MB BChE incubated with different concentrations of BChE and the calibration plot of SWV response against BChE concentration are shown in Figure 5A.3 and A.4, respectively.

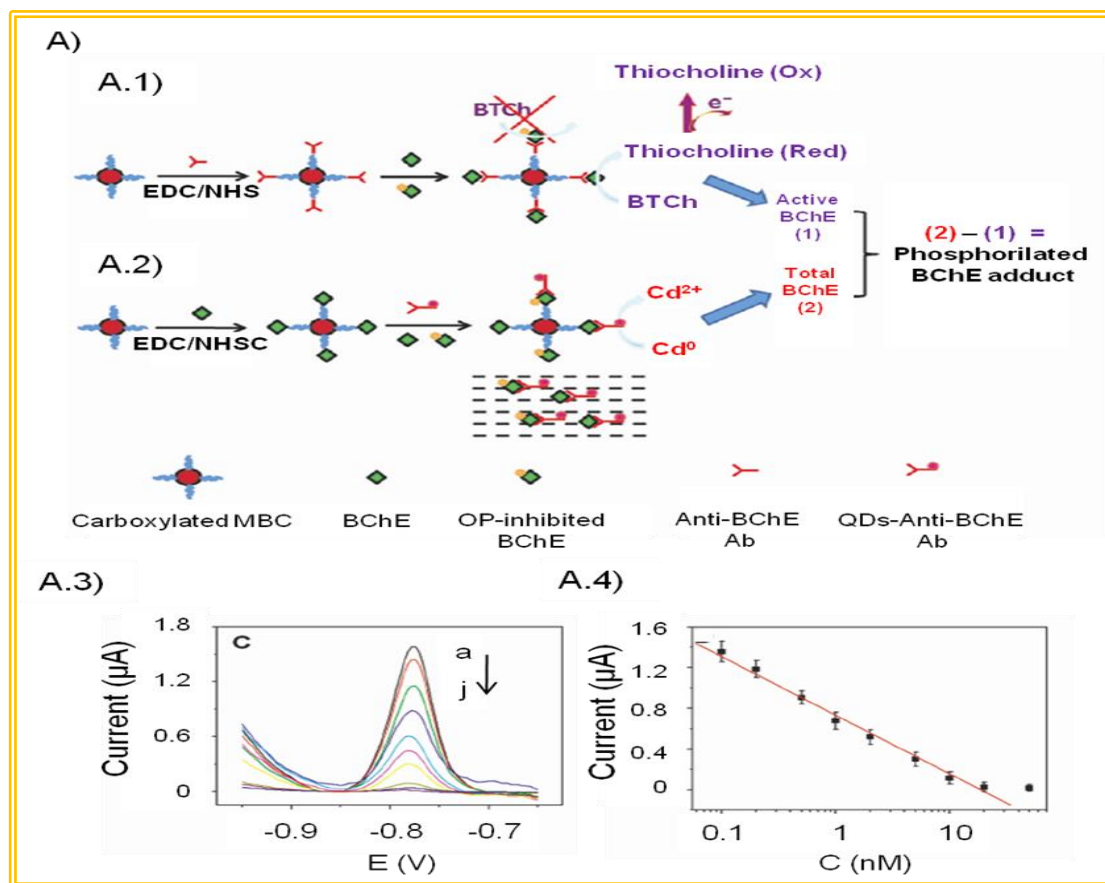


**Figure 5:** A) Schematic illustrations of the principle of immunosensing platform based on (A.1) Immunodetection of enzyme activity and (A.2) Immunoassay of total amount of enzyme simultaneously for biomonitoring of OP exposure; A.3) SWV responses for MBChE incubated with different concentrations of BChE; (A.4) Calibration plot for the immunosensor response.

Beyond the inhibition process, other detection strategy has been used in the detection of pollutants compounds. For example the toxic compound can be transformed by an enzyme giving a secondary product easy to be measured. Different platforms using nanomaterials in particular for screening and analysis of phenols compounds able to be metabolized from the tyrosinase enzyme have been reported in the last years.

Mayorga et al <sup>48</sup> propose for example an interesting connection between the enzyme tyrosinase and the bismuth nanoparticles. This biosensing platform shows not only the effectiveness of bismuth nanoparticles to improve the electron transfer between the active centre of tyrosinase and the electrode surface but also to improve the

immobilization of the enzyme over the electrode surface. The authors were able to quantify two different phenols compounds with a simple biosensing system ( Fig 6 A) showing the effectiveness of this nanomaterial (Fig 6B) that allowed to obtain a linear response for catechol and phenol achieving a good performance for both pollutants (Fig 6 C, Fig 6B)

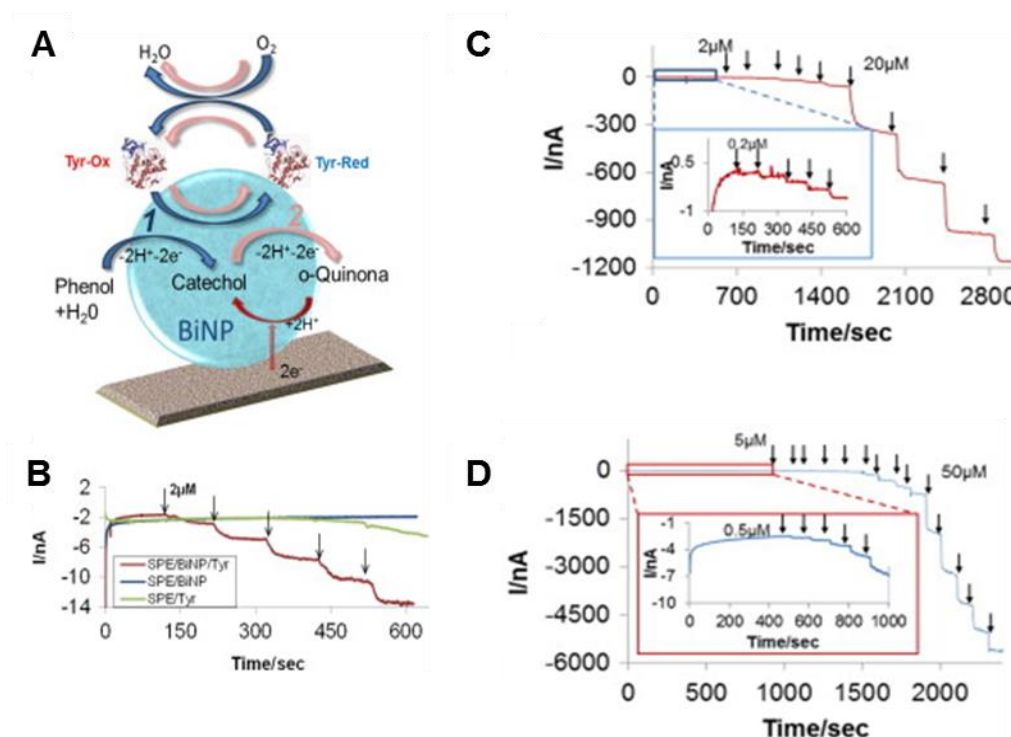


**Figure 6** A) Proposed mechanism for the phenol and catechol electrocatalytic detection by using BiNP based biosensor; B) Current–time response curves of bare SPE, SPE/BiNP and SPE/BiNP/Tyr modified electrodes upon successive additions of 2 μM phenol; C) typical current–time response curves for the successive additions of 0.2, 2 and 20 μM of phenol, inset magnification of the initial steps; D) typical current–time response curves for the successive additions and 0.5, 5 and 50 μM of catechol, inset magnification of the initial steps.

48

Qu et al.<sup>49</sup> describe a similar strategy for detection of phenols compounds such as catechol and bisphenol using the Graphene-silk peptide nanosheet connected to the tyrosinase deposited over the glassy carbon electrode. The transfer charge and the stability of the biosystem take advantage of the intrinsic characteristic of the graphene.



The obtained results (detection limits) are below the allowed limit defined by law for these pollutants and show also a high sensitivity

Mei et al.<sup>50</sup> report also a biosensing platform for detection of phenols compounds using graphene. In their work graphene is used as a support to avoid the agglomeration of bimetallic nanoparticles (Fig 7A) that have to enhance the transfer of charge between the laccase enzyme to the electrode surface.

The results obtained (Fig 7B) showed a linear response for this enzyme-based sensing system. Nevertheless the system seems rather complicated comparing to those one using only the graphene as mediator and stabilizer.

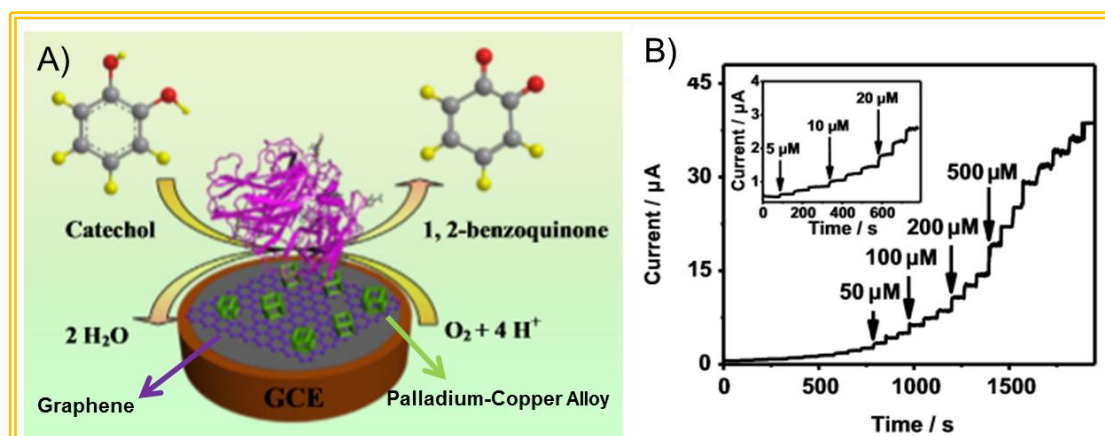


**Figure 7** A) Schematic illustrations of the principle of the enzyme platform based on the reduced graphene oxide supported palladium-copper alloyed nanocage. B) Chronoamperometric graphic of the different additions of catechol.

### 1.3.3 MIPs and Other Host–Guest-Like Systems

The production of high-affinity specific antibodies used in immunoassays is one of the most complicated problems in the development of such sensing systems when antibodies to a particular pesticide are difficult to be obtained. In addition, natural antibodies are highly expensive and may undergo mutation, thus varying the interaction capacity of the recognition sites. Molecular imprinted polymers (MIPs) have attracted considerable attention as an alternative for preparing molecular recognition systems mimicking the

specific binding events of Abs. , Moreover despite the high sensitivity enzyme-based pesticide detection systems, they suffer from poor chemical/physical stability, which prevents their use in harsh environments (e.g., acidic or basic media, organic solvents, high temperatures, etc.). Thus, replacement of biological receptors with synthetic counterparts such as recognition elements also is extremely important for electrochemical-based systems. To this end, MIPs represent a good alternative in the pollutants detection.

Generally, MIPs are prepared via polymerization of the appropriate monomer(s) in the presence of the target molecule or template (e.g., pesticide). After polymerization, the target is chemically removed, leaving behind nanocavities with the exact size, shape, and corresponding functional groups capable of rebinding the target with a high degree of selectivity. A general scheme of MIP preparation is shown in Figure 8.

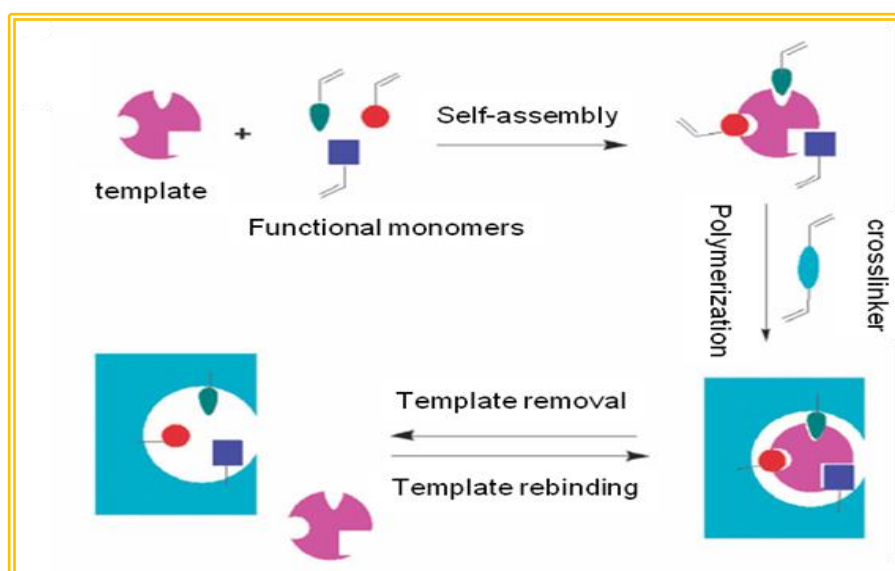


**Figure 8:** General scheme of MIPs preparation

A nice example of an MIP-based system recently published by Xie et al. can be seen in Figure 9.<sup>51</sup> The authors report a surface molecular self-assembly strategy for molecular imprinting in electropolymerized polyaminothiophenol (PATP) membranes at the surface of AuNP-modified glassy carbon electrodes (GCEs) for the electrochemical detection of chlorpyrifos (CPF). Figure 9A and 9B depicts the procedure for preparing the imprinted PATP–AuNP's–GCE electrodes: electrodeposition of AuNP's of the GCE surface; followed by electrodeposition of ATP on the surface of GCE; and finally, removal of the imprinting

CPF molecules (Figure 9A). Figure 9C displays the cyclic voltammetric responses of the system to different amounts of CPF. Well-defined peaks are shown, with the current increasing as CPF concentration increases. A linear relationship in the range from 0.5 to 10  $\mu\text{M}$  CPF was obtained with a detection limit of 0.33  $\mu\text{M}$  of CPF. The AuNP's not only enhance the signal but also increase the mass transport, which is a normal drawback for these sensing methods.

Du and collaborators reported a similar system, which involves use of imprinted poly(o-phenylenediamine) and AgNP's instead of AuNP's and cyclic voltammetry as the detection technique.<sup>52</sup> They achieved detection limits of 2.2 nM for the pesticide dimethoate detection.

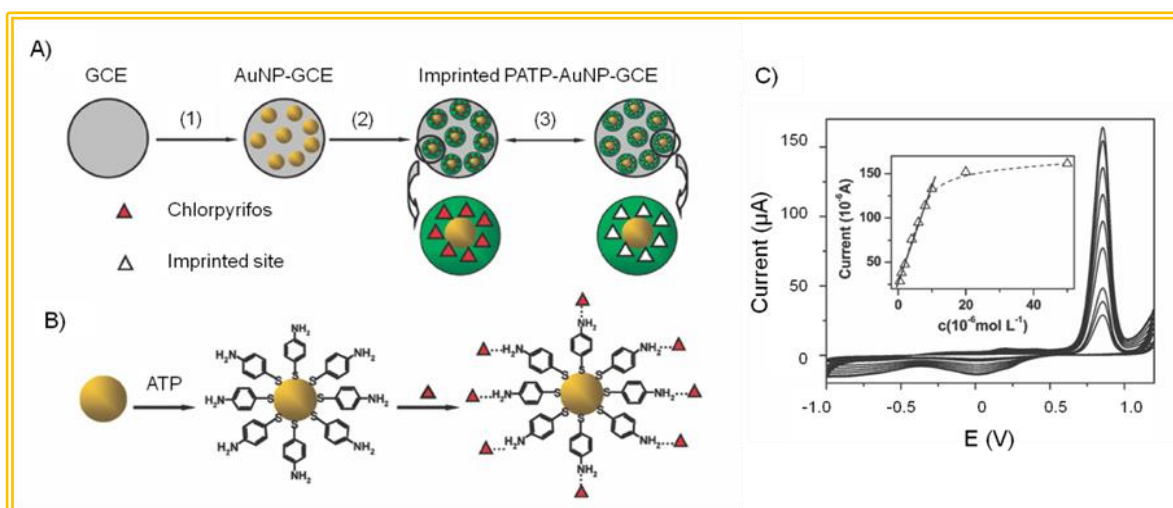


**Figure 9** A) Preparation procedures of the imprinted PATP-AuNP-gc electrode: (1) electrodeposition of AuNPs on the surface of the glassy carbon electrode (GCE); (2) electropolymerization of ATP on the surface of the AuNP-gc electrode; (3) removal/rebinding of chlorpyrifos on the imprinted sites of the imprinted PATP-AuNP-GCE. B) Schematic illustration for the adsorption of the ATP molecule at the AuNP surface and the further self-assembly of CPF at ATP-modified AuNP-GCE. C) Cyclic voltammograms of increasing CPF concentration in 0.05 M PBS (pH ) 6.86) containing 0.1 M KCl. The inset shows the calibration curve of CPF.

Pan et al<sup>53</sup> propose a nice example of MIP using nitrogen-doped graphene nanoribbons (NGNRs) and Ionic liquid for the determination of 4-nonyl-phenol using a glassy carbon electrode. In this interesting work the authors highlight that the phenols showed better electrochemical response at GNRs than at multi-wall carbon nanotubes (MWCNTs) or

---

graphene modified GCE. The results achieved by this biosensing system show a great sensibility and reproducibility in real samples.

### 1.3.4 Other Electrochemical Strategies

An alternative of using antibodies and enzymes is the use of nucleic acid (NA) as a biological element in the biosensing system assay. It is well known that NA molecules have the function of carrying and passing on genetic information with wide range physical, chemical and biological activities. Normally and with a lot of interest the NA are able to detect and quantify single strain of DNA giving fundamental information in the field of the health care. Furthermore specific DNA sequences for example can be indicators of pathogens correlated so to food and water contamination and so to environmental monitoring.

In addition the connection of DNA with nanomaterial has well evaluated for the detection of pollutants compounds. In addition to the aforementioned methodologies described for pesticide detection, there are other analytical methods being evaluated to develop new, simple, low-cost, portable, and sensitive devices that do not require biological or synthetic receptors. For example, Li et al. recently reported a novel photoelectrochemical sensor for electrochemical detection of dichlofenthion.<sup>54</sup>

They harnessed nanosized titania to obtain electroactive compounds by photocatalytic degradation of dichlofenthion, which they then readily detected using differential pulse anodic stripping voltammetry (DPASV). For dichlofenthion, the detection limit appears to be in the nanomolar range. In the future, this strategy could be applied for other non-electroactive compounds.

Kaushik et al. used  $\text{Fe}_3\text{O}_4$  NPs for electrochemical detection of pyrethroids.<sup>55</sup> Their system is not based on AChE inhibition but rather on the binding of pesticides to single-stranded calf thymus DNA (ssCT-DNA). The ssCT-DNA is immobilized onto a chitosan (CH)- $\text{Fe}_3\text{O}_4$  NPs/ITO electrode. When pesticides are recognized by the DNA strand, the current intensity decreases, and this change is detected by DPV.

---

Musameh et al. recently reported on the use of CNT-webs for methyl parathion detection.<sup>56</sup> They define CNT-webs as “a novel form of CNT(s) produced by drawing CNT(s) away from the front face of specially grown ‘forests’ of aligned CNT(s)”, a method which generates high porosity surfaces. Because of this large surface area and good electrochemical properties, CNT-webs represent great surfaces for the adsorption of molecules and their subsequent electrochemical detection. Using DPV, they achieved detection limits of 1.0 nM for methyl parathion. Furthermore, they demonstrated that their new system outperforms a system based on a bare GCE. The main aim of such technologies is to provide a nonanalyte restricted system with the purpose of general pesticides analysis using electrochemical techniques.

## 1.4 Conclusions

In the last few decades, the development of novel methods for pesticides detection with high accuracy, precision, reproducibility and low detection limits has been a challenge for the scientific community.

The attractive physico-chemical properties of nanostructured materials (metal nanoparticles, quantum dots, magnetic nanoparticles, carbon nanotubes, or graphene among others) such as strong absorption ability, excellent electron transfer or large surface-to-volume area make them particularly attractive for their use as either transducing platforms or labels in optical or electrochemical sensors and biosensors.

Gold nanoparticles are the nanoparticles of choice in most of the developed optical detection systems due to their small size, sensitivity, robust manufacturing methods and easy functionalization and the fact that they can be even seen at naked eye. Regarding fluorescence based detection systems, they mainly take advantage of the great properties of quantum dots (QDs) as labels compared to other traditional organic dyes: higher brightness and higher photostability.

Carbon nanostructured materials (i.e. carbon nanotubes, graphene) are the most common materials used as electrochemical transducing platforms for pesticides detection due to the dramatic increase on the sensitivity that these materials present owing to their large specific surface area and high surface free energy. The use of nanomaterials as

immobilization matrices in the pesticides detection field leads to an increase in the system sensitivity due to the excellent response on storage of the recognition/degradation elements.

Besides the nanomaterials based transducing platforms, some nanomaterials can also be used as electrochemical labels with interest for immunosensing systems. Specially, QDs are very well-known as electrochemical labels owing to their easy and low detection limits achieved due to the possibility of using electrochemical stripping techniques. In addition, they also offer the possibility of barcodes development owing to the unique voltammetric stripping signatures depending on the QDs composition (i.e. Cd(II), Zn(II), Pb(II) etc) these can display.

Recognition elements (i.e. antibodies, host-guest systems) play also a key role on the selectivity and sensibility of the designed pesticides detection systems. A compromise between sensibility, selectivity and stability should be taken when deciding the recognition element used in each system. Beside recognition elements, enzymatic inhibition based on cholinesterases has been extensively used for pesticides detection. Such inhibition is found to be further detected using different strategies (i.e. optical and electrochemical).

In this regard, pesticides monitoring systems based upon many of the aforementioned nanomaterials look promising; however, most have not been yet studied in 'real-world' applications. Efforts must be focused on the final aim which is the in-field application of the developed devices so as to achieve a real cost-efficient tool with a fast response for pesticides detection/screening in polluted areas/objects. In this context the development of lateral flow devices that incorporate nanoparticles as labels or other nanomaterials may be future excellent alternatives.

Moreover, nanomaterials can also be used for pesticides degradation and/or removal. The use of metal nanoparticles for catalytic degradation is an exciting and rapidly growing area. It is crucial to keep in mind a few advantages of such nanomaterials with respect to the conventional technologies used for catalysis applied in chemical degradation or removal. First, high surface area is a critical factor in the performance of catalysis allowing the improving in the performance of such technology. In addition, novel reactions can be accomplished at the nanoscale due to an increase in the number of surface atoms which are not possible with analogous bulk material. And finally, more adsorbent atoms are

present per unit mass of the adsorbent and thus the removal percentage of chemical may be higher.

---

## 1.5 Bibliography

1. Soler L.; Sánchez S. *Nanoscale* **2014**, 6, 7175-7182.
2. Rodgers K. R. *Anal. Chim. Acta* **2006**, 568, 222-231.
3. <http://www.who.int/mediacentre/factsheets/fs313/en/>.
4. 98/93/EC Directive on quality of water intended for human consumption.
5. [www.who.int](http://www.who.int).
6. [www.eco-usa.net](http://www.eco-usa.net).
7. [www.panna.org](http://www.panna.org).
8. <http://www.epa.gov>.
9. Laine M.; Jorgensen K. *Appl. Environ. Microbiol.* **1996**, 54, 1507-1513.
10. Hansh C.; Mccarns S.; Smith C.; Dodittle D. *Chem. Biol. Interact.* **2000**, 127, 61-72.
11. Thévenot D. R.; Toth K.; Durst R.A.; Wilson G. S. *Biosens. Bioelectron.* **2001**, 16, 121–131.
12. Selected Analytical Methods for Environmental Remediation and Recovery, EPA600-R-12-555SAM2012.pdf.
13. Stan H. *Comprehen. Anal. Chem.* **2005**, 43, 269-337.
14. Cavalcanti A.; Shirinzadeh B.; Zhang M.; Kretly L. *Sensors* **2008**, 8, 2932-2958.
15. Zhanga W.; Asirib A.M.; Liua D.; Dua D.; Linb Y. *Trends in Anal. Chemistry* **2014** 54, 1-10.
16. De la Escosura-Muñiz A.; Parolo C.; Merkoçi A. *Materials Today* **2010**, 13, 24-34.
17. Suri, C.R.; Boro, R.; Nangia, Y.; Gandhi, S.; Sharma, P.; Wangoo, N.; Rajesh, K.; Shekhawat, G.S. *TrAC, Trends Anal. Chem.* **2009**, 28, 29-39.
18. Ahn K.C.; Kim H.; McCoy M.R.; Gee S.J.; Hammock B.D. *J. Agricult. Food Chem.* **2011**, 59, 2792-2802.
19. Yuan M.; Liu B.; Liu E.; Sheng W.; Zhang Y.; Crossan A.; Kennedy I.; Wang S. *Anal. Chem.* **2011**, 83, 4767–4774.
20. Xu Z.; Shen Y.; Zheng W.; Beier R.C.; Xie G.; Dong J.; Yang J.; Wang H.; Lei H.; She Z.; Sun Y. *Anal. Chem.* **2010**, 82, 9314–9321.
21. Boro R.C.; Kaushal J.; Nangia Y.; Wangoo N.; Bhasin A.; Suri C.R. *Analyst* **2011**, 136, 2125-2130.
22. Liu G.; Lin Y, *Talanta* **2007**, 74, 308-317.
23. Kimmel D.W.; LeBlanc G.; Meschievitz M.E.; Cliffe D.E. *Anal. Chem* **2012**, 84 , 685–707.
24. Cao X.; Ye Y.; Liu S. *Anal. Biochem.* **2011**, 417, 1-16.
25. Tang L.; Zeng G.; Shen G.; Li Y.; Zhang Y.; Huang D. *Environ. Sci. Technol.* **2008**, 42, 1207–1212.



- 
26. Chen L.; Zeng G.; Zhang Y.; Tang L.; Huang D.; Liu C.; Pang Y.; Luo J. *Anal. Biochem.*, **2010**, 407, 172-179.
  27. Valera E.; Azcon J.R.; Barranco A.; Alfaro B.; Baeza F.S.; Marco M.P.; Rodriguez A. *Food Chem.* **2010**, 122, 888-894.
  28. Sharma P.; Sablok K.; Bhalla V.; Suri C.R. *Biosens. Bioelectron.* **2011**, 26, 4209-4212.
  29. Wang H.; Wang J.; Timchalk C.; Lin Y. *Anal. Chem.* **2008**, 22, 8477-8484.
  30. Liu G.; Wang J.; Barry R.; Petersen C.; Timchalk C.; Gassman P.L.; Lin Y. *Chem. Eur. J.* **2008**, 14, 9951-9959.
  31. Lu D.; Shao G.; Du D.; Wang J.; Wang L.; Wang W.; Lin Y. *Lab Chip* **2011**, 11, 381-384.
  32. Zamfir L.; Rotariu L.; Bala C. *Biosens. Bioelectron.* **2011**, 26, 3692-3695
  33. Chen, H.; Zuo, X.; Su, S.; Tang, Z.; Wu, A.; Song, S.; Zhang, D.; Fan, C. *Analyst*, **2008**, 133, 1182-1186.
  34. Jha, N.; Ramaprabhu, S. *Nanoscale* **2010**, 2, 806-810.
  35. Du D.; Chen W.; Zhang W.; Liu D.; Li H.; Lin Y. *Biosens. Bioelectron.* **2010**, 25, 1370-1375.
  36. Chen, S.; Huang J.; Du D.; Li J.; Tu H.; Liu D.; Zhang, A. *Biosens. Bioelectron.* **2011**, 26, 4320-4325.
  37. Novoselov K.S.; Geim, A.K.; Morozov, S.V.; Jiang, D.; Zhang, Y.; Dubonos, S.V.I.; Grigorieva, V.; Firsov, A.A. *Science* **2004**, 306, 666-669.
  38. Brownson D.A.C.; Banks C.E. *Analyst* **2010**, 135, 2768-2778.
  39. Wang Y.; Zhang S.; Du D.; Shao Y.; Li Z.; Wang J.; Engelhard, M.H.; Li J.; Lin Y. *J. Mat.Chem.* **2011**, 21, 5319-5325.
  40. Wang, H.; Wang, J.; Choi, D.W.; Tang, Z.W.; Wu, H.; Lin, Y.H. *Biosens. Bioelectron.* **2009**, 24, 2377-2383.
  41. Viswanathan, S.; Radecka, H.; Radecki, J. *Biosens. Bioelectron.* **2009**, 24, 2772-2777.
  42. Choi, B.G.; Park, H.; Park, T.J.; Yang, M.H.; Kim, J.S.; Jang, S.; Heo, N.S.; Lee, S.Y.; Kong, J.; Hong, W.H. *NANO*, **2010**, 4, 2910-2918.
  43. Liu, T.; Su, H.; Qu, X.; Ju, P.; Cui, L.; Ai, S. *Sens. Actuators, B* **2011**, 160, 1255-1261.
-

- 
44. Ganesana, M.; Istarnboulie, G.; Marty, J.; Noguier, T.; Andreescu, S. *Biosens. Bioelectron.* **2011**, *30*, 43-48.
  45. Chauhan N.; Narang J.; Pundir C.S. *Biosens. Bioelectron.* **2011**, *29*, 82-88.
  46. Won, Y.H.; Jang, H.S.; Kim, S.M.; Stach, E.; Ganesana, M.; Andreescu, S.; Stanciu, L. *Langmuir* **2009**, *26*, 4320–4326.
  47. Du, D.; Wang, J.; Wang, L.; Lu, D.; Smith, J.N.; Timchalk, C.; Lin, Y. *Anal. Chem.* **2011**, *83*, 3770-3777.
  48. Mayorga-Martinez C. C.; Cadevall M.; Guix M.; Ros J.; Merkoçi A. *Biosens. Bioelectr.* **2013**, *40*, 57-62
  49. Qu Y.; Ma M.; Wang Z.; Zhan G.; Li B.; Wang X.; Fang H. Zhang H.; Li C. *Biosens. Bioelectr.* **2013**, *44*, 85-88.
  50. Mei L. P.; Feng J. J.; Wu L.; Zhou J. Y.; Chen J. R.; Wang A. J. *Biosensor. Bioelectronic.* **2015**, *74*, 347-352.
  51. Xie, C.; Li, H.; Li, S.; Wu, J.; Zhang, Z. *Anal. Chem.* **2010**, *82*, 241-249.
  52. Du, D.; Chen, S.; Cai, J.; Tao, Y.; Tu, H.; Zhang, A. *Electrochim. Acta* **2008**, *53*, 6589-6595.
  53. Pan Y; Shang L; Zhao F.; Zeng B. *Electrochimica Acta* **2015**, *151*, 423–428.
  54. Li H.; Li J.; Yang, Z.; Xu Q.; Hu, X. *Anal. Chem.* **2011**, *83*, 5290-5295.
  55. Kaushik A.; Solanki P.R.; Ansari A.A.; Malhotrab B.D.; Ahmad S. *Biochem. Engin. J.* **2009**, *46*, 132–140.
  56. Musameh M.; Notivoli M.R.; Hickey M.; Kyratzis I.L.; Gao Y.; Huynh C.; Hawkins S.C. *Adv. Mat.* **2011**, *23*, 906-910.
-



# Chapter 2.

# Objectives



## 2.1 General Objectives

The main objective of this PhD thesis is the development of nanomaterials-based (bio)sensing systems with interest for pesticides and phenolic compounds detection with interest for environmental monitoring.

More in details the objectives can be summarized as following:

### **1. Development of an enzymatic inhibition based system using boron doped diamond electrode (BBDE) as a platform for chlorpyrifos detection.**

- 1.1 Electrochemical characterization of BBDE.
- 1.2 Study of the mechanism of detection of the pesticide using BDDE.
- 1.3 Evaluation of the analytic performance of the enzymatic inhibition based system for chlorpyrifos detection.
- 1.4 Pesticide sensing in real samples.

### **2. Development of dual (bio)sensing system for chlorpyrifos and catechol detection using IrOx nanoparticles.**

- 2.1 Morphologic characterization of IrOx Nanoparticles (NPs)
- 2.2 Electrochemical characterization of the implemented system using electrochemical impedance spectroscopy.
- 2.3 Implementation and evaluation of the analytical performance of the system for dual detection of chlorpyrifos and catechol.

### **3 Development of CuO nanoparticles based system for free enzymatic detection of phenolic compounds and pesticide (diuron).**

3.1 Morphologic study of copper oxide (CuO) nanoparticles.

3.2 Electrochemical characterization of the properties of CuO nanoparticles.

3.3 Implementation and evaluation of analytical performance of free enzymatic sensing system based on CuO nanoparticles for detection of phenolic compounds and pesticides (diuron).





## Chapter 3

# Magnetic Enzymatic Platform for Organophosphate Pesticide Detection Using Boron-doped Diamond Electrodes

Related publication

---

Flavio Pino, Tribidasari A. Ivandini, Kazuya Nakata, Akira Fujishima, Arben Merkoçi, and Yasuaki Einaga. **Analytical Sciences** 2015 In press

---



## Magnetic Enzymatic Platform for Organophosphate Pesticide Detection Using Boron-doped Diamond Electrodes

### 3.1 INTRODUCTION

Electrochemical transducer systems based on acetylcholinesterase (AChE) are particularly promising for pesticide detections due to more advantages being offered compared to chromatography<sup>1-3</sup> or electrophoresis methods.<sup>4,5</sup> AChE is a well-known key enzyme in many important areas, such as neurobiology, toxicology and pharmacology, since AChE catalyzes the hydrolysis of acetylthiocholine to thiocholine.<sup>6</sup> It is also known that different types of pollutants, especially various types of pesticides, like organophosphorus, carbamates and organochlorine, inhibit the enzymatic reactions of AChE.<sup>6-8</sup> Their derivatives are harmful compounds found in insecticides, pesticides and chemical-warfare agents.<sup>2,9,10</sup> Taking advantage of the inhibition behavior of pesticide, a pesticide sensor could be developed by monitoring the enzymatic activity during the reaction of acetylthiocholine/thiocholine.<sup>8,9,11-13</sup>

Meanwhile, colorimetric and spectrophotometric are the standard methods used to detect thiocholine.<sup>14-16</sup> However, those methods require some chemicals to generate color<sup>14,15</sup> or fluorescent products,<sup>16</sup> which is less favorable compared to an easy and economic detection system based on the electrochemical oxidation of thiocholine at solid electrodes.<sup>9,17-25</sup> Accordingly, direct detections of thiocholine using different types of solid electrodes were developed, including at gold<sup>17-19</sup> and platinum-based<sup>20</sup> electrodes. The use of carbon-based electrodes was also reported, including graphite paste,<sup>21</sup> screen-printed carbon electrodes,<sup>22,23</sup> and carbon nanotubes combined with other solid electrode.<sup>9</sup> However, generally the use of some mediators, such as 7,7,8,8-tetracyanoquinonodimethane,<sup>21,22</sup> cobalt (II) phthalocyanine,<sup>23</sup> and prussian blue,<sup>24,25</sup> to improve the kinetic reaction was also been documented.

On the other hand, boron-doped diamond (BDD) electrodes are established as superior electrodes among other solid electrodes due to their wide potential windows, low background currents and excellent stability regarding physical and chemical properties.<sup>26</sup>

Moreover, the biocompatibility is also satisfactory.<sup>27</sup> The applications of BDD electrodes as detectors and sensors for some important materials have been reported.<sup>26-29</sup> However, it is very rare that enzymatic systems have been developed using BDD electrodes, since it is difficult to perform chemical modifications, such as enzyme immobilization, at a BDD surface.<sup>26</sup> In this work, the electrochemical detection of chlorpyrifos (CPF), as a model of organophosphorus pesticides, was developed based on thiocholine oxidation at bare BDD electrodes. AChE was used to generate thiocholine through the enzymatic hydrolysis of acetylthiocholine. Acetylcholine chloride (AT-Cl) was found to produce a more selective oxidation peak potential of thiocholine than acetylthiocholine iodide (AT-I). Furthermore, the extraordinary property of a collection of magnetic beads<sup>30-33</sup> was utilized to immobilize AChE at a BDD surface. Then, the inhibition effect by CPF in AChE activity was used as a signal.

Meanwhile, the immobilization of AChE on magnetic beads has already been documented based on the adsorption,<sup>31</sup> nickel-histidine affinity,<sup>32</sup> and covalent coupling using glutaraldehyde.<sup>33</sup> In this work, streptavidin-biotin interaction was used to perform self-assembly AChE immobilization on the magnetic beads. A selective and sensitive detection of CPF injected in tap water was successfully demonstrated. High stability of the current responses and a very low limit of detection (LOD) can be achieved. The results suggested that the combination of using magnetic beads with the superior properties of bare BDD electrodes is suitable for organophosphorous pesticide detection, especially CPF.

## 3.2 Experimental section

### 3.2.1 Reagent and Solution

Acetylcholinesterase (AChE, 844 U/mg from electric eel) was purchased from Sigma-Aldrich. The activity was confirmed by monitoring the appearance of thionitrobenzene using a UV/Vis spectrometer at 412 nm, resulting from the reaction of 5,5'-dithiobis(2'-nitrobenzoic acid) (DTNB) with thiocholine produced from the enzymatic hydrolysis of acetylthiocholine by AChE.<sup>32</sup> The magnetic beads were a streptavidin-coupled bead solution (Dynabeads M-280) with a bead diameter of 2.80  $\mu\text{m}$ , purchased from Invitrogen AG (Basel, Switzerland). The stock concentration of Dynabeads M-280 is 10 mg ( $6-7 \times 10^{-8}$  Dynabeads particles) per mL. Sulfo-NHS-biotin was supplied by Pierce.

Acetylthiocholine iodide (AT-I), acetylthiocholine chloride (AT-Cl), Tris-HCl, bovine serum albumin (BSA), chlorpyrifos (CPF), nonionic surfactant Tween-20 (product No. 167-11515) and other chemicals were supplied by Wako, Japan.

### 3.2.2 Electrode preparation

BDD thin films were deposited on Si(111) wafers in a microwave plasma chemical vapor deposition system (Cornes Technology). Acetone was used as a carbon source, whereas trimethoxyborane was used as a boron source with a 1% B/C ratio. The details of the preparation are described elsewhere.<sup>26</sup> The surface morphology and the crystalline structure of the films characterized using a scanning electronic microscope (SEM) showed a polycrystalline diamond grain size of ~5  $\mu\text{m}$  with ~13  $\mu\text{m}$  thickness. Raman spectroscopy showed a peak at ~1300  $\text{cm}^{-1}$  attributable to the  $\text{sp}^3$  hybridization of diamond. The absence of a peak at ~1600  $\text{cm}^{-1}$  suggested a fine quality of the diamond films.<sup>26</sup> Prior to use, the BDD film was cleaned by ultrasonication in 2-propanol for 10 min, followed by rinsing with high-purity water. In order to oxidize the surface of BDD, the as-deposited BDD was electrochemically oxidized in 0.1 M  $\text{H}_2\text{SO}_4$  at +3.0 V (vs. Ag/AgCl) for 20 min.<sup>26,34</sup> Characterization with XPS showed that the process increased the O/C ratio of BDD from 0.03 to 0.3.<sup>26</sup>

### 3.2.3 Methods and Procedure

Prior to use, the magnetic beads were cleaned based on a procedure proposed by Dynal Biotech. A volume of 15  $\mu\text{L}$  of the bead solution was homogenized and equilibrated in a vial containing 150  $\mu\text{L}$  of a 50 mM phosphate buffer solution (PBS). The process was repeated three times. Meanwhile, the AChE was modified with biotin according to a procedure proposed by Gao et. al.<sup>13</sup> Briefly, the AChE was reconstituted in PBS and desalted over a PD-10 column equilibrated in PBS. An aliquote of sulfo-NHS-biotin was added into a 2.5 mL solution of 50 mM PBS pH 7.4 containing 75 mU AChE, then conjugated for 60 min at room temperature. Finally, 50  $\mu\text{L}$  biotinylized AChE was added and mixed in a vial of washed magnetic beads, and allowed to undergo a conjugation process for 24 h at 40C to obtain the AChE-modified magnetic beads. Prior to use, the vial was normalized at room temperature, followed by a three-times washing process to

remove any excess of enzyme, and allowed to exist in the form of a suspension in 150  $\mu\text{L}$  PBS before being measured.

### 3.2.4 Electrochemical measurements

The electrochemical experiments were performed in a conventional three-electrode cell system with a BDD film used as a working electrode, an Ag/AgCl electrode as a reference electrode, and a platinum wire as a counter electrode. The volume of the cell was 5 mL. The BDD working electrode along with the conducting silicon substrate was pressed against the bottom of the cell using a Viton O-ring (3 mm diameter). Electrical contact was made through the backside of the silicon by contacting to a brass plate. A piece of magnet bar with a diameter of 3 mm was then placed under the brass plate at the same position as the working electrode. Electrochemical measurements were carried out in 50 mM PBS at ambient temperature using a galvanostat (ALS CHI BAS).

### 3.2.5 Enzymatic Assay

The AChE-modified magnetic beads suspension from the vial was added into a cell that contained 1 mL of CPF in PBS. In order to dissolve CPF, a mixture of methanol and NaOH solution is required. After the optimum inhibition time, 3 mL of acetylthiocholine chloride in PBS was added, and final concentration was adjusted to 1 mM. Cyclic voltammetry was conducted after an optimum contact time between AChE and acetylthiocholine chloride. Schematic steps of the electrochemical measurements of the enzymatic assay are displayed in Fig. 1. The measurements were performed for various concentrations of CPF standard solutions, and repeated three times. The application of a real sample was performed using a Yokohama (Japan) tap-water sample. Prior to analysis, the sample was filtered using a filter paper (Whatmann-41, pore diameter of 20-25  $\mu\text{m}$ ). Then, a volume of 5 mL filtered tap water was injected by a CPF standard solution. A volume of 1 mL of the

CPF-injected sample was then filled into the cell to be treated using the same procedure as the standard solution of CPF for electrochemical measurements.

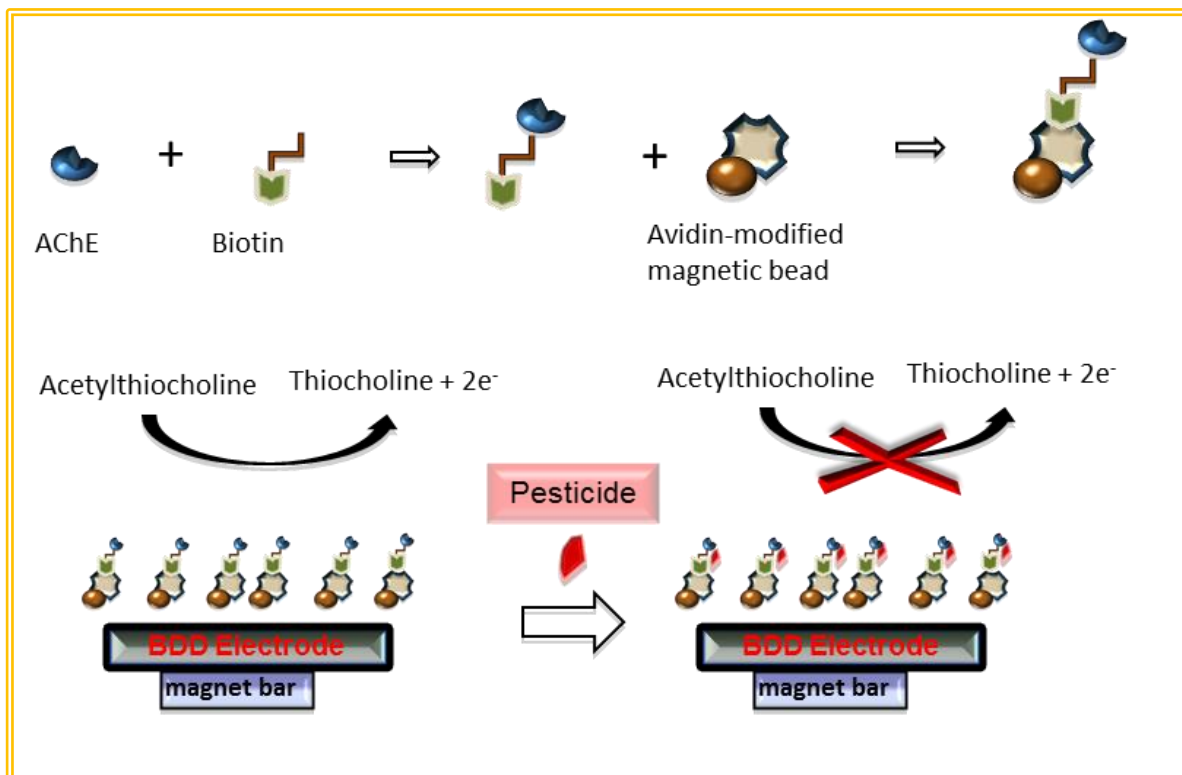


**Figure 1** Schematic illustration of the biotin-avidin complex over the magnetic beads and the magnetic-enzymatic platform system

### 3.3 RESULTS AND DISCUSSION

#### 3.3.1 Electrochemical Characteristic of Thiocholine at BDD electrodes

Figure 2 shows cyclic voltammograms (CVs) performed using BDD electrodes for 0.1 M PBS pH 7.4 in both the absence and the presence of 1 mM AT-I and AT-CI at a BDD electrode. There was no peak observed in the absence of both types of acetylthiocholine in the potential range of -0.5 to +1.5 V (vs. Ag/AgCl). However, when AT-I was added to the system, two well-defined oxidation and reduction peaks were observed at potentials of +1.1 and -0.2 V, respectively (Fig. 2(A)). On the contrary, these peaks did not appear

when AT-I was substituted by AT-Cl (Fig. 2(B)), suggesting that the oxidation and reduction reactions occurred in the system with AT-I only.

It is well known that acetylthiocholine is not electroactive.<sup>9,19</sup> On the other hand, the electrochemical detection of iodide at BDD electrodes was reported by our group,<sup>35</sup> in which two well-defined oxidation peaks and one reduction peak have been observed in the CV of a potassium iodide solution, and were proposed to be attributed to the oxidation and reduction of iodide ions. Meanwhile, evidence of the observable iodide peaks in the CVs of AT-I was also reported to interfere with the thiocholine peaks at screen-printed electrodes.<sup>36</sup>

Taking account of those reports, the oxidation and reduction peaks in Fig. 2(A) could be attributed to the oxidation of iodide ions, which are presented in the system as counter ions of AT-I.

In the presence of AChE, both AT-I and AT-Cl are hydrolyzed to thiocholine, which is known to be electroactive due to its S-H functional groups.<sup>34,37</sup> Figures 2(C) and 2(D) show the CVs of 1 mM AT-I and 1 mM AT-Cl at 5 min contact time after the addition of 25 mU AChE, respectively. The figures show that there was practically no difference between the CVs of AT-I before (Fig. 2(A)) and after (Fig. 2(C)) the addition of 25 mU AChE, although a small increase in the peak current was observed. On the contrary, a well-defined oxidation peak appeared at the potential of +0.8 V in the CV of AT-Cl (Fig. 2 (D)), which indicated that this peak has a strong relation to the presence of thiocholine. This peak cannot be observed in the AT-I system, since it was covered by the onset of iodide oxidation, which appears at around the same potential.<sup>35</sup> Considering that the current of the thiocholine oxidation peak was relatively small in comparison to those of iodide oxidation, and therefore was predicted to be decomposed in the presence of iodide ions, AT-Cl was then used for the next experiments.

A comparison was also performed with the oxidation peak of thiocholine at glassy carbon electrodes, as shown in the inset of Fig. 2(D). Although a similar oxidation potential as well as current were observed at both the glassy carbon and BDD electrodes, a lower



background current of the BDD electrode results in about a order higher signal-to-background ratio of the current, which generally leads to better limits of detection.<sup>26</sup>

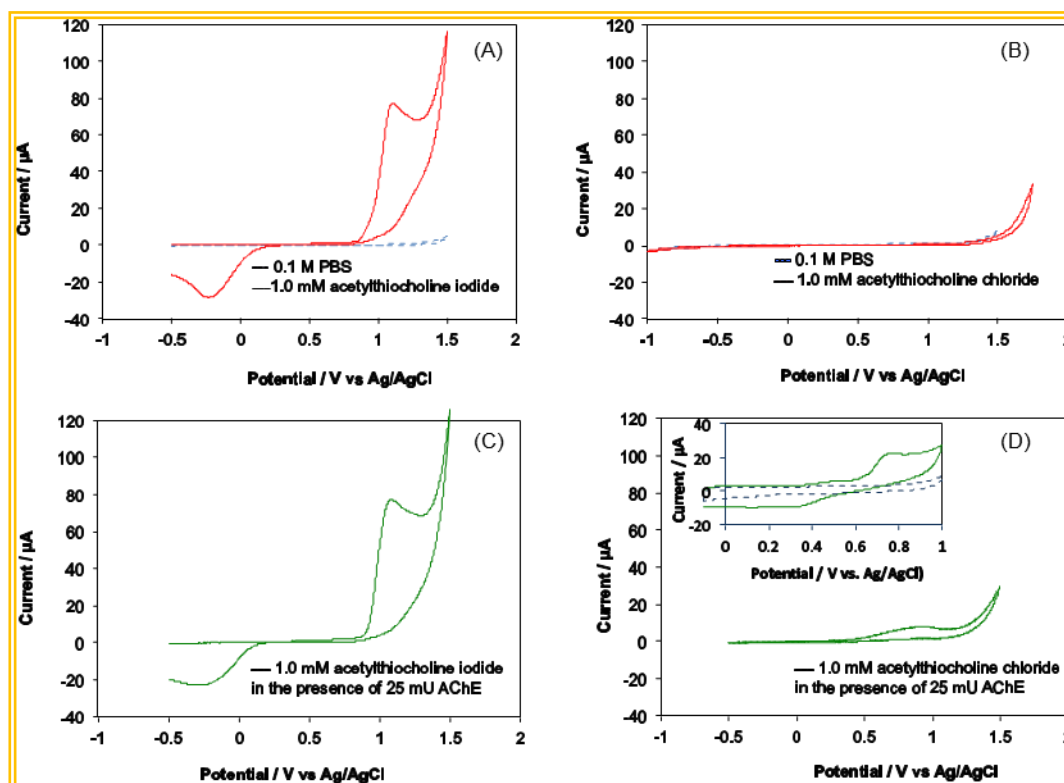
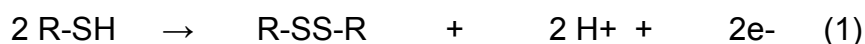


**Figure 2** Voltammograms performed for 1 mM acetylthiocholine iodide in 0.1 M PBS pH 7.4 in the absence of AChE, and at the 5th min after the addition of 50 mU AChE at (A) AD-BDD and (B) AO-BDD electrodes. Scan rate was 100 mV/s.

Evidence of the oxidation peak at around +0.8 V at neutral pH is in agreement to the oxidation of the -S-H functional group at BDD electrodes, as reported by Terashima et. al.<sup>34</sup> Based on this report, it is predicted that the -S-H bond was oxidized to be the S-S functional group, as follows:



The oxidation can continue to -S-O-S- at the higher potential. However, in this work we limited the measurements at +1.5 V and used the peak at +0.8 V for the following experiments.

The peak current at +0.8 V increases with the contact time between AT-I and AChE, then reaches the maximum currents after 30 min (Figs. 3(A) and 3(B)). Therefore, a contact time of 30 min was fixed for the next experiments. Furthermore, using 1 mM AT-Cl as the substrate, the oxidation peak currents at +0.9 V were linear ( $R^2 = 0.99$ ) in the AChE activity range from 5 mU to 30 mU (Figs. 3(C) and 3(D)). The results suggested that this system is promising to be utilized to monitor the activity of AChE.

The dependence of the peak current of thiocholine on the scan rate was also investigated from the scan rate of 5 to 400 mV/s. A linearity ( $R^2 = 0.99$ ) to the square root of the scan rate was achieved, suggesting that the oxidation mechanism was under diffusion control.

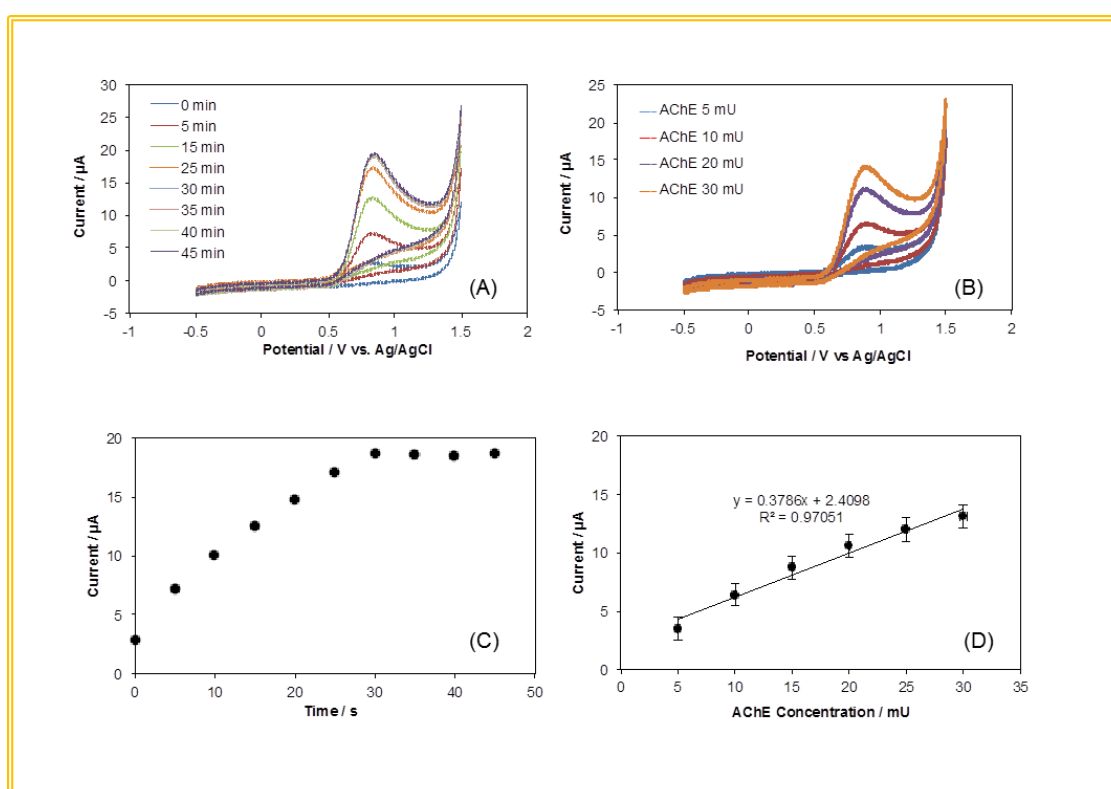


**Figure 3** Cyclic voltammograms performed for 1 mM acetylthiocholine chloride in 0.1 M PBS pH 7.4 (a) at the various contact times with 25 mU AChE and (b) at 30 min after the addition of various concentrations of AChE. Figures (c) and (d) show plots of the dependence of peak currents on the contact times and the AChE concentrations. Other conditions were similar to Fig. 2.

Basically, the enzymatic assay was performed using an inhibition reaction of AChE by organophosphorus compounds. Since organophosphorus compounds have very similar molecule structures with acetylthiocholine, they can irreversibly bind to the active site of AChE through the phosphorylation adduct.<sup>36</sup> In order to avoid any competition between

acetylthiocholine and CPF to react with AChE in this sensor, AT-CI needs to be added after the inhibition reaction of CPF to AChE is completed. Furthermore, since this reaction involves enzymatic activity, it is important to control the pH. Accordingly, the oxidation current of thiocholine was investigated at different pH values in the presence of CPF. Solutions of 1 mM CPF with different pHs were conjugated to 25 mU AChE for 10 min, then, an AT-CI solution was added into the solution. The final concentration of AT-CI was adjusted to 1 mM and voltammetry was performed after 30 min contact. Fig. 4(A) shows plots of the peak currents at a potential of + 0.8 V.

The presence of CPF decreases the peak current of thiocholine oxidation, since CPF inhibits the AChE activity. The maximum decrease occurred at pH 7.4, and remained the same when the pH was continually decreased to 7.0. Therefore, pH 7.4 was selected for the condition of the following experiments.

Further, the influence of the inhibition time of AChE by CPF was investigated. A solution series of 1 mM CPF was conjugated to 25 mU AChE in 0.1 M PBS pH 7.4 for various inhibition times of from 0 to 25 min. Then, AT-CI was added and cyclic voltammetry was conducted. Fig. 4(B) shows that increasing the inhibition time by CPF resulted in a decrease of the oxidation peak current at +0.8 V. As the decrease reached its maximum after 15 min, the inhibition time of 15 min was fixed for the next experiments.

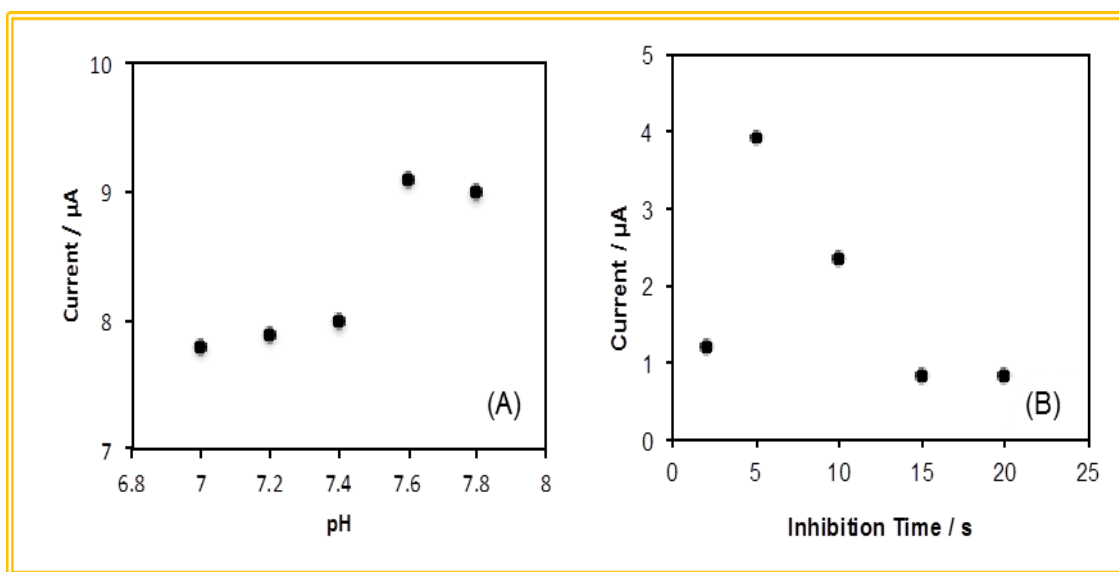


**Figure 3** Dependence of the peak currents at +0.8 V extracted from cyclic voltammograms of 1 mM acetylthiocholine chloride in 0.1 M PBS at (a) various pH after the inhibition time of 10 min and (b) in various inhibition times to AChE at pH 7.4.

Concentrations of 25 mU AChE and 1 mM CPF were used. Other conditions were similar to Fig. 2.

### 3.3.2 Modification of magnetic beads with AChE

Modification of the magnetic beads was performed using a specific interaction between streptavidin and biotin. Streptavidin-modified magnetic beads supplied from Invitrogen AG (Basel, Switzerland) were used, whereas the AChE was an in-house modified with biotin to provide the attachment of AChE on the magnetic beads. Sulfo-NHS biotin was used to perform biotinylated AChE. Then, biotinylated AChE was conjugated to the magnetic beads. The steps involved in the assembly of the structure of the enzymatic assay for the determination of CPF are shown in Fig. 1. Since streptavidin is a tetrameric protein in which each sub unit binds to one molecule of biotin,<sup>13</sup> larger capacities of streptavidin than biotin allow the immobilization of biotinyl AChE on the surface of magnetic beads. An amount of 15  $\mu$ L of the magnetic bead suspensions is expected to cover the active site for 75 mU of biotinylated AChE. However, problems related to unspecific sites need to be considered, including the unspecific sites of the magnetic beads that was not covered by AChE, and the surface of sulfo-NHS-biotinyl-streptavidin at the magnetic beads as the result of the reaction between sulfo-NHS-biotin with magnetic beads. In order to cover the unspecific sites, BSA was then added.

Prior to measurements, a method was examined for measuring 1 mM CPF using unmodified magnetic beads (without AChE) at 30 min after the addition of AT-Cl, as shown in Fig. 5(A). Another measurement of 1 mM using AChE-modified magnetic beads without the addition of AT-Cl in the solutions was also tested, as shown in Fig. 5(B). Two very small oxidation peaks at potentials of around +0.3 V and +0.6 V are shown in the CVs of both tests. Theoretically, there is no thiocholine peak that will be generated at the system in the absence of AChE or AT-Cl. It was previously reported that Bovine Serum Albumin (BSA) are electroactive at hydrogen terminated BDD but not at oxidized terminated BDD electrodes.<sup>38</sup> Since the oxidized terminated one was employed in this work, it can be presumed that the oxidation peaks that appeared at the CVs were related to the oxidation

of biotin-streptavidin systems. Furthermore, these peaks appeared at different potentials with very small currents in comparison with the thiocholine peak. Therefore, these peaks can be ignored, and the system can be considered to be suitable for the detection of CPF.

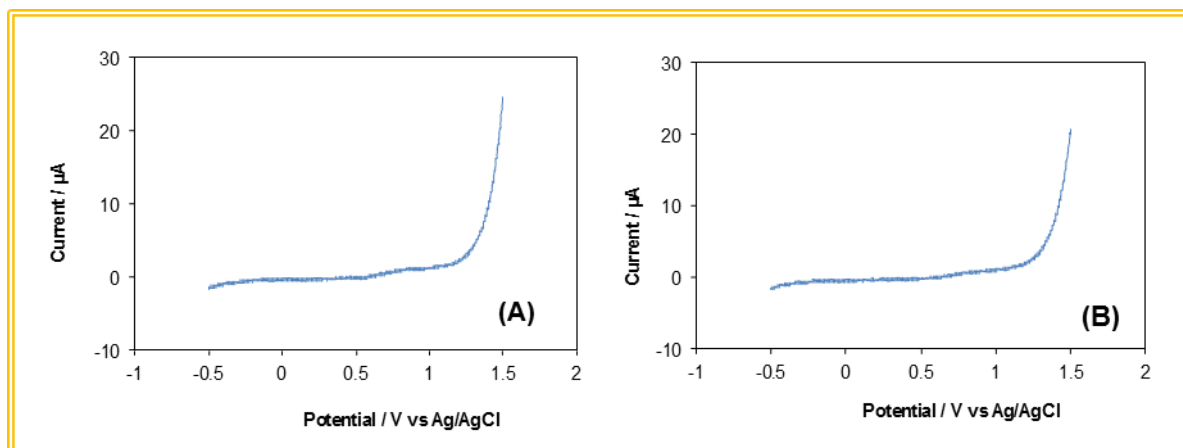


**Figure 5** Linear-sweep voltammograms performed in the system of 1mM CPF in 0.1 M PBS pH 7.4 (a) with unmodified magnetic beads at 15 min after the addition 1 mM acetylthiocholine chloride and (b) with AChE-modified magnetic beads without the presence of acetylthiocholine chloride (b). Scan rate was 100 mV/s.

### 3.3.3 Application of AChE-modified magnetic beads in Chlorpyrifos Sensors

The AChE-modified magnetic beads were then applied for electrochemical sensors of CPF. A comparison was made with the system with free AChE. Figure 6 shows typical CVs resulted from those systems with free AChE (Fig. 6(A)) and with immobilized AChE at magnetic beads (Fig. 6(B)) in the presence of various concentrations of CPF. The same number of enzyme activity, i.e. 25 mU, and the same concentration of AT-Cl, i.e. 1 mM, were employed. In the CVs of both systems, a well-defined peak was observed at around +0.7 V. This peak potential is slightly shifted compared to the thiocholine peak in Figs. 2 and 3 due to the change of the pH, since methanol and NaOH are required to dissolve CPF.

The dependences of the inhibition percentage of AChE to the CPF concentrations are shown in Figs. 6(C) and (D). Good linearity in the CPF concentrations range from  $10^{-9}$  to

$10^{-5}$  M was shown at both systems ( $R^2 > 0.9$ ). However, a slightly higher slope was observed for the system using the magnetic beads. Small error bars shown in these figures, suggested good stability of the current responses, which indicated the stability of the BDD surfaces. Furthermore, the sensor's performance was also examined for 50 and 10% AChE inhibition ( $IC_{50}$  and  $IC_{10}$ , respectively).<sup>40</sup> About one order lower  $IC_{50}$  and  $IC_{10}$  can be achieved using a system with immobilized AChE.

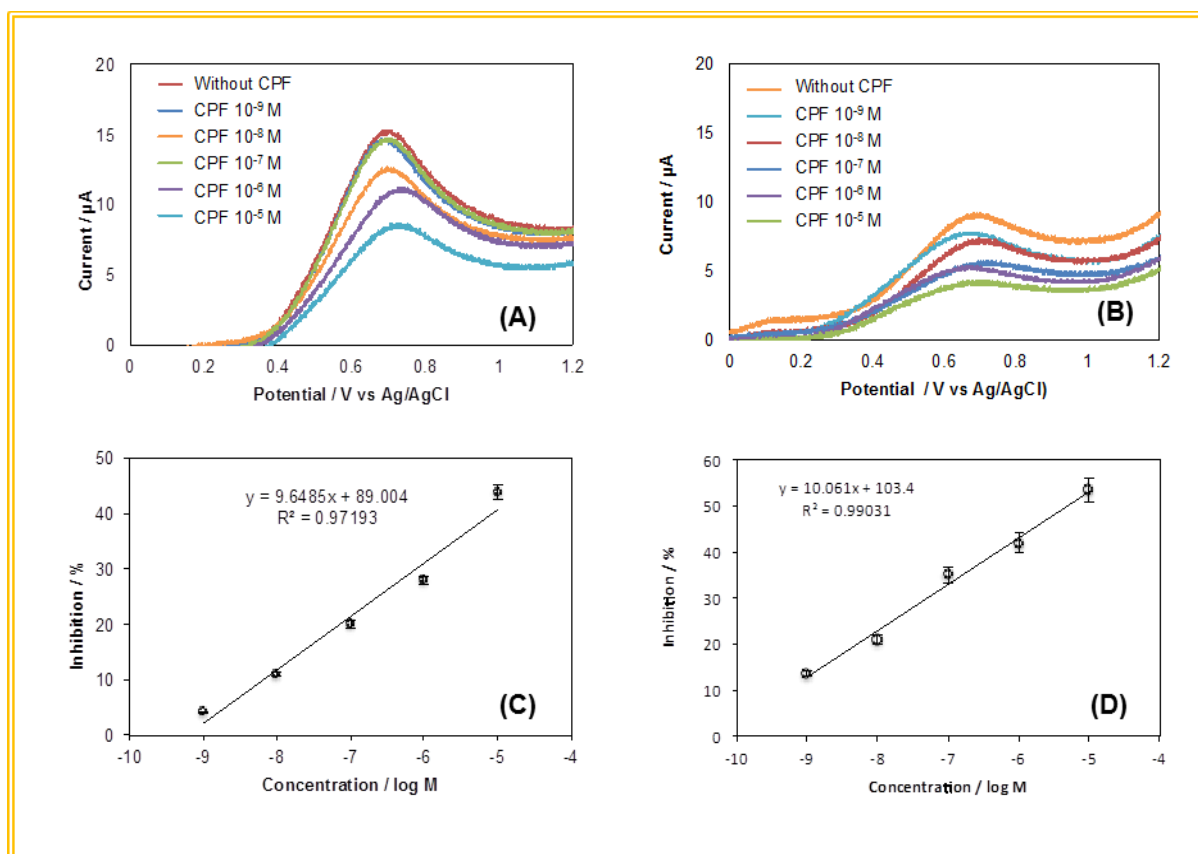


**Figure 6** Linear sweep voltammograms performed for 1 mM acetylthiocholine chloride in 0.1 M PBS pH 7.4 at 15 min after being added in various concentrations of CPF conjugated to (a) free AChE in the solutions and (b) immobilized AChE at 15  $\mu$ L magnetic beads.

The limits of detection (LODs) were then estimated using  $IC_{10}$ , which showed LOD values of  $6.5 \times 10^{-9}$  and  $5.7 \times 10^{-10}$  M for free and immobilized AChE, respectively. The results suggested that the immobilization of AChE at magnetic beads system provides better performance in the measurements of CPF. A summary of the analytical performance is displayed in Table 1.

**Table 1** Performance of the CPF detection using free and immobilized AChE at magnetic beads using BDD electrodes.

	Free AChE	Immobilized AChE
CPF Concentration Range	$10^{-9}$ to $10^{-5}$ M	$10^{-9}$ to $10^{-5}$ M
Linear Equation	$y = 9.65 x + 89$ ( $R^2 = 0.97$ )	$y = 10.06 x + 103.4$ ( $R^2 = 0.99$ )
IC <sub>50</sub>	$9.1 \times 10^{-5}$ M	$5.4 \times 10^{-6}$ M
IC <sub>10</sub>	$6.5 \times 10^{-9}$ M	$5.7 \times 10^{-10}$ M
RSD (n=3)	9.7 %	7.7 %

These LODs are also comparable to other reported detection methods based on thiocholine (Table 2), considering that the system applied by cyclic voltammetry instead of amperometry.<sup>17,18,22,25,39-43</sup> The AChE-modified magnetic beads could be stored in 4°C for 30 days with less than a 5% change of the current response.

However, the recovery of the magnetic beads (ex. using a microfluidic system) for repetitive measurements is an important aspect to be considered in the future.<sup>25</sup>

**Table 1** Performance of the CPF detection using free and immobilized AChE at magnetic beads using BDD electrodes.

Electrode	Immobilization Support	Linearity / M	LOD / M	Ref. No.
Bare BDD	Magnetic beads	$10^{-9}$ to $10^{-5}$	$5.7 \times 10^{-10}$	This work
CNT-SPE	Strip test	$5 \times 10^{-11}$ to $10^{-8}$	$2 \times 10^{-11}$	39
CNT-GC	7,7,8,8-tetracyanoquinodimethan	Not clear	$4 \times 10^{-10}$	22
SPE	PEDOT	Not clear	$4 \times 10^{-9}$	40
Au-BDD	Carbon nanopshere	$10^{-11}$ to $10^{-7}$	$4.9 \times 10^{-13}$	19
Au-GC	Chitosan	$4 \times 10^{-10}$ to $8 \times 10^{-8}$	$2.8 \times 10^{10}$	41
CNT-Au	Chitosan/Prussian Blue	$5 \times 10^{-11}$ to $7.5 \times 10^{-9}$	$5 \times 10^{-11}$	25
MWCNT-Au	Fe <sub>3</sub> O <sub>4</sub>	$10^{-10}$ to $5 \times 10^{-8}$	$1 \times 10^{-10}$	42
Au	ZnS and poly(indole-5-carboxylic acid)	$1.5 \times 10^{-9}$ to $4 \times 10^{-10}$	$1.5 \times 10^{-9}$	17
Au	PANI/CNT wrapped with ssDNA	$10^{-11}$ to $10^{-6}$	$1 \times 10^{-12}$	18
Pt-Graphene-GC	Tyr	$7.1 \times 10^{-10}$ to $2.9 \times 10^{-8}$	$5.7 \times 10^{-10}$	43

### 3.3.4 Analysis of chlorpyrifos in tap water

In order to study the interference effect, Yokohama (Japan) Tap Water spiked with CPF was selected as a model sample. The tap water, according to Yokohama Waterworks

Bureau, can be used as drinking water. The water is well controlled and its quality information is available to be accessed by public with a pH of 6.99 and contains in ppm of 0.04 Al, - Ca, 6.5 Cl<sup>-</sup>, 0.01 Fe, 49 Mg, and 1.17 NO<sub>3</sub><sup>-</sup>. Negative contents of Cu, As, Zn, Cr, and Pb have been reported. While Ca<sup>2+</sup>, Cl<sup>-</sup>, and NO<sub>3</sub><sup>-</sup> ions are known not to be electroactive, Al, Fe, and Mg was found to have oxidation-reduction potentials far from +0.8 V (vs. Ag/AgCl).<sup>26</sup> Therefore, the interference was expected to come from the inhibition of AChE by these compounds.

The CPF-injected tap water solutions of 10<sup>-7</sup> and 10<sup>-6</sup> M were measured using systems with free and immobilized AChE. While the free AChE systems showed that the interference of tap water increases the signals, the immobilized AChE systems showed a better recovery of the measurements. Apparently, the accumulation of AChE immobilized at magnetic beads at the surface of BDD limits the interference of some metals to AChE. It is well known that activity of AChE decreases with the presence of metals.<sup>6-8</sup>

The results suggested that the detection of CPF based on thiocholine oxidation using an AChE-modified BDD electrode using a magnetic platform is more selective and suitable at BDD electrodes. A summary of the detection of CPF injected in Yokohama Tap Water is displayed in Table 3.

**Table 3** *The measurements of % recoveries of CPF injected in Yokohama Tap Water using free and Immobilized AChE at magnetic beads*

Chlorpyrifos Added / M	Free AChE		Immobilized AChE	
	Found / M	% recovery	Found / M	% recovery
1.00 x 10 <sup>-7</sup>	1.28 x 10 <sup>-7</sup>	128 ± 18	9.8 x 10 <sup>-8</sup>	98 ± 5
1.00 x 10 <sup>-6</sup>	1.09 x 10 <sup>-8</sup>	109 ± 9	8.8 x 10 <sup>-8</sup>	88 ± 7



### 3.4 Conclusion

Detection of chlorpyrifos (CPF) based on thiocholine oxidation using acetylcholinesterase (AChE) immobilized at magnetic beads has been successfully performed at boron-doped diamond (BDD) electrodes. Good linearity of the current responses was demonstrated. Very low limit of detection ( $3.10 \times 10^{-10}$  M) as well as low interference in the direct detection of CPF injected in tap water solution could be obtained using anodically oxidized (AO) BDD. In addition, the system with immobilized AChE at magnetic beads provided a better limit detection compare to that of free enzyme. It can be previewed that the developed pesticide detection system can be implemented easily in (micro) fluidic measurements for on-line monitoring as well and can be extended to several other analytes with interest for environment, health and safety, and security field

### 3.5 Bibliography

1. Aragay G.; Pino F.; Merkoci A. *Chem. Rev.* **2012**, 112, 5317-5338.
2. Dirtu A.C.; Van den Eede N.; Malarvannan G.; Ionas A.C.; Covaci A. *Anal. Bioanal. Chem.* **2012**, 404, 2555-2581.
3. Ye J.; Zhao M.; Liu J.; Liu W. *Env. Pollution* **2010**, 158, 2371-2383.
4. Wang J.; Chatrathi M.P.; Mulchandani A.; Chen W. *Anal. Chem.* **2001**, 73, 1804-1808.
5. Wang J.; Pumera M.; Chatrathi M.P.; Escarpa A.; Musameh M.; Collins G.; Muchandani A.; Lin Y.; Olsen K. *Anal. Chem.* **2002**, 74, 1187-1191.
6. Racchi M.; Mazzucchelli M.; Porrello E.; Lanni C.; Govoni S. *Pharmacol. Res.* **2004**, 50, 441-451.
7. Nenner M. *Arch. Toxicol.* **1973**, 30, 87-94.
8. Pundir C.S.; Chauhan N. *Anal. Biochem.* **2012**, 429, 19-31.
9. Liu G.C.; Riechers S.L.; Mellen M.C.; Lin Y.H. *Electrochem. Commun.* **2005**, 7, 1163-1169.
10. Kim K.; Tsay O.G.; Atwood D.A.; Churchill D.G. *Chem. Rev.* **2011**, 111, 5345-5403.
11. Periasamy A.P.; Umasankar Y.; Chen S-M. *Sensors* **2009**, 9, 4034-4055.
12. Booth L.H.; Hodge S.; O'Halloran K. *Bull. Environ. Contam. Toxicol.* **2001**, 67, 633-640.
13. Gao Y.; Kyratzis I.; Taylor R.; Huynh C.; Hickey M. *Anal. Lett.* **2009**, 42, 2711-2727.
14. Yamada M.; Marui Y.; Hayashi C.; Miki Y.; Takemura S. *Clin. Chem.* **2001**, 47, 1962-1966.
15. Dietz A.; Rubinstein H.; Lubrano T. *Clin. Chem.* **1973**, 19, 1309-1313.
16. Parvari R.; Pecht I.; Soreq H. *Anal. Biochem.* **1983**, 133, 450-456.
17. Chauhan N.; Narang J.; S. Pundir C. *Biosens. Bioelectron.*, **2011**, 29, 82-88.
18. Viswanathan R.; Radecka H.; Radecki J. *Biosens. Bioelectron.* **2009**, 24, 2772-2777.
19. Wei M.; Zeng G.; Lu Q. *Microchim. Acta* **2014**, 181, 121-127.
20. Gruss R.; Scheller F.; Shao M.J.; Liu C.C. *Anal. Lett.* **1989**, 222, 1159-1169
21. Martorell D.; Cespedes F.; Martinez-Fabregas E.; Alegret S., *Anal. Chim. Acta* **1997**, 337, 305-313.
22. Hart J.P.; Hartley I.C. *Analyst* **1994**, 119, 259-263.
23. Rotariu L.; Zamfir L. G.; Bala C. *Anal. Chim. Acta* **2012**, 748, 81-88.
24. Ricci F.; Arduini F.; Amine A.; Moscone D.; Palleschi G. *J. Electroanal. Chem.* **2004**, 563, 229-237.

25. Zhai C.; Sun X.; Zhao W. P.; Gong Z. L.; Wang X. Y. *Biosens. Bioelectron.* **2013**, *42*, 124-130.
26. Fujishima A.; Einaga Y.; Rao T.N.; Tryk D.A. ed. *Diamond Electrochemistry BKC-Elsevier*, Tokyo, **2005**.
27. Ivandini T.A., Saepudin E.; Wardah H. Harmesa H.; Dewangga N.; Einaga Y. *Anal. Chem.* **2012**, *84*, 9825-9832.
28. Wahyuni W. T.; Ivandini T. A.; Jiwanti P. K.; Saepudin E.; Gunlazuardi J.; Einaga Y. *Electrochemistry* **2015**, *83*, 357-362.
29. Ishii Y.; Ivandini T. A.; Murata K.; Einaga Y. *Anal. Chem.* **2013**, *85*, 4284-4288.
30. Wang J.; Musameh M.; Laochareoensuk R. *Electrochem. Commun.* **2005**, *7*, 652-656.
31. Llopis X.; Pumera M.; Alegret S.; Merkoçi A. *Lab Chip* **2009**, *9*, 213-218.
32. Istamboulie G.; Andreescu S.; Marty J. L.; Noguer T. *Biosens. Bioelectron.* **2007**, *23*, 506-512.
33. Oujji N. B.; Bakas I.; Istamboulie G.; Ait-Ichou I.; Ait-Addi E.; Rouillon R.; Noguer T. *Sensors* **2012**, *12*, 7893-7904.
34. Terashima C.; Rao T. N.; Sarada B. V.; Kubota Y.; Fujishima A.; *Anal. Chem.* **2003**, *75*, 1564-1572.
35. Fierro S.; Comninellis C.; Einaga Y. *Talanta* **2013**, *103*, 33-37.
36. Bucur M.-P.; Bucur B.; and Radu G.-L. *Sensors* **2013**, *13*, 1603-1613.
37. Chailapakul O.; Siangproh W.; Sarada B. V.; Terashima C.; Rao T. N.; Tryk D. A.; Fujishima, A. *Analyst* **2002**, *127*, 1164-1168.
38. Chiku M.; Ivandini T. A.; Kamiya A.; Fujishima A.; Einaga Y. *J. Electroanal. Chem.* **2008**, *612*, 201-207.
39. Du D.; Wang J.; Wang L. M. *Anal. Chem.* **2012**, *84*, 1380-1385.
40. Istamboulie G., Sikora T., Jubete E., Ochoteco E., Marty J. L., and Noguer T., *Talanta* **2010**, *82*, 957-961.
41. Sun X.; Zhai C.; Wang X. Y.; *IEEE Sens. J.* **2013**, *13*, 172-179.
42. Chauhan N.; Pundir C. S. *Anal. Chim. Acta* **2011** *701*, 66-74.
43. Liu T.; Xu M. R.; Yin H. S.; Ai S. Y.; Qu X. J.; Zong S. S. *Microchim. Acta* **2011**, *175*, 129-135.



# Chapter 4

## Electrochemical detection of phenol compound and pesticide using IrOx nanoparticles

### Related publication

---

Carmen Mayorga, Flavio Pino, Sevinc Kurbanoglua, Lourdes Rivas, Sibel A Ozkan and Arben Merkoçi . Journal of Materials Chemistry B, **2014**, 2, 2233-2239

---



## Electrochemical detection of phenol compounds and pesticide using IrOx nanoparticles.

### 4.1 Introduction

Environmental pollution control technology has a great demand for detection and screening systems. Moreover, analytical systems are highly requested for the dual detection of different pollutants using the same platform. Among all pollutant compounds, organophosphate pesticide (OP) and phenol compounds are the most toxic and dangerous ones for human being.<sup>1,2</sup>

It is well known that pesticide and phenol compounds possess high acute toxicity. For instance, chlorpyrifos (CPF), one of the most widely used OP, interferes with brain development in part due to alterations in the activity of transcription factors involved in the basal machinery of cell replication and differentiation<sup>3</sup> and phenol is potential human carcinogen and is of considerable health concern, even at low levels.<sup>4</sup>

Pesticides are extensively used in farming and domestic purposes.<sup>5</sup> Phenol compounds have limited use in industry process for different purposes.<sup>6</sup> In fact, everyday those compounds are easily released in different water systems affecting the ecosystem.

Nowadays, the detection of pesticides and phenol compounds is performed using large and expensive automated analysers such as liquid chromatography coupled with mass spectroscopy<sup>7,8</sup> and high pressure liquid chromatography.<sup>9,10</sup>

These techniques reach low limit of detection and high reproducibility but involve extraction of large volumes of water, require extensive purification and expensive equipment. Therefore, there is a high demand to obtain simple analytical devices and related nanomaterials for the detection of the mentioned hazard compounds in environment and health related samples.

The main prospective of the future detection systems are to be cheap, reliable, easy to be used and disposable. At the same time, it would be necessary to have devices that can detect different family of pollutants.

Currently different approaches for the detection of pesticides, including immunoassay<sup>11</sup> and enzymatic activity<sup>12</sup> have been developed. Enzymatic biosensors are the most reliable for this type of analysis due to their simplicity, efficiency and their easy usage. In fact, numerous biosensors about using inhibition-based enzymatic systems in particularly those based on the inhibition of AChE<sup>13, 14</sup> have been reported. Furthermore, tyrosinase (Tyr) was used for phenolic compound detection and based on the inhibition of this enzyme few pesticide detections have been reported.<sup>15, 16</sup>

The advantage of the Tyr based electrochemical biosensor is its achieved selectivity due to the fact that the effect of interfering species such as other electroactive compounds is low given its low working potential (-0.2V or less)<sup>17-19</sup> in comparison to acetyl cholinesterase (AChE) and free mediators based biosystems that mostly use to work at 0.6 V.<sup>20</sup>

Meanwhile, the request for a disposable analytical platform could be reached through the use of micro-transducers like screen printed carbon electrode (SPCE). In fact in the last twenty years, the application of these devices for in-situ and user-friendly measurements is significantly increased.

The key factor in an enzymatic micro-device platform is the immobilization procedure of the enzyme. This process is usually performed in different ways; adsorption, entrapment and cross –linking are the most reported. The main-objective of the enzyme immobilization alternatives has always been the increase of the biosensor stability and its reproducibility being fouling of the working electrode surface the most important drawback to overcome.<sup>21, 22</sup>

The explosion in nanomaterials research, especially nanoparticles, has influence also the research, in the field of enzymatic biosensor.<sup>23, 24</sup> The connection of enzymatic systems with nanoparticles has a high impact on improving the performance of the platform used for detection of toxic compounds. This is due to the unique, chemical, physical and electronic properties at nanoscale effect possessed by nanoparticles (normally in the range of 1 – 100 nm).<sup>25, 26</sup>

Iridium oxide (IrOx) films have been used in biosensors as electrodes (enzymes can be immobilized) due to their high conductivity.<sup>27</sup> Furthermore, IrOx nanoparticles, as new



emerging metal nanoparticles, possess useful electronic and conductivity switching properties which make them highly attractive for biosensors development as well.<sup>28</sup>

In the present study, an enzymatic biosensor for dual detection of two different pollutants, catechol (a phenol derivate) and chlorpyrifos (an organophosphate pesticide) is proposed. Such sensing is achieved through a SPCE modified with IrOx NPs and Tyrosinase. The proposed biosensor reports improvement in the limit of detection (0.08  $\mu\text{M}$ ) and sensitivity for catechol compared to previously reported biosensors.

This biosensor shows also low limit of detection (0.003  $\mu\text{M}$ ) for CPF while being used in a tyrosinase inhibition mode operation. Finally the efficiency of this biosensor for real applications in CPF detection in river and tap water was also explored showing great possibilities for future application as a low cost platform for pesticide detection.

## **4.2 Experimental section**

### **4.2.1 Apparatus and electrodes**

Electrochemical experiments were performed using an electrochemical analyzer Autolab 20 (Eco-Chemie, The Netherlands) which was connected to a personal computer using a software package GPS 4.9 (General Purpose Electrochemical System). Impedance measurements were performed by using an Autolab302 potentiostat/galvanostat/frequency-response analyzer PGST30, controlled by GPES/FRA Version 4.9. Scanning electrochemical microscopy (SEM) images were acquired using a Field Emission-Scanning Electron Microscopy (Merlin, Carl Zeiss) and Transmission electron microscope (TEM) images were taken with a JEM-2011(Jeol,Ltd., Japan).

A thermoshaker TS1 (Biometra) was used to stir the samples during inhibition process operating at controlled temperature of 37.5 °C and 350 rpm of shaking.

Homemade screen printed carbon electrodes (SPCEs), were used as the electrochemical transducer which are constituted by three electrodes in a single strip: carbon working

electrode with diameter of 3 mm, Ag/AgCl reference electrode and carbon counter electrode.

### 4.2.2 Reagents and solutions

Tyrosinase from mushroom ( $\geq 1000$  unit/mg), bovine serum albumin (BSA), glutaraldehyde (GA, 25%), chlorpyrifos and catechol were purchased from Sigma-Aldrich (St. Louis, MO). For the synthesis of iridium oxide nanoparticles, potassium hexachloroiridate-(IV), sodium hydrogencitrate, were purchased from Sigma-Aldrich (St. Louis, MO). Milli-Q water was obtained from purification system and all solutions were prepared with ultra-pure water from a Millipore-MilliQ system. All reagents and other inorganic chemicals were supplied by Sigma-Aldrich or Fluka, unless otherwise stated.

### 4.2.3 Synthesis of iridium oxide nanoparticles

Iridium oxide nanoparticles were prepared according to the previously reported procedure.<sup>29</sup> Potassium hexachloroiridate-(IV)  $2.6 \times 10^{-5}$  M solution was mixed with sodium hydrogencitrate  $1.6 \times 10^{-2}$  M solution. The pH of the red brown solution was adjusted to pH 7.5 with a 0.25 M NaOH solution and then refluxed in an oil bath with constant stirring for 30 min. As the mixture cooled to room temperature, the pH was again adjusted to 7.5 with a reflux for 30 min. This procedure was repeated until pH reached a constant value of 7.5. Finally the solution was refluxed 2 h more with oxygen bubbling. At the end of this step, a deep blue solution of IrOx nanoparticles was obtained. The solution was stocked in a glass-stoppered flask and at 4°C when not in use.

### 4.2.4 Preparation and modification of Screen Printed Electrodes

Screen printing electrodes were fabricated by sequential deposition of a graphite ink, Ag/AgCl ink and insulating ink on a polyester substrate. The polyester substrate was dried

---

at 120 °C for 45 min (graphite) and 30 min (Ag/AgCl and insulating) after the deposition of each layer. Before modification, SPCEs were activated at 3  $\mu$ A for 120 sec in 0.1 M H<sub>2</sub>SO<sub>4</sub>. A 5  $\mu$ L solution of IrOx NPs suspension was dropped onto the working surface of SPCE. 0.25 % of gluteraldehyde (GA) was prepared in ultra-pure water and from this solution 5  $\mu$ L was dropped onto the SPCE/IrOx surface. 2  $\mu$ L of the solution of Tyr (1mg/50mL) in BSA 5% (1:1) was dropped onto SPCE/IrOx/GA surface. Tyr and BSA solution were prepared in 0.1 M phosphate buffer at pH 6.5 %. In between all steps, electrodes were allowed to be dried at 37.5 °C for 30 min.

## 4.2.5 Electrochemical measurements

The surface characterization of the modified electrodes was performed by electrochemical impedance spectroscopy (EIS) studies in 1mM [Fe(CN)<sub>6</sub>]<sup>3-/4-</sup> with 0.1 M KCl as redox probe. A sinusoidal potential modulation of  $\pm$  50 mV amplitude in the 0.1 Hz to 100 kHz frequency range, with logarithmic scale of 10 points per decade, was superimposed onto the formal potential of the redox couple, [Fe(CN)<sub>6</sub>]<sup>6/4-</sup> (0.24 V vs Ag/AgCl). Nyquist diagrams were also recorded.

Chrono-amperometric measurements were conducted at -200 mV; magnetic stirrer was used to provide the convective transport in 10 mL of 0.1 M phosphate buffer with 0.1 M KCl. Electrochemical experiments were carried out at room temperature.

## 4.3 Results and discussion

### 4.3.1 Morphological studies

Transmission electron microscographs of IrOx NPs were obtained to determine the particle sizes and their homogeneity. Figure 4.1A displays the typical TEM image of the synthesized IrOx nanoparticles (12.5  $\pm$  2.5 nm). Although the dispersion of these nanoparticles was not homogenous in the solution, most of the formed IrOx NPs exhibited special shape. These nanoparticles seem to be cluster of other smaller nanoparticles with diameter around 1.5  $\pm$  0.3 nm.

IrOx NPs were immobilized onto working electrode of SPCE, then glutaraldehyde (GA) was used as cross-linking agent followed by a modification with a solution composed of tyrosinase and BSA. The obtained biosensor was carefully characterized in each of the fabrication step by using optical and electrochemical methods. Figure 4.1B shows a scanning electron microscopy (SEM) image of SPCE. Figure 4.1C displays the distribution of the IrOx NPs onto the working electrode surface of the SPCE and the effect of glutaraldehyde as a binding matrix; finally figure 4.1D shows a good entrapment of the IrOx NPs, glutaraldehyde and Tyrosinase-BSA.

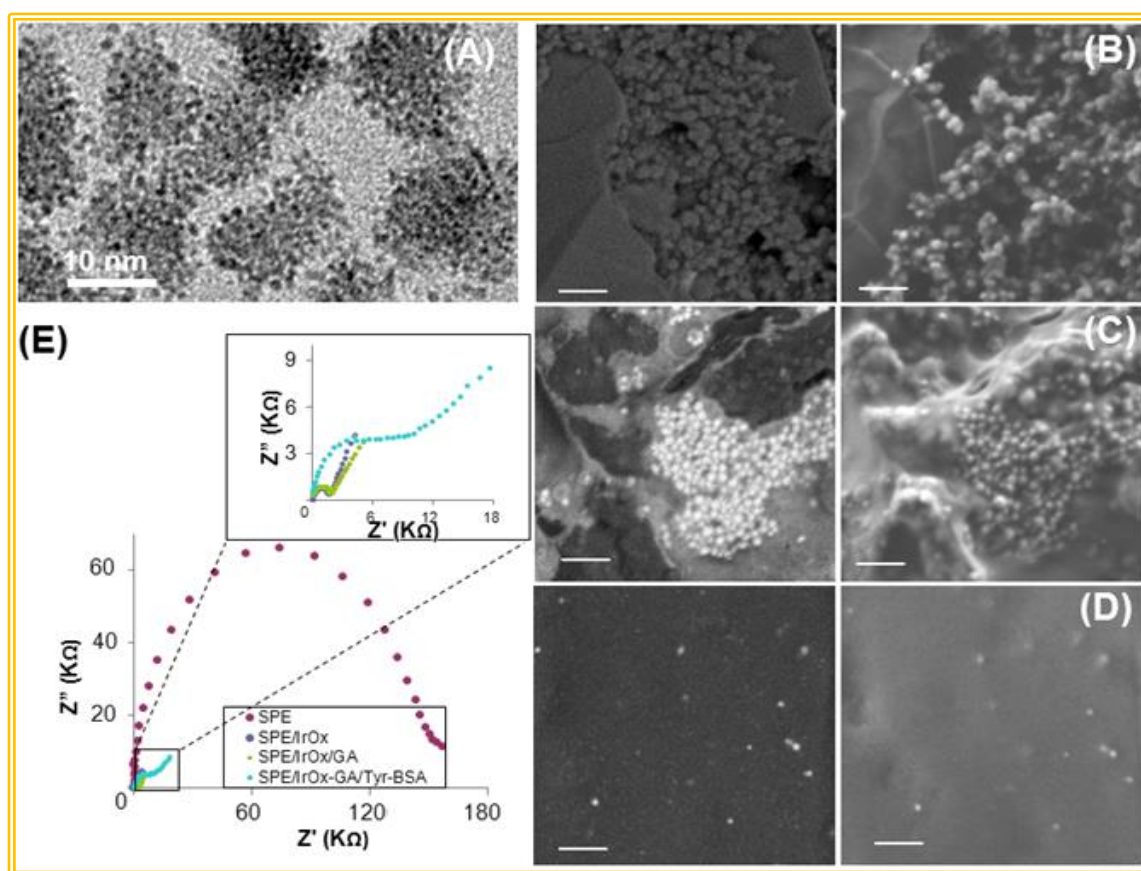


**Figure 1** Surface characterization. (A) TEM images of IrOx NPs. SEM images of SPCE (B), SPCE/IrOx/GA (C) and SPCE/IrOx/GA/IrOx-BSA (D). Impedance studies (E) of the modified electrodes surfaces. Left SEM images were taken using backscattered electrons mode. The scale bar of SEM images is 200 nm.

To study the surface features of the modified electrodes, electrochemical impedances spectroscopy was used. The EIS curve presented as Nyquist plot consists in two parts:

one part is the semicircle section, located at higher frequencies corresponding to the electron transfer limited process.

The second part is relate to the electron-transfer resistance ( $R_{ct}$ ) and can be obtained by measuring its diameter. Another important part of Nyquist plot is the linear section, which brings the information related to the diffusion process held in solution and located at lower frequencies. The increase of electron transference due to the presence of IrOx NPs layer was observed with the decreasing of  $R_{ct}$  in the Nyquist plot (see Figure 1E). These improvements were due to the fact that IrOx is a metallic oxide known for its high conductivity.<sup>27, 30</sup>

The adsorption of glutaraldehyde onto the IrOx (see  $R_{ct}$  increase at Figure 1E) indicates the effect of glutaraldehyde as a good binding / entrapment matrix. Finally, when the solution composed of Tyr-BSA was introduced (adsorbed onto the electrode surface) an increasing of  $R_{ct}$  as result of a successful immobilization of the enzyme could be observed (Fig. 1 E).

### 4.3.2 Analytical measurements

The SPCE/ IrOx/Tyr biosensor operation for the catechol detection was evaluated by chrono-amperometric responses for the different enzyme modified sensors upon successive addition of 5  $\mu$ M catechol (Fig 4.2). This biosensor showed a higher current change in comparison to the SPCE/Tyr (Fig. 4.2B). The observed reduction of the current was attributed to the direct reduction of o-quinone to catechol, released from the enzyme-catalyzed reaction on the electrode surface (see Fig.4.2A).

Tyrosinase has oxidase activity for oxidation of catechol to o-quinone (see Figure 4.2B). At moderate negative potential the o-quinone product of phenol oxidation may be electrochemically reduced to catechol (Figure 4.2B). Oxidation by the enzyme followed by reduction at the electrode may result in cycling between the catechol and o-quinone.<sup>18</sup>

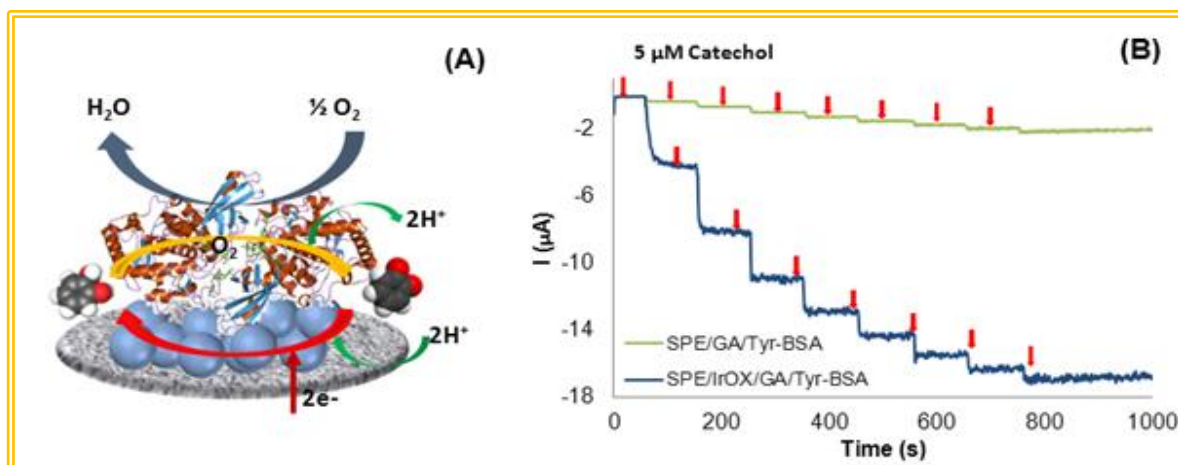


**Figure. 4.2** Schematic representation of proposed detection mechanism, displaying the tyrosinase and reaction involved in the catechol detection (A). Current-time responses of SPCE/GA/Tyr-BSA and SPCE/IrOx/GA/Tyr-BSA for the successive addition of 5  $\mu\text{M}$  catechol solution, during stirring conditions within a working potential of  $-0.2\text{V}$  using 0.1 M phosphate buffer (PB) at pH 6.5 with 0.1 M KCl.

Chrono-amperometric response of the SPCE/IrOx/Tyr biosensor to successive additions of catechol solution (Figure 4.3A) is further evaluated under optimized experimental conditions.

The linear biosensor response within the range from 0.25  $\mu\text{M}$  – 27.5 $\mu\text{M}$  catechol with  $r=0.99$  was observed.

The biosensor shows sensitive bioelectrocatalytic response, reaching about 95% of the steady-state current within 10s after each addition of catechol.

The typical calibration curves of the SPCE/IrOx/Tyr for catechol is showed in Figure 4.3B. Moreover, LOD and LOQ were calculated according to the 3 times  $s/m$  and 10  $s/m$  criterions, respectively, where 's' is the standard deviation of the peak currents of low concentration of the analyte (five runs) and 'm' is the slope of the related calibration graph. <sup>31-35</sup> SPCE/IrOx/Tyr biosensor shows LOD=0.08  $\mu\text{M}$  and LOQ=0.24  $\mu\text{M}$  for catechol.

The results of triplicate sets indicated by error bars reveal the in-day repeatability (Figure 4.3B) of the measurements with a relative standard deviation (RSD) lower than 10%. Between day repeatability also obtained with a RSD value lower than 15%.

Pesticides are known to inhibit different enzymatic systems being tyrosinase one of these.<sup>15</sup>

To evaluate pesticide inhibition activity onto the tyrosinase biosensor, the 'percentage inhibition' method was followed. The Tyr biosensor is immersed into a buffer solution under stirring condition and addition of catechol 5  $\mu\text{M}$  was performed waiting until achieving a steady state current response.

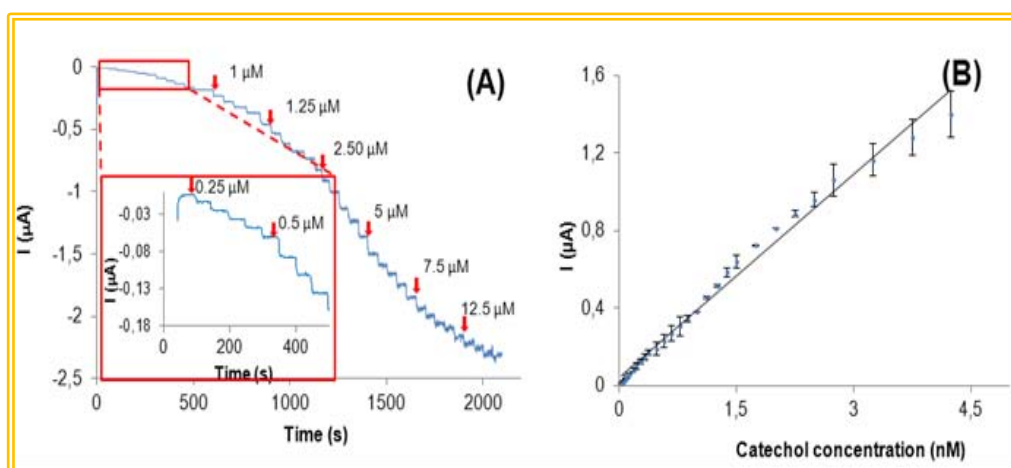


**Figure 4.3** Typical current–time response curves for the successive additions of different catechol concentration (A); inset: magnification of the initial steps. Biosensor calibration curve gives as current versus catechol concentration (B).

The stationary state current after each addition ( $I_{ss}$ ) is related to the enzyme activity of the biosensor when the inhibitor is not present. After that the same biosensor is incubated during a fixed interval of time (30 min) with chlorpyrifos pesticide. The pesticide incubated biosensor was measured again after the addition of the same concentration of catechol (5  $\mu\text{M}$ ). Lower steady state-currents ( $I_p$ ) were obtained due to the inhibition by pesticide. The Tyr biosensor inhibition percentage is calculated using the following equation:

$$I(\%) = \left[ \frac{(I_{ss} - I_p)}{I_{ss}} \right] * 100$$

In order to optimize the testing variables for pesticide detection using tyrosinase inhibition, catechol concentration and incubation time were evaluated in presence of 0.1  $\mu\text{M}$  chlorpyrifos. Figure 4A shows the optimum catechol concentration value to be used as working substrate for Tyr inhibition experiments. Herein different concentrations of catechol (1, 2 and 5  $\mu\text{M}$ ) were used, and the best inhibition response was found to be achieved for a 5  $\mu\text{M}$  substrate solution. The incubation time was also evaluated (see Figure 4.4B) showing that when the incubation time increased the inhibition also increased. A 30 min incubation time (under stirring condition at 37.5  $^{\circ}\text{C}$ ) was used for the following experiments.

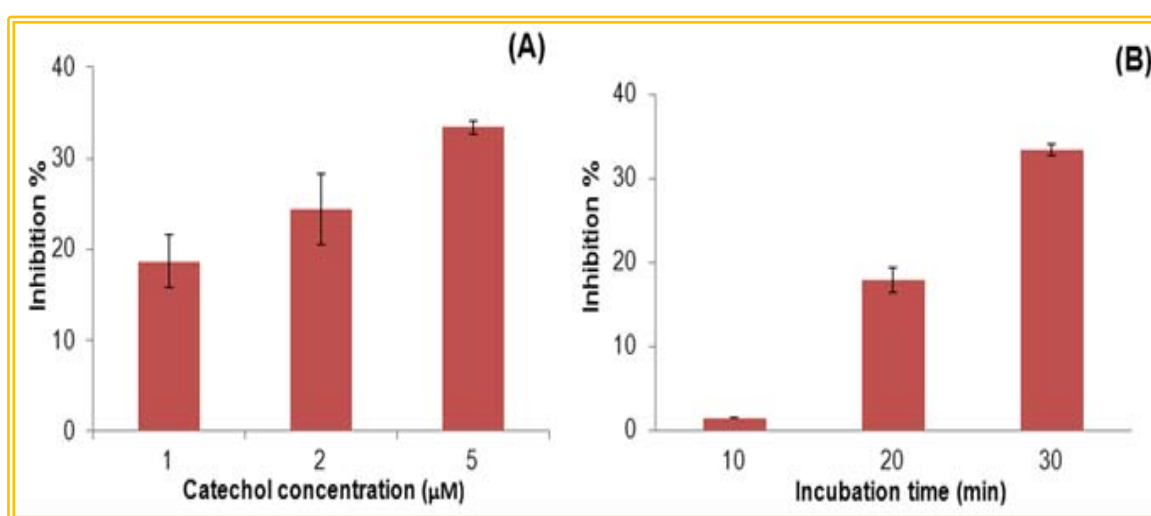


**Figure 4.4** Effect of substrate amount (A) and incubation time (B) in the residual activity of the catechol biosensor after pesticide incubation.

Plots of the biosensor inhibition percentage as a function of pesticide concentration are shown in Figure 5A. The proposed biosensor provides linear range for chlorpyrifos concentration from 0.01 to 0.1  $\mu\text{M}$  with a correlation coefficient of 0.99 with a LOD=0.003  $\mu\text{M}$  and LOQ=0.010  $\mu\text{M}$ . As the pesticide irreversibly inhibits the enzyme, a new biosensor has to be used for each point of the calibration after being exposed to the pesticide. The results indicated by error bars reveal the in-day repeatability (Figure 4.5A) of the measurements with a relative standard deviation (RSD) lower than 15%.



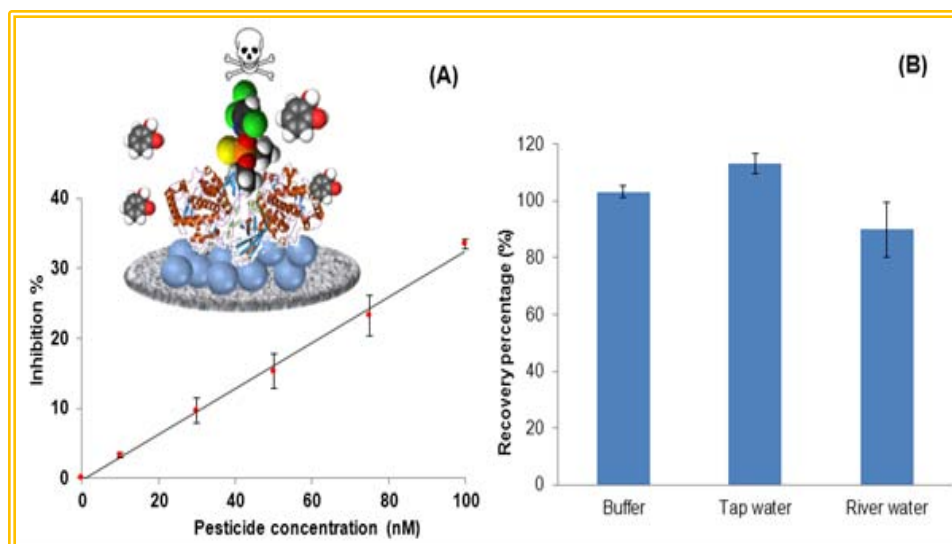


**Figure 4.5** Calibration curve of the biosensor as a function of the CPF concentration and the inhibition percentage (A). CPF recovery percentage from PBS, tap water and river water, using catechol biosensor (B).

Between day repeatability was also obtained with a RSD value lower than 15%. These biosensors for CFP detection present high analytical performances in term of sensitivity and LOD (table 4.1).

**Table 4.1** Comparison between different chlorpyrifos biosensors reported in the literature.

Electrode	Enzyme	Linear Range ( $\mu\text{M}$ )	LOD ( $\mu\text{M}$ )	Sample	Working Potential (mV)	Ref
Gold disk electrode	AChE	$1.0 \text{ e}^{-5} - 1.0 \text{ e}^{-6}$	$1.0 \text{ e}^{-6}$	Spiked river water	350	[5]
Mini carbon pate electrode	AChE	$1.0 \text{ e}^{-5} - 1.0 \text{ e}^{-0}$	$4.0 \text{ e}^{-6}$		50	[23]
Gold electrode	AChE	$5.0 \text{ e}^{-5} - 7.5 \text{ e}^{-2}$	$5.0 \text{ e}^{-5}$	Vegetable sample	600	[20]
Glassy carbon electrode	TYR	$7.1 \text{ e}^{-4} - 2.9 \text{ e}^{-2}$	$5.7 \text{ e}^{-4}$		60	[15]
SPE	TYR	$1.0 \text{ e}^{-2} - 1.0 \text{ e}^{-1}$	$3.0 \text{ e}^{-3}$	Spiked tap and river water	-200	This work

To further demonstrate the applicability of the proposed biosensor, recovery tests by adding chlorpyrifos 0.1  $\mu\text{M}$  into river and tap water were also performed. The results are presented in Figure 5B. Recovery percentages of 113 %  $\pm$  3.6 and 90 %  $\pm$  9.6 for tap and river water respectively with RSD lower than 10% (n=3) were found. This indicates that the proposed biosensor can be used for trace pesticide level detection in real samples. In addition it is possible to detect catechol and CPF using the same platform given the fact that the catechol detection is almost instantaneous (10 s response time) and CPF detection requires a longer response (30 min) (See Figure 4. 6.). It also can be extended to other kind of enzymes and pollutants detection with interest for environmental monitoring.

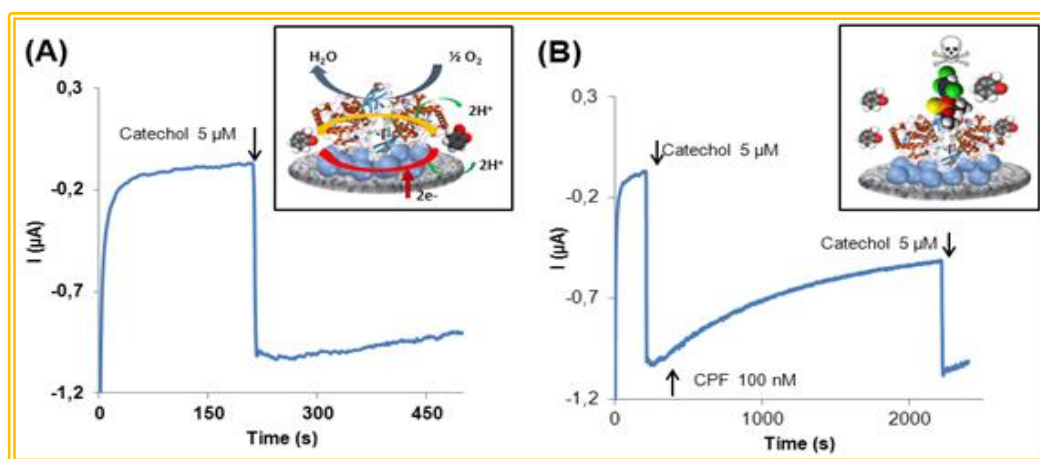


**Figure 4.6** IrOx Nanoparticles induced dual catalytic/inhibition based detection of catechol (A) and CPF (B) using the same platform.

To further demonstrate the applicability of the proposed biosensor, recovery tests by adding chlorpyrifos 0.1  $\mu\text{M}$  into river and tap water were also performed. The results are presented in Figure 5B. Recovery percentages of 113 %  $\pm$  3.6 and 90 %  $\pm$  9.6 for tap and river water respectively with RSD lower than 10% (n=3) were found. This indicates that the proposed biosensor can be used for trace pesticide level detection in real samples. In addition it is possible to detect catechol and CPF using the same platform given the fact that the catechol detection is almost instantaneous (10 s response time) and CPF

detection requires a longer response (30 min) (See figure 6). It also can be extended to other kind of enzymes and pollutants detection with interest for environmental monitoring.

## 4.4 Conclusion

An IrOx NPs based biosensing platform with effective tyrosinase immobilization properties and corresponding catalytic effect toward catechol is developed. Due to the high conductive and the surface active area of the IrOx NPs, the proposed biosensor displays dramatic improvements of the analytical performance in terms of a wider linear range of response along with a good LOD and sensitivity for catechol detection. Moreover the chlorpyrifos pesticide is detected using the same biosensor through the enzyme inhibition mechanism. The LOD was found to be 0.003  $\mu\text{M}$  which is lower than the maximum contaminant level recommended by the European Environment Bureau.<sup>36</sup> In addition to the analytical performance the use of this biosensor for chlorpyrifos detection has advantages in comparison to other ones reported before (Table 4.1.) due to the fact that it is related to a simple cost/efficient screen-printed carbon electrode. In addition it is possible to detect catechol and CPF using the same platform. A careful operation of this platform should be versatile and efficient enough for dual detection applications. This dual phenol/pesticide detection biosensing system can be extended to other enzymes and consequently to other pollutants combining direct (catalytic) and indirect (inhibition) detections in the same platform.

## Bibliography

1. Aragay G.; Pino F. ; Merkoçi A. *Chem. Rev.* **2012**, 112, 5317–5338 .
2. Heath C.W. *Cancer* **1997**, 80, 1887-1888.
3. Ridanoa M.; E.; Raccaa A. C.; Flores-Martina J.; Camolottoa S. A.; Magnarelli de Potasb G.; Genti-Raimondia S.; Panzetta-Dutaria M. G. *Reprod. Toxicol.* **2012**, 33 331– 338.
4. Bódalo, Gómez E., Hidalgo A. M., Gómez M., Murcia M.D; López I. *Desalination* **2009**, 245, 680–686.
5. Viswanathan S.; Radecka H.; Radecki J. *Biosens. Bioelectron.* **2009**, 24, 2772-2777.
6. Zhonga W.; Wanga D.; Xua X.; *J. Hazard Mater.* **2012**, 217, 286– 292.
7. Vermeulen A.; Welvaert K.;Vercammen J. *J Chromatogr. A* **2005**, 1071, 41-46.
8. Gundel J., Angerer M. J. *J. Chromatogr. B* **2000**, 738, 47-55.
9. Sherma J. *Anal. Chem.* **1995**, 65, 40R-54R.
10. Valenzuela I.; Lorenzini R.; Redondo M. J.; Font G. *J. Chromatogr. A* **1999**, 839, 101–107.
11. 11 Wang H.; Wang J.; Timchalk C.; Lin Y. H. *Anal. Chem.* **2008**, 80, 8477-8484.
12. 12 Du D., Chen W., Zhang W., Liu D., Li H. Lin Y., *Biosens. Bioelectron.* **2010**, 25, 1370-1375.
13. Gong J.; Guan Z.; Song D.; *Biosens. Bioelectron.* **2013**, 39, 320-323.
14. Arduini F.; Guidone S.; Amine A.; Palleschi G.; Moscone D. *Sensor. Actuat. B-Chem* **2013**, 179, 201– 208.
15. Liu T.; Xu M.; Yin H.; Ai S.; Qu X.; Zong S. *Microchim. Acta* **2011**, 175, 129-135.
16. Solé S.; Merkoçi A.; Alegret S. *Crit. Rev. Anal. Chem* **2003**, 33, 89–126.
17. Tanimoto Y. de Albuquerque D.; Ferreira L. F. *Anal. Chim. Acta* **2006**, 596, 210-221.
18. Mayorga-Martinez C. C.; Cadevall M.; Guix M.; Ros J.; Merkoçi A. *Biosens. Bioelectron.* **2013**, 40, 57–62.
19. Pérez-López B.; Merkoçi A.; *Adv. Funct. Mat.* **2011**, 21, 255-260.
20. Zhai C.; Sun X.; Sao W.; Gong Z.; Wang X. *Biosens. Bioelectron.* **2013**, 42, 124-130.
21. Andrescu S., Barthelmebs L., Marty J. L., *Anal. Chim. Acta* **2002**, 464,171-180.
22. Hart J. P.; Wring S. A. *Trends Anal. Chem.* **1997**, 16, 89-103.
23. Zamifir L.; Rotariu L.; Bala C. *Biosens. Bioelectron.* **2011**, 26, 3692-3695.
24. Lin Y.; Lu F.; Wang J. *Electroanalysis* **2004**, 16, 145-149.
25. Taufik S.; Yusof N.A.T.; Tee W.; Ramli I. *Int. J. Electrochem.* **2011**, 6, 1880–1891.
26. Katz E.; Willner I. *Angew. Chem. Int. Ed.* **2004**, 43, 6042–6108.
27. Mayorga Martinez C. C.; Madrid R. E.; Felice C. J. *Sensor. Actuat. B-Chem* **2008**, 133, 682– 686.
28. Tang J.; Tang D.; Niessner R.; Knopp D. *Anal Bioanal Chem* **2011**, 400, 2041–2051.

29. Kuwabara T.; Tomita E.; Sakita S.; Hasegawa D.; Sone K. ; Yagi M. *J. Phys. Chem. C* **2008**, 112, 3774-3779.
30. Meyer R.; Cogan S.; Nguyen T.; Rauh R. *IEEE Trans. Neural. Sys. Rehabil. Eng.* **2001**, 9, 2–10.
31. Riley C. M.; Rosanske T. M. *Development and validation of analytical methods*. Elsevier, New York **1996**.
32. Swartz M. E.; Krull I. S. *Analytical method development and validation*. Marcel Dekker **1997**, New York.
33. Ermer J.; JHMcB M. *Method validation in pharmaceutical analysis*. Weinheim, Wiley VCH **2005**.
34. De Bievre P.; Gunzler H. *Validation in chemical measurements* **2005**. Springer, Berlin.
35. Ozkan S.A. *Electroanalytical Methods in Pharmaceutical Analysis and Their Validation*, HNB Publishing **2012**, New York.
36. Council Directive 98/83/EC **1998** on the quality of water intended for human consumption, Official Journal of the European Communities, <http://eurlex.europa.eu/LexUriServ/LexUriServ.do?uri=OJ:L:1998:330:0032:0054:EN:PDF>.



**Chapter 5**  
**CuO nanoparticles based system for**  
**free enzymatic detection of phenolic**  
**compounds and pesticide**





## **CuO nanoparticles based system for free enzymatic detection of phenolic compounds and pesticide.**

### **5.1 INTRODUCTION**

The multidetection of pollutants like phenolic compounds and pesticides are critically important in environmental control. In this century it is well known that the pollution is one of the main threats and challenges that humanity faces today. Different types of pollutants in fact are released every day from industry or from intensive farming in the environment. For example the United States Environmental Protection Agency (EPA) in one of the last report shows that only in USA over 1 billion of tons of pesticide have been used in the farming for improving the agriculture production.<sup>1</sup>

Meanwhile all the minimum levels of the toxic compounds like phenolic compounds and pesticide as 3-(3,4-dichlorophenyl)-1,1-dimethylurea (DCMU) are controlled by the governmental environmental agencies. Moreover, different research centers worldwide are dedicated to developing different sensor systems to detect those toxic compounds.<sup>2</sup>

The phenols compound furthermore are common contaminants, whose origin are either natural either industrial.<sup>3</sup> Those compounds are highly toxic towards environment and human being, in fact could be absorbed through oral dermal and respiratory tracts.<sup>4,5</sup>

At the same time DCMU have an highly toxicity to aquatic organisms and may cause long term effects in the aquatic environment for its specific and sensitive inhibitory activity of photosynthesis.<sup>6,7</sup>

In this contest there is an high demand of new tools and techniques for pollutants detection with fundamental targets to reach: high sensitivity, selectivity, rapidness, cost efficiency, and easy to use also for not training users.<sup>8,9</sup>

The currently analytical methods, such liquid/gas chromatography or mass spectrometry can detect different toxic compounds with low detection limit, high reproducibility, optimum sensitivity and sensibility. However those techniques involve complicate sample preparation, using high expensive instrumentation and need high qualified technicians.<sup>10,11</sup>

Meanwhile, the latest trends in (nano)materials and micro and nanotechnologies are offering new opportunities for development bio/sensors with high analytical performances and the possible integration with existing simple platforms and technologies beside the development of new ones that.<sup>12,13</sup>

Particularly, nanoparticles due to their small dimension (1-100 nM) present unique, chemical, physical and electronic properties at nanoscale possessed.<sup>14</sup> Taking advantage of those incredible compounds, (bio)sensing systems increase their strength, their sensitivity and their application in complex matrix.<sup>15</sup>

Moreover the research on the field of novel nanostructured materials integrated on cheap design, highly selective, fast and reliable non-enzymatic sensors is of significant interest nowadays.<sup>16</sup>

Considering the drawbacks of the biological recognition element in particularly the low stability and difficult procedure to purify in the last period there is an increasing interest of mimic those biomolecules artificially, and nanomaterials represent an alternative due to their catalytic properties.<sup>17</sup>

Among all the nanomaterials a great interest have been dedicated in the last period to copper oxide nanomaterials, for their different properties that make them suitable for different purpose: antioxidant<sup>18</sup>, conductivity<sup>19</sup>, catalytic<sup>20</sup> and solar cells applications.<sup>21</sup> Despite all those characteristics CuO nanoparticles in basic medium have been used for free enzymatic electrochemical glucose sensor and other related molecules<sup>22,23</sup> with optimum results.

This part, the interaction of different phenolic compounds (Catechol, Phenol and 4-dichlorophenol) and DCMU pesticide are studied by standard electrochemistry techniques, the result shows that CuO NPs represent an interesting multidetection pollutants platform.

The sensing system is achieved through a SPCE with low LOD and high reproducibility and it is suitable for make in situ measurement and also could be used by no training users.

## 5.2 Experimental section

### 5.2.1 Instruments and Methods

All the electrochemical experiments were performed using an electrochemical analyzer Autolab 20 (Eco-Chemie, The Netherlands) which was connected to a personal computer using a software package GPS 4.9 (General Purpose Electrochemical System). The optic characterization of Copperoxide nanoparticles were obtained through a JEM-2011(Jeol,Ltd., Japan) transmission electron microscope (TEM). XPS measurements were obtained using a Phoibos 150 analyzer (SPECS GmbH, Berlin, Germany) in ultra-high vacuum conditions (base pressure 1E-10mbar) with a monochromatic aluminium Kalpha x-ray source (1486.74eV). X-ray powder diffraction (XRPD) measurements were performed on an X'Pert MPDP analytical diffractometers (Panalytical).

Absorbance measurements have been performed using specocroscopic analyser (Perkin Elmer, Massachusetts, USA) Disposable devices as home-made screen printed electrodes (SPE) have been produced (DEK 248, DEK International, Switzerland), which are constituted by three electrodes in a single strip: a carbon working electrode with a diameter of 3 mm, an Ag/AgCl reference electrode and a carbon counter electrode.

### 5.2.2. Reagents

For the synthesis of the copperoxide nanoparticles have been used the follow reagents : copper acetate monohydrate [Cu(CH<sub>3</sub>COO)<sub>2</sub>] (98%), sodium hydroxide (NaOH, 96% purity), acetic acid (99 % ), ethanol (99.5 %). Monobasic potassium phosphate (99%), dibasic potassium phosphate (98 %), potassium chloride (99%), phenol (98 %), catechol(98%), 4-chlorophenol (99%) and DCMU (98%) also were used. All the reagents were analytical grade and used without further purification and were purchased from Sigma-Aldrich (St. Louis, MO).

### 5.2.3 Synthesis of Copper oxide nanoparticles

A quick faster low temperature reaction has been applied for the synthesis of Copper Oxide nanoparticles .

The nanoparticles were prepared following a previous procedure.<sup>24</sup> Initially an aqueous solution of 0.02 M copper acetate ( $[\text{Cu}(\text{CH}_3\text{COOH})_2]$ ) was mixed with 0.5 mL acetic acid in a round-bottomed flask equipped with a refluxing device, after the temperature reached 100°C 0.8 g of pellets of NaOH was rapidly added into the above boiling solution until the pH value of the mixture reached 6–7, after that a large amount of black precipitate was simultaneously produced.

The precipitate was centrifuged, washed three times with absolute ethanol and one with distilled water. The precipitate was dissolved in water and storage at 4°C.

### 5.2.4 Methods

Home-made screen-printed-electrodes (SPE) consist of counter-electrode, reference electrode of Ag/AgCl and working electrode. They are fabricated on sheets of polyester substrate by the sequential deposition of three different ink layers, first the graphite ink layer on the polyester substrate for working electrode and counter-electrode, next the Ag/AgCl ink for the pseudo reference electrode and finally the isolating ink was printed. Each layer was printed using a screen printing machine. After its deposition each layer was cured by keeping the printed sheet at 120 °C for 30 min.

Before start the proper detection process the surface of the working electrode has been activated by applying 3  $\mu\text{A}$  for 120 s in a solution of  $\text{H}_2\text{SO}_4$ . Chrono-amperometric measurements were conducted at -200 mV in 50 $\mu\text{L}$  of 0.1 M phosphate buffer with 0.1 M KCl pH 6.5. Electrochemical experiments were carried out at room temperature.

## 5.3 Results and discussion

### 5.3.1 Morphological studies

The CuO NPs were characterized by optical and spectroscopy technique to obtain a detailed knowledge of the shape, the dimension and the oxidation level. The Figure 1 shows the TEM image of CuO, nanoparticles with highly regular and uniform average diameter of around  $5.5 \pm 0.2$  nm (see inset Fig. 1A).

Moreover, HRTEM images (Figure 1B) obtained from copper oxide nanoparticles exhibited well-defined lattice fringes. The spacings of these lattice fringes is 28 nm that corresponds of a typical structure of monoclinic CuO. In fact, these results are similar to those obtained in previous publications (<sup>24</sup>) like the XRD pattern of the CuO nanoparticles presented in Figure 1D.

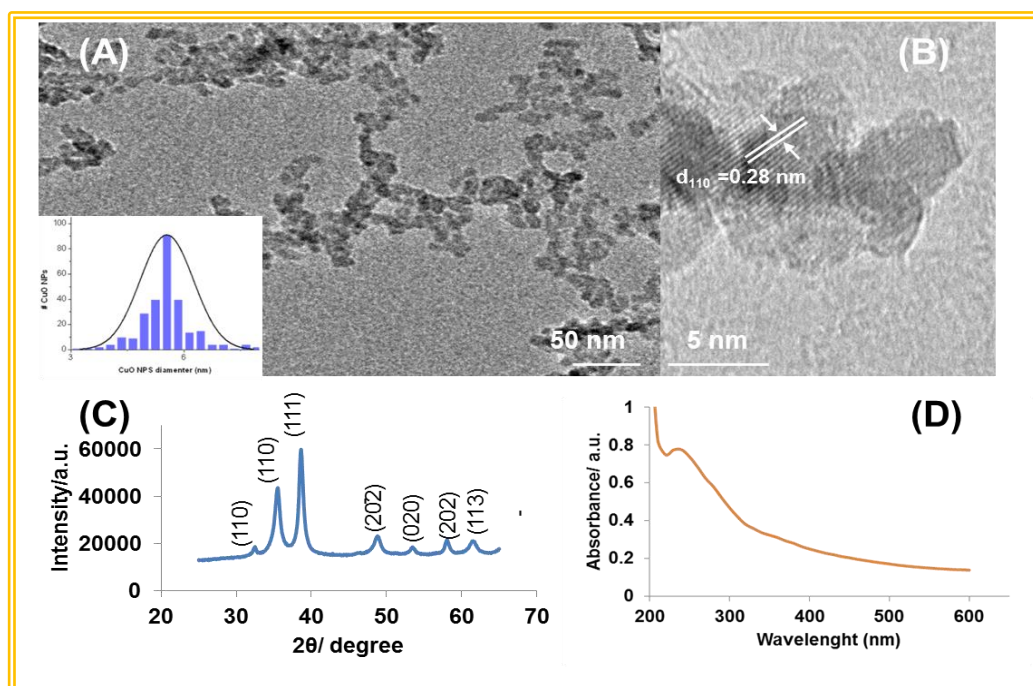
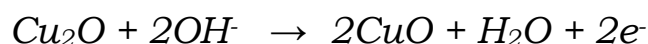


**Figure 1** Surface characterization: (A) TEM images of CuO NPs, in the inset the distribution and (C) XRD pattern, (D) Spectroscopic graph of the absorbance of CuOx NPs.

All diffraction peaks can be indexed in a single-phase with a monoclinic structure of CuO. Other peaks of possible impurities are not observed. The spectroscopy absorbance peak (285 nm) shows in the picture 1 D clarify also the efficiency of the synthesis . Even if different value of absorbance peak is attributed to the CuO nanomaterial, various studies confirm that depending on the shape and the dimension diverse value of peak of absorbance. <sup>25</sup>

### 5.3.2 Electrochemical behavior of the CuO NPs

The electrochemical behavior of CuO NPs drop-cast onto the SPE is evaluated using cyclic voltammetry measurements (Figure 2A) in phosphate buffer with pH 6.5 0.1 M KCl. Two main peaks, one anodic and one cathodic are observed at 0 V and -0.1V respectively. The anodic one correspond to the oxidation of Cu(I) to Cu(II) in agreement with the following reaction:



While, the catodic peak represents the reduccion of Cu (II) to Cu (I) (see schematic representation in Figure 2B). Different amounts of CuO NPs are evaluated, in order to study the dependence with the redox response (see inset of Figure2A).

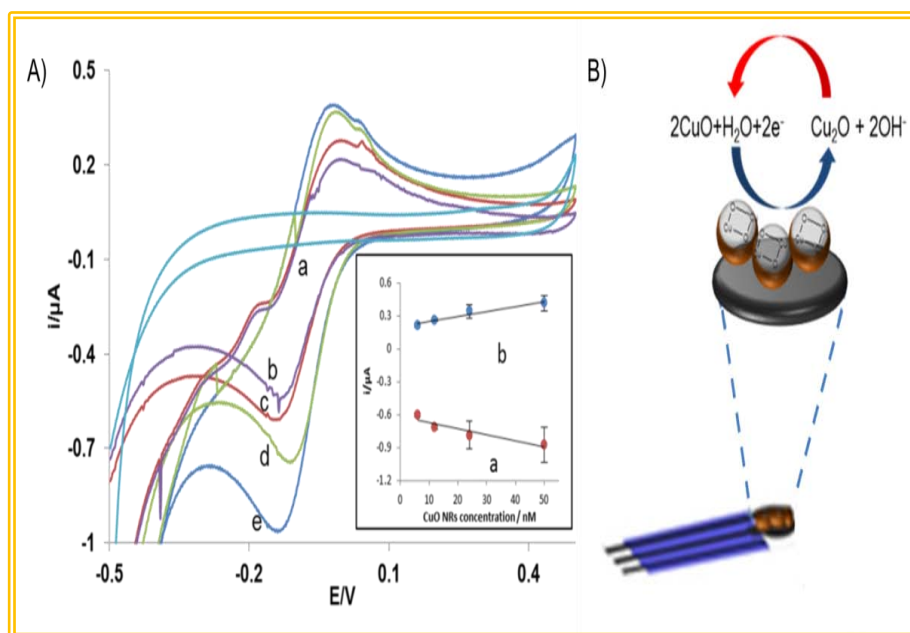


**Figure 2.** (A) Cyclic voltammograms of different concentration (a=0, b=6, c=12, d=24 and e= 50 nM) of CuO NPs drop-casted onto SPCE. PBS pH 6.5 + KCl 0.1 M and scan rate, 50 mV/s. Inset: Plots of peak current of oxidation of Cu(I) to Cu(II) and reduction of Cu (II) to Cu (I) against varying concentration of CuO NRs drop-cast onto SPCE. (B) Schematic of electrochemistry behaviour of CuO NPs.

### 5.3.3 Phenolics Compounds detection

Cyclic voltammetry studies of fixed amount of CuO NPs with and without the presence of 0.5 μM catechol have been performed (see Figure 3). In presence of catechol, a decreased of the reduction peak was observed. This behaviour may be due to a complex formation between catechol and CuO NPs (inset Figure 3).

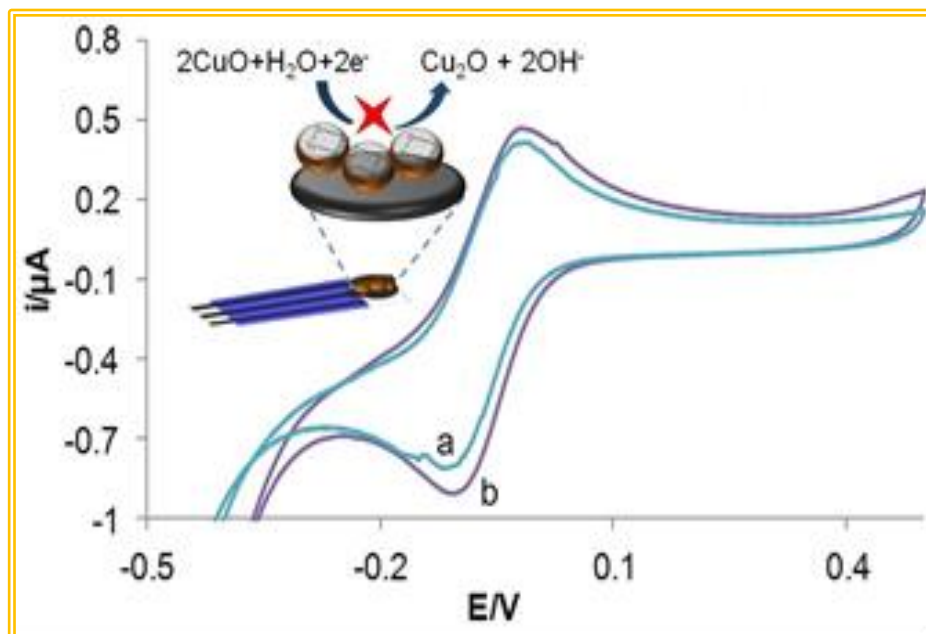


**Figure. 3** Cyclic voltammograms of 12 nM CuO NPs suspension with (a) and without (b) 0.5  $\mu\text{M}$  of catechol. Condition: PBS pH 6.5 + KCl 0.1 M, scan rate of 50 mV/s.

The chronoamperometry technique is used to evaluate the CuO NPs (12 nM) responses using reduction behaviour given that the reduction peak in CVs showed greater stability and reproducibility. In consequence, different reduction potentials were evaluated in order to obtain the best chronoamperometric response.

The best response is observed at  $-0.2$  V (see inset Figure 4). The chronoamperometric responses of the complex of CuO NPs with different phenolic compounds (catechol, phenol, 4-chlorophenol) have been studied at the fixed potential of  $-0.2$  V. Figure 4 shows the calibration curves of the phenolic compounds studied as a function of the reduction current.



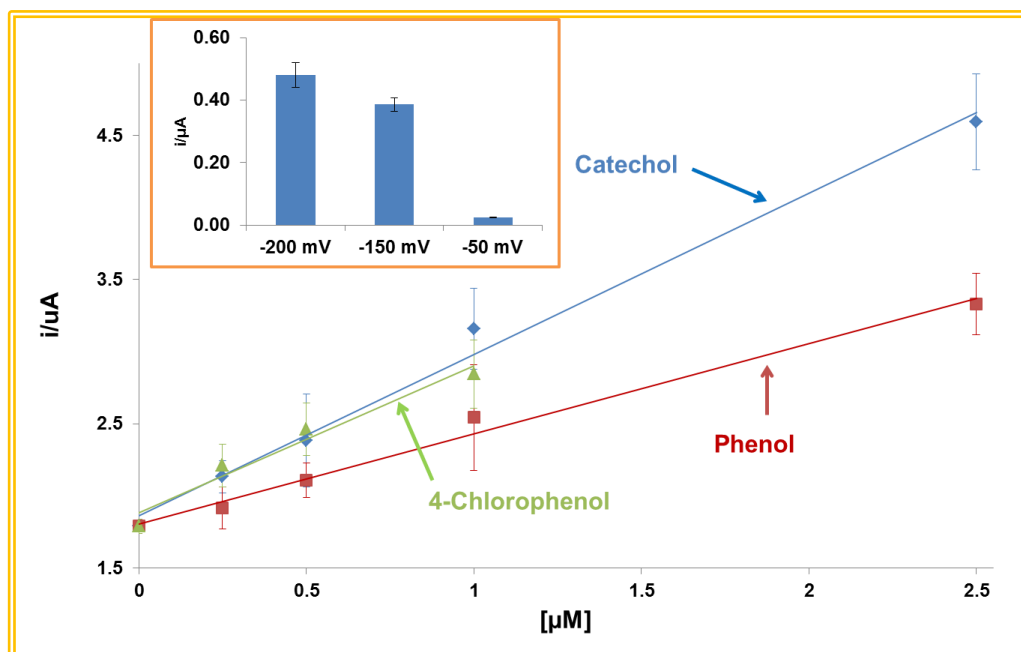


**Figure 4.** Calibration curves of current response as a function of different concentrations of phenolic compounds: catechol (blue), 4-chlorophenol (green) and phenol (red). The calibration curves are obtained through chronoamperometric measurement recorded at -0.2 V in presence of CuO NPs 12nM. Inset: Potential dependence of chronoamperometric response of CuO NPs.

The analytical performances of these three detection systems in terms of limit of detection (LOD) (catechol 0.30, phenol 0.69 and 4-chlorophenol 0.43  $\mu\text{M}$ ), limit of quantification (LOQ) (catechol 0.99, phenol 1.4 and 4-chlorophenol 2.3  $\mu\text{M}$ ) linear range (catechol 0.25-2.5, phenol 0.25-2.5 and 4-chlorophenol 0.25-1  $\mu\text{M}$ ), sensitivity (catechol 1.12, phenol 0.63 and 4-chlorophenol 1.03  $\mu\text{M} \cdot \mu\text{A}^{-1}$ ) and reproducibility (RSD % of 7, 6 and 7 for catechol, phenol and 4-chlorophenol respectively) are also evaluated. The LOD and LOQ were calculated as 3 times s/m and 10 s/m criterions, respectively, where 's' is the standard deviation of the peak currents of low concentration of the analyte (five runs) and 'm' is the slope of the related calibration graph. (25-28) The observed sensitivities in the linear calibration regions of the order: catechol > 4-chlorophenol > phenol is probably related to the affinity of the phenolic compounds toward CuO NPs to form complexes. The obtained detection limits for the three phenolic compounds are lower than the allowed levels of phenols in water as given by the EPA<sup>29</sup> and are similar with biosensors based on Tyrosinase.<sup>30-32</sup>

DCMU is a pesticide that inhibits the enzyme activity of tyrosinase<sup>(33)</sup>. In this work the effect of this pesticide on the CuO NPs is also studied. First of all, following the normal procedure of an inhibition system the incubation time between the DCMU and the CuO NPs has been studied. Figure 5A shows the inhibition percentage obtained after different incubation times (10, 20 and 30 min). The highest response is observed after 30 min of incubation. A calibration plot of the inhibition percentage as a function of DCMU concentration is shown in Figure 5B. This system provides a linear range of 0.5 to 2.5  $\mu\text{M}$  with good linearity ( $r = 0.992$ ). The LOD ( $0.047\mu\text{M}$ ) and LOQ ( $0.159 \mu\text{M}$ ) are also calculated using the same method described before. Good inter electrode reproducibility (RSD %) equal to 7% detection is also observed.

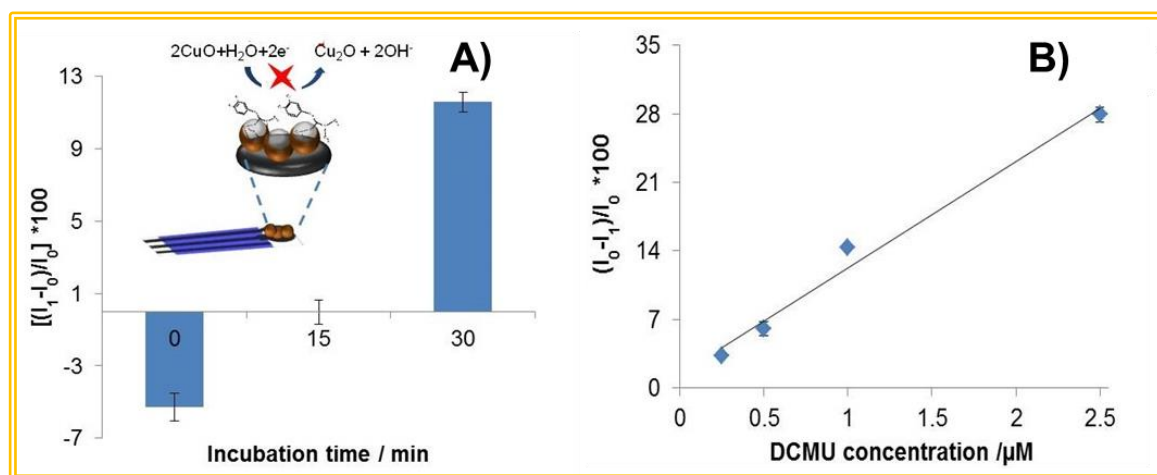


**Figure 5** (A) Inhibition % and incubation time relation in the presence of  $1\mu\text{M}$  of DCMU. (B) Dependency of the inhibition percentage from the different concentrations of DCMU . Inset: proposed mechanism for pesticide detection.

## 5.4 Conclusion

In this work a CuO NPs sensing platform with high catalytic effect toward phenolic compounds and DCMU is developed. The obtained results have shown that the CuO NPs lead to a simple and reliable sensor system with an improved analytical performance that would be useful as alternative to enzyme-based inhibition sensors. The high reproducibility

and sensitivity obtained for the detection of different phenolic compounds below the threshold values make the developed device a promising system for environmental monitoring. Furthermore, the LOD (0.159  $\mu\text{M}$ ) obtained to detect DCMU using the same system is in the same order of magnitude as the values recommended by WHO<sup>34,35</sup> and EQS-MA (34) for drinking water and sea water respectively. The interaction between CuO NPs and these pollutants also may suggest the use of this nanomaterial to remove these pollutants with interest for future sensor removal applications.<sup>36</sup>

## 5.5 Bibliography

- 1) United States Environmental Protection Agency. September, **2012**, 20.
- 2) Heath C. W. *Cancer* **1997**, 80, 1887-1888.
- 3) Karim F.; Fakruddin A.N.M. *Rev Environm Sci Biotechnol.* **2012**, 11, 261-274.
- 4) Shan D.; Zhang J.; Xue H-G.; Zhang Y.C.; Cosnier S.; Ding S.-N. *Biosensor and Bioelectronics* **2009**, 24, 3671-3676.
- 5) Aragay G.; Pino F.; Merkoci A.; *Chem Rev.* **2012**, 112, 5317-5338.
- 6) Pipi A. R.F.; Sirés I.; De Andrade A. R.; Brillas E. *Chemosphere*, **2014**, 109,49–55.
- 7) Giacomazzi S.; Cochet N. *Chemosphere* **2004**, 56, 1021–1032.
- 8) Liu D.; Chen W.; Wei J.; Li X.; Whang Z.; Jiang X. *Anal. Chem.* **2012**, 84, 4185-4191.
- 9) Mayorga-Martinez C.C.; Cadevall M.; Guix M.; Ros J.; Merkoçi A. *Biosens. Bioelectr.* **2013**, 15, 57-62.
- 10) Shan D.; Zhang J.; Xue H-G.; Zhang Y.-C.; Cosnier S.; Ding S.-N. *Biosens. Bioelectr.* **2009**, 24, 3671-3676.
- 11) Turner A. P. F. *Chem. Soc. Rev.* **2013**. 42, 3175-3184.
- 12) Nichkova M.; Dosev D.; Davies A. E.; Gee S. J.; Hammock B. D.; Kennedy I. M. *Anal. Chem.* **2005**, 77, 6864-6873.
- 13) Du D.; Wang J.; Smith J. N.; Timchalk C.; Lin Y. *Anal. Chem.* **2009**, 81, 9314–9320.
- 14) Merkoci A. ed. *Biosensing using nanomaterials*, Wiley, New Jersey, **2009**.
- 16) Mayorga-Martinez C. C.; Guix M.; Madrid R. E.; Merkoçi A.; *Chem. Commun.* **2012**, 48, 1686-1688.
- 17) Chen X.; Wu G.; Cai Z.; Oyama M.; Chen X.; *Microch. Acta* **2014**, 181, 689-705.
- 18) Das D.; Nath B.; Phukon P.; Dolui S.; *Coll. Surf. B.* **2013**, 111, 430-433.
- 19) Jammi S.; Sakthivel S.; Rout L.; Mukherjee T.; Mandal S.; Mitra R.; Punniyamurthy T. *J. Org. Chem.* **2009**, 74,1971–1976.
- 20) Zhou K.; Wang R.; Xu B.; Li Y. *Nanotechnology* **2006**, 17, 3939-3943.
- 21) Anandan S.; Wen X.; Yang S. *Mat. Chem. and Pysic.* **2005**, 93, 35-40.
- 22) Jiang L-C.; Zhang W.D.. *Biosens. Bioelectr.* **2010**, 25, 1402-1407.
- 23) Zhang X.; Wang G.; Zhang W.; Hu N.; Fang B. *J. Phys. Chem. C.* **2008**, 112. 8856-8862.
- 24) Ahmad R.; Vaseem M.; Tripathy N.; Hahn Y.-B. *Anal. Chem.* **2013**, 26, 10448-10454.
- 25) Lin X. Z.; Liu P.; Yu J. M.; Yang. G. W. *J. Phys. Chem. C.* **2009**, 113, 17543–17547.
- 26) C.M. Riley and T. Rosanke, *Development o and Validation of analytical methods*, Elisivier, New York “**1996**.
- 27) Swartz M. E. *Analytical Method development and validation*, Marcel Decker, New York **1997**.

- 28) J Ermer and M. JH. Method validation in pharmaceutical analysis. Wiley VCH Weinheim.
- 29) Alarcón Ángeles G.; Guix M.; Ambrosi A.; Ramirez Silva M.T., Palomar Pardave M. E., Merkoçi A. *Nanotechnology* **2010**, 21, 245502- 245511.
- 30) Mayorga-Martinez C. C.; Hlavata L., Miserere S.; López- Marzo A.; Labuda J.; Pons J; Merkoçi A. . *Biosens. and Bioelectr.* **2014**, 55, 355–359.
- 31) Mayorga-Martinez C. C.; Hlavata L., Miserere S.; López- Marzo A.; Labuda J.; Pons J; Merkoçi A. *Electroph.* **2013**, 34, 2011–2016.
- 32) Malzahn K., Windmiller J. R., Ramirez G. V., Schoning M. J., Wang J., *Analyst* **2011**, 136, 2912-2917.
- 33). Amine A.; Mohammadia H.; Bouraisa I.; Palleschi G. *Biosens. and Bioelectr.* **2006**, 21, 1405–1423.
- 34) Anh T. M. ; Dzyadevych S. V.; Van M. C.; Nicole Renault J.; Duc C. N.; Chovelon J.-M *Talanta* **2004**, 63, 365-370.
- 35) Sharma P., Sablok K., Bhalla V., Raman Suri C., *Biosens. and Bioelectr.* **2011**, 26, 4209–4212.
- 36) Tian L.; Gao Y.; , Li L.; Wu W D. Sun, J. Lu, T. Li, *Microchim. Acta*, 2013, 180, 607;



# **Chapter 6**

## **General conclusions and future perspectives**





## General conclusions and future perspectives

### 6.1 General conclusions

Three different electrochemical biosensing platforms have been developed and optimized in this PhD Thesis. The obtained results are with interest for further applications of the developed biosensing systems in environmental monitoring following the permitted levels of each contaminant according to the established rules by law. The developed electrochemical biosensing systems have evidenced the role of nanomaterials for improving their performance in general and especially of the sensitivity, which is one of the critical issues for environmental monitoring.

Considering the detailed objectives described in Chapter 2 and the achieved results described in Chapters 3, 4 and 5, the conclusions are detailed as follows:

**Firstly, a simple electrochemical biosensing platform for OP pesticide detection has been developed.** The detection of chlorpyrifos (CPF) is based on thiocholine oxidation using acetylcholinesterase (AChE) immobilized onto magnetic beads as a pre-concentration platform being the boron-doped diamond (BDD) electrode the transducer. The system presents good linearity of the current responses, very low limit of detection ( $3.10 \times 10^{-10}$  M CPF) as well as low interferences in the direct detection of CPF injected in tap water solution while using anodically oxidized (AO) BDD. In addition, the system with immobilized AChE at magnetic beads provided a better limit of detection in comparison to that of free enzyme.

**Secondly, an IrOx NPs based biosensing platform with effective tyrosinase immobilization for dual detection of catechol and chlorpyrifos pesticide is implemented.** Due to the high conductivity and the surface active area of the IrOx NPs, the proposed biosensor displays significant improvements of the analytical performance in terms of a wider linear range of response along with a good LOD and sensitivity for

catechol detection. Moreover the chlorpyrifos pesticide is detected using the same biosensor through the enzyme inhibition mechanism. The LOD was found to be 0.003  $\mu\text{M}$  which is lower than the maximum contaminant level recommended by the European Environment Bureau. In addition to the analytical performance the use of this biosensor for chlorpyrifos detection has advantages in comparison to other ones reported before due to the fact that it is related to a simple cost/efficient screen-printed carbon electrode. A careful operation of this platform should be versatile and efficient enough for dual detection applications.

**Thirdly, a CuO NPs sensing platform with high catalytic effect toward phenolic compounds and Diuron (DCMU) is developed.** The obtained results have shown that the CuO NPs lead to a simple and reliable sensor system with an improved analytical performance that would be useful as alternative to enzyme-based inhibition sensors. The high reproducibility and sensitivity obtained for the detection of different phenolic compounds below the threshold values make the developed device a promising system for environmental monitoring. Furthermore, the LOD (0.159  $\mu\text{M}$ ) obtained to detect DCMU using the same system is in the same order of magnitude as the values recommended by WHO and EQS-MA for drinking water and sea water respectively.

## 6.2 Future Perspectives

The results obtained in this PhD thesis confirm how the nanomaterials may improve the bio/sensing systems for environmental monitoring of pesticides and phenolic compounds.

The developed system based on IrOx NPs, for the dual phenol/pesticide detection biosensing system can be extended to other enzymes and consequently to other pollutants combining direct (catalytic) and indirect (inhibition) detections in the same platform.

Regarding the biosensing platform based on BDDE and using MB modified with acetyl cholinesterase, it can be previewed that the developed pesticide detection system can be

---

implemented easily in (micro) fluidic measurements for on-line monitoring as well and can be extended to several other analytes with interest for environment, health and safety, and security fields.

The well orienting of biological receptor through the magnetic beads and low background currents and excellent stability regarding physical and chemical properties the boron doped diamond can prospectively be a breakthrough in the field of environmental monitoring through electrochemical biosensors. Future improving in the miniaturization of the system like the connection with the screen printed process and the same time the inclusion in lab on chip system would able to create a biosensing system with interest for continuous monitoring of pollutants.

On the other hand, the phenolic compounds and DCMU detection based on CuO NPs, offers the possibility to develop robust and stable free enzymatic systems for long time pollutants monitoring. Another possible application of this system is for removing of phenolic compounds and pesticides from contaminated waters (for example rivers, lakes etc.) due to the possible interaction of those nanoparticles through complex formation with the hazard compounds.



# ANNEX A

# Iridium oxide nanoparticle induced dual catalytic/inhibition based detection of phenol and pesticide compounds†

Cite this: *J. Mater. Chem. B*, 2014, 2, 2233

Carmen C. Mayorga-Martinez,<sup>‡a</sup> Flavio Pino,<sup>‡a</sup> Sevinc Kurbanoglu,<sup>‡ab</sup> Lourdes Rivas,<sup>a</sup> Sibel A. Ozkan<sup>b</sup> and Arben Merkoçi<sup>\*ac</sup>

Environmental pollution control technology has a great demand for detection systems, particularly for pesticides and phenolic compounds. Moreover, analytical systems are highly required for the dual detection of different pollutants using the same platform. In that direction, a new, reliable, easy to use and disposable biosensor for the detection of catechol and chlorpyrifos is proposed. The designed biosensor with synergic properties between the high conductivity of iridium oxide nanoparticles, low-cost screen printed electrodes and the efficiency of tyrosinase shows broad linearity ranges for catechol and chlorpyrifos detection. Using this biosensor, very low limits of detection for catechol (0.08  $\mu\text{M}$ ) and chlorpyrifos (0.003  $\mu\text{M}$ ) are observed and recoveries of spiked tap and river water samples have also been studied showing very good recoveries.

Received 11th December 2013  
Accepted 28th January 2014

DOI: 10.1039/c3tb21765e

[www.rsc.org/MaterialsB](http://www.rsc.org/MaterialsB)

## Introduction

The detection of polluting compounds is a major concern for health and environmental government institutions. Among all pollutant compounds, organophosphate pesticide (OP) and phenol compounds are the most toxic and dangerous ones for human beings.<sup>1,2</sup> It is well known that pesticide and phenol compounds possess highly acute toxicity. For instance, chlorpyrifos (CPF), one of the most widely used OPs, interferes with brain development in part due to alterations in the activity of transcription factors involved in the basal machinery of cell replication and differentiation,<sup>3</sup> and phenol is a potential human carcinogen and is of considerable health concern, even at low levels.<sup>4</sup>

Pesticides are extensively used in farming and for domestic purposes.<sup>5</sup> Phenol compounds have limited use in industrial processes for different purposes.<sup>6</sup> In fact, every day these compounds are easily released in different water systems affecting the ecosystem.

Nowadays, the detection of pesticides and phenol compounds is performed using large and expensive automated

analysers such as liquid chromatography coupled with mass spectrometry<sup>7,8</sup> and high pressure liquid chromatography.<sup>9,10</sup> These techniques reach low limits of detection and have high reproducibility, but they involve extraction of large volumes of water, require extensive purification and expensive equipment. Therefore, there is a high demand to obtain simple analytical devices and related nanomaterials for the detection of the mentioned hazardous compounds in environment and health related samples. The main requirements of the future detection systems are to be cheap, reliable, easy to use and disposable. At the same time, it would be necessary to have devices that can detect different families of pollutants.

Currently different approaches for the detection of pesticides, including immunoassay<sup>11</sup> and enzymatic activity,<sup>12</sup> have been developed. Enzymatic biosensors are the most reliable for this type of analysis due to their simplicity, efficiency and their easy usage. In fact, numerous biosensors using inhibition-based enzymatic systems, in particular those based on the inhibition of acetyl cholinesterase (AChE),<sup>13,14</sup> have been reported. Furthermore, tyrosinase (Tyr) has been used for phenolic compound detection, and based on the inhibition of this enzyme some pesticide detections have been reported.<sup>15,16</sup>

The advantage of the Tyr based electrochemical biosensor is its achieved selectivity due to the fact that the effect of interfering species such as other electroactive compounds is low given its low working potential ( $-0.2$  V or less)<sup>17-19</sup> in comparison to AChE and free mediator based biosystems that mostly work at 0.6 V.<sup>20</sup>

Meanwhile, the need for a disposable analytical platform could be reached through the use of micro-transducers like screen printed carbon electrodes (SPCEs). In fact in the last

<sup>a</sup>Nanobioelectronics & Biosensors Group, ICN2-Institut Catala de Nanociencia i Nanotecnologia, Campus UAB, 08193, Bellaterra, Barcelona, Spain. E-mail: arben.merkoci@icn.cat

<sup>b</sup>Ankara University, Faculty of Pharmacy, Department of Analytical Chemistry, 06100, Tandogan, Ankara, Turkey

<sup>c</sup>ICREA, Barcelona, Catalonia, Spain

† Electronic supplementary information (ESI) available. See DOI: 10.1039/c3tb21765e

‡ C. C. M.-M., F. P. and S. K. contributed equally to this work.

twenty years, the application of these devices for *in situ* and user-friendly measurements has significantly increased. The key factor in an enzymatic micro-device platform is the immobilization procedure of the enzyme. This process is usually performed in different ways; adsorption, entrapment and cross-linking are the most reported. The main objective of the enzyme immobilization alternatives has always been the increase of the biosensor stability and its reproducibility, fouling of the working electrode surface being the most important drawback to overcome.<sup>21,22</sup>

The explosion in nanomaterials research, especially nanoparticles, has also influenced the research in the field of enzymatic biosensors.<sup>23,24</sup> The connection of enzymatic systems with nanoparticles has a high impact on improving the performance of the platform used for detection of toxic compounds. This is due to the unique, chemical, physical and electronic properties at nanoscale possessed by nanoparticles (normally in the range of 1–100 nm).<sup>25,26</sup> Iridium oxide (IrOx) films have been used in biosensors as electrodes (enzymes can be immobilized) due to their high conductivity.<sup>27</sup> Furthermore, IrOx nanoparticles possess useful electronic and conductivity switching properties which make them highly attractive for biosensor development as well.<sup>28</sup>

In the present study, an enzymatic biosensor for dual detection of two different pollutants, catechol (a phenol derivative) and chlorpyrifos (an organophosphate pesticide) is proposed. Such sensing is achieved through a SPCE modified with IrOx NPs and tyrosinase. The proposed biosensor reports improvement in the limit of detection (0.08  $\mu\text{M}$ ) and sensitivity for catechol compared to previously reported biosensors. This biosensor shows also a low limit of detection (0.003  $\mu\text{M}$ ) for CPF while being used in a tyrosinase inhibition mode operation. Finally the efficiency of this biosensor for real applications in CPF detection in river and tap water was also explored showing great possibilities for future application as a low cost platform for pesticide detection.

## Experimental

### Materials and apparatus

Electrochemical experiments were performed using an electrochemical analyzer Autolab 20 (Eco-Chemie, The Netherlands) which was connected to a personal computer using a software package GPS 4.9 (General Purpose Electrochemical System). Impedance measurements were performed by using an Autolab302 potentiostat/galvanostat/frequency-response analyzer PGST30, controlled by GPES/FRA Version 4.9. Scanning electrochemical microscopy (SEM) images were acquired using a field emission-scanning electron microscope (Merlin, Carl Zeiss) and transmission electron microscope (TEM) images were taken with a JEM-2011 (Jeol, Ltd., Japan). A thermoshaker TS1 (Biometra) was used to stir the samples during the inhibition process operating at a controlled temperature of 37.5 °C and shaking at 350 rpm. Homemade screen printed carbon electrodes (SPCEs) were used as electrochemical transducers, which are constituted by three electrodes in a single strip: a

carbon working electrode with a diameter of 3 mm, an Ag/AgCl reference electrode and a carbon counter electrode.

### Reagents and solutions

Tyrosinase from mushroom ( $\geq 1000$  unit per mg), bovine serum albumin (BSA), glutaraldehyde (GA, 25%), chlorpyrifos and catechol were purchased from Sigma-Aldrich (St. Louis, MO). For the synthesis of iridium oxide nanoparticles, potassium hexachloroiridate(IV) and sodium hydrogencitrate were purchased from Sigma-Aldrich (St. Louis, MO). Milli-Q water was obtained from a purification system and all solutions were prepared with ultra-pure water from a Millipore-MilliQ system. All reagents and other inorganic chemicals were supplied by Sigma-Aldrich or Fluka, unless otherwise stated.

### Synthesis of iridium oxide nanoparticles

Iridium oxide nanoparticles were prepared according to the previously reported procedure.<sup>29</sup> Potassium hexachloroiridate(IV)  $2.6 \times 10^{-5}$  M solution was mixed with sodium hydrogencitrate  $1.6 \times 10^{-2}$  M solution. The pH of the red-brown solution was adjusted to 7.5 with a 0.25 M NaOH solution and then refluxed in an oil bath with constant stirring for 30 min. As the mixture cooled to room temperature, the pH was again adjusted to 7.5 with refluxing for 30 min. This procedure was repeated until the pH reached a constant value of 7.5. Finally the solution was refluxed for a further 2 h with oxygen bubbling. At the end of this step, a deep blue solution of IrOx nanoparticles was obtained. The solution was stored in a glass-stoppered flask and at 4 °C when not in use.

### Preparation and modification of screen printed electrodes

Screen printed electrodes were fabricated by sequential deposition of a graphite ink, Ag/AgCl ink and insulating ink on a polyester substrate. The polyester substrate was dried at 120 °C for 45 min (graphite) and 30 min (Ag/AgCl and insulating) after the deposition of each layer. Before modification, SPCEs were activated at 3  $\mu\text{A}$  for 120 s in 0.1 M  $\text{H}_2\text{SO}_4$ . A 5  $\mu\text{L}$  solution of IrOx NPs suspension was dropped onto the working surface of SPCE. 0.25% of glutaraldehyde (GA) was prepared in ultra-pure water and from this solution 5  $\mu\text{L}$  was dropped onto the SPCE/IrOx surface. 2  $\mu\text{L}$  of the solution of Tyr (1 mg per 50  $\mu\text{L}$ ) in 5% BSA (1 : 1) was dropped onto the SPCE/IrOx/GA surface. Tyr and BSA solutions were prepared in 0.1 M phosphate buffer at pH 6.5. In between all steps, electrodes were dried at 37.5 °C for 30 min.

### Electrochemical measurements

The surface characterization of the modified electrodes was performed by electrochemical impedance spectroscopy (EIS) studies in 1 mM  $[\text{Fe}(\text{CN})_6]^{3-/4-}$  with 0.1 M KCl as redox probe. A sinusoidal potential modulation of  $\pm 50$  mV amplitude in the 0.1 Hz to 100 kHz frequency range, with a logarithmic scale of 10 points per decade, was superimposed onto the formal potential of the redox couple,  $[\text{Fe}(\text{CN})_6]^{3-/4-}$  (0.24 V vs. Ag/AgCl). Nyquist diagrams were also recorded.

Chrono-amperometric measurements were conducted at  $-200$  mV; a magnetic stirrer was used to provide the convective transport in 10 mL of 0.1 M phosphate buffer with 0.1 M KCl. Electrochemical experiments were carried out at room temperature.

## Results and discussion

### Morphological studies

Transmission electron micrographs of IrOx NPs were obtained to determine the particle sizes and homogeneity. Fig. 1A displays a typical TEM image of the synthesized IrOx nanoparticles ( $12.5 \pm 2.5$  nm) (see inset in Fig. 1A). Although the dispersion of these nanoparticles was not homogenous in the solution, most of the formed IrOx NPs exhibited spherical shape. These nanoparticles seem to be clusters of other smaller nanoparticles with diameters around  $1.5 \pm 0.3$  nm.

The XPS spectra of IrOx NPs (Fig. S1†) showed the shifting of the Ir  $4f_{7/2}$  and  $4f_{5/2}$  peaks to  $\sim 62.3$  and  $\sim 65.1$  eV, and an increase of the O 1s peak intensity at 531.6 eV (main peak) and 533.7 eV (small peak), these results being in good agreement with the characteristics of a high oxidation state  $4^+$  of iridium.

IrOx NPs were immobilized onto an SPCE working electrode, then GA was used as cross-linking agent followed by modification with a solution composed of tyrosinase and BSA. The obtained biosensor was carefully characterized in each of the fabrication steps by using optical and electrochemical methods. Fig. 1B shows an SEM image of SPCE (left image corresponds to backscattered electrons mode). Fig. 1C displays the distribution of the IrOx NPs onto the working electrode surface of the SPCE.

IrOx NPs appear brighter in the backscattered electrons image (Fig. 1C left), while the effect of glutaraldehyde as a binding matrix was more evident in normal mode (Fig. 1C right). An enhancement of the contrast between objects of different chemical compositions using backscattered electrons mode is observed, since heavy elements backscatter electrons more strongly than light elements. Finally Fig. 1D shows a good entrapment of the IrOx NPs, glutaraldehyde and tyrosinase-BSA.

To study the surface features of the modified electrodes, electrochemical impedances spectroscopy was used. The EIS curve presented as Nyquist plot consists of two parts: one part is the semicircle section, located at higher frequencies corresponding to the electron transfer limited process; the second part is related to the electron-transfer resistance ( $R_{ct}$ ) and can be obtained by measuring its diameter. Another important part of the Nyquist plot is the linear section, which provides information related to the diffusion process held in solution and located at lower frequencies. The increase of electron transference due to the presence of the IrOx NP layer was observed with the decreasing of  $R_{ct}$  in the Nyquist plot (see Fig. 1E). These improvements were due to the fact that IrOx is a metallic oxide known for its high conductivity that corresponds to the high oxidation state ( $4^+$ ) of iridium.<sup>27,30</sup> Additionally, this nanostructured platform based on IrOx NPs has a high surface area that contributes to the conductivity improvement.

The adsorption of glutaraldehyde onto the IrOx (see  $R_{ct}$  increase in Fig. 1E) indicates the effect of glutaraldehyde as a good binding/entrapment matrix. Finally, when the solution composed of Tyr-BSA was introduced (adsorbed onto the

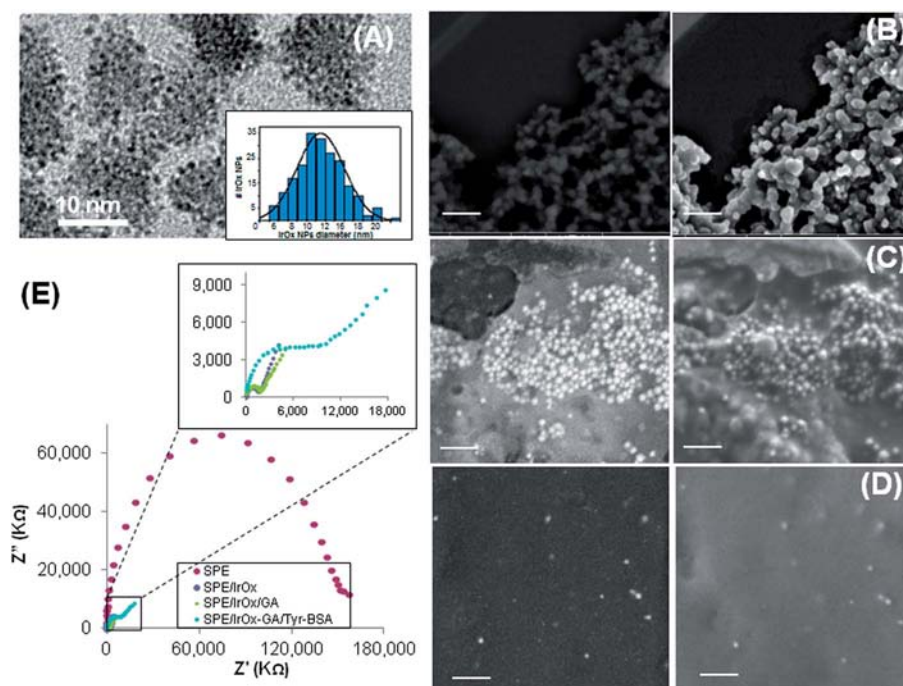


Fig. 1 Surface characterization. (A) TEM images of IrOx NPs. SEM images of SPCE (B), SPCE/IrOx/GA (C) and SPCE/IrOx/GA/IrOx-BSA (D). Impedance studies (E) of the modified electrodes surfaces. Left SEM images were taken using backscattered electrons mode. The scale bar of SEM images is 200 nm.



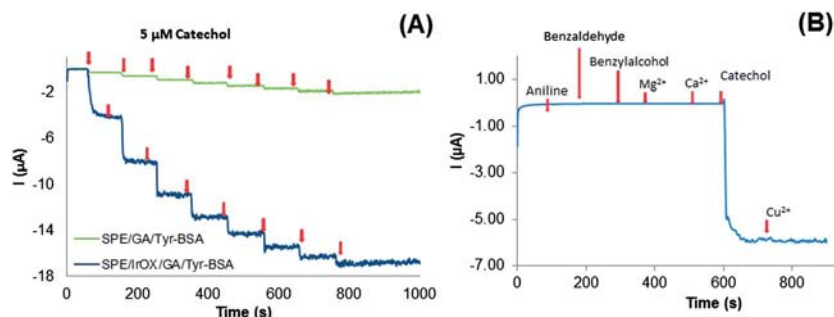


Fig. 2 Current–time responses of SPCE/GA/Tyr-BSA and SPCE/IrOx/GA/Tyr-BSA for the successive addition of 5 μM catechol solution, during stirring within a working potential of  $-0.2$  V using 0.1 M phosphate buffer (PB) at pH 6.5 with 0.1 M KCl (A). Selectivity evaluation for catechol biosensor in the presence of successive additions of 50 μM aniline, benzaldehyde, benzyl alcohol,  $Mg^{2+}$ ,  $Ca^{2+}$ , 5 μM catechol and 25 μM  $Cu^{2+}$  (B).

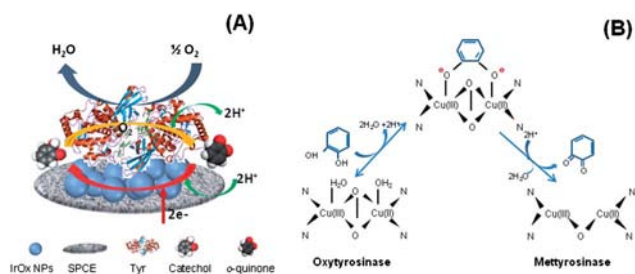


Fig. 3 Schematic representation of proposed detection mechanism, displaying the tyrosinase (Tyr) and reaction involved in the catechol detection at the SPCE modified with IrOx NPs (A). Catalytic cycles of the oxidation of catechol to *o*-quinone over two Cu atoms within the active site of tyrosinase enzymes (B).

electrode surface) an increase of  $R_{ct}$  as a result of the successful immobilization of the enzyme could be observed (Fig. 1E).

The SPCE/IrOx/Tyr biosensor operation for the catechol detection was evaluated by chrono-amperometric responses for the different enzyme modified sensors upon successive addition of 5 μM catechol (Fig. 2). This biosensor showed a higher current change in comparison to SPCE/Tyr (Fig. 2A). The observed reduction of the current was attributed to the direct reduction of *o*-quinone to catechol, released from the enzyme-catalyzed reaction on the electrode surface (see Fig. 3A and B). Tyrosinase has oxidase activity for oxidation of catechol to *o*-quinone (see Fig. 3B). At moderate negative potentials the *o*-

quinone product of phenol oxidation may be electrochemically reduced to catechol (Fig. 2A). Oxidation by the enzyme followed by reduction at the electrode may result in cycling between the catechol and *o*-quinone.<sup>18</sup>

Fig. 2B shows a good selectivity of this biosensor toward catechol detection that is evident by the shown negligible responses toward interfering species. The chrono-amperometric responses toward aniline, benzaldehyde, benzyl alcohol,  $Mg^{2+}$ ,  $Ca^{2+}$  (each one at a concentration 10 times higher than the phenol concentration) and  $Cu^{2+}$  (5 times higher than the phenol concentration) were measured. The selected species for interference studies seem to be the ones usually present with phenolic compounds in contaminated samples.<sup>18</sup>

#### Analytical characterization of the biosensor

The chrono-amperometric response of the SPCE/IrOx/Tyr biosensor to successive additions of catechol solution (Fig. 4A) was further evaluated under optimized experimental conditions (data not shown). A linear biosensor response within the range from 0.25–27.5 μM catechol with  $r = 0.99$  was observed. The biosensor shows sensitive bioelectrocatalytic response, reaching about 95% of the steady-state current within 10 s after each addition of catechol.

The typical calibration curve of the SPCE/IrOx/Tyr biosensor for catechol is shown in Fig. 4B. Moreover, LOD and LOQ were calculated according to the 3 times  $s/m$  and 10 times  $s/m$  criteria, respectively, where 's' is the standard deviation of the peak

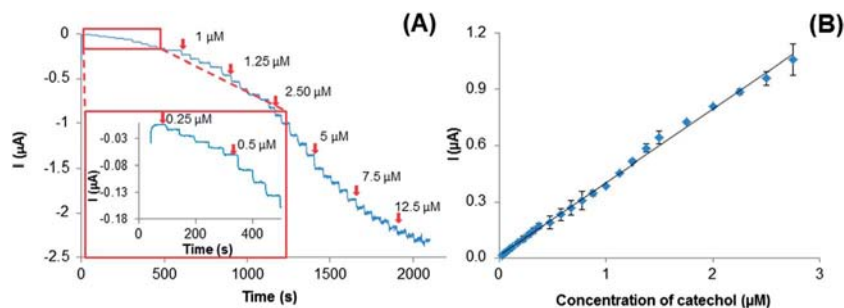


Fig. 4 Typical current–time response curves for the successive additions of different catechol concentrations (A); inset: magnification of the initial steps. Biosensor calibration given as current versus catechol concentration (B).

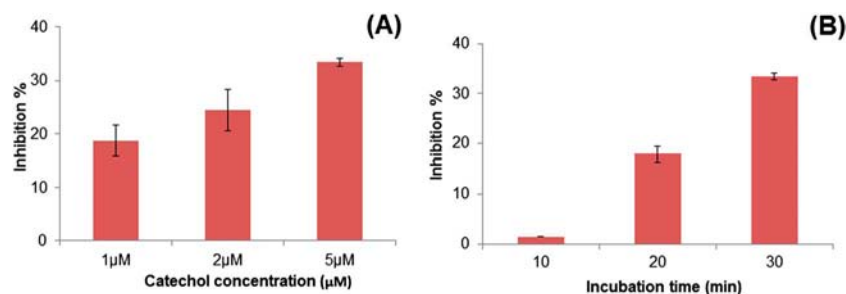


Fig. 5 Effects of substrate amount (A) and incubation time (B) on the residual activity of the catechol biosensor after pesticide incubation.

current of low concentration of the analyte (five runs) and ‘*m*’ is the slope of the related calibration graph.<sup>31–35</sup> The SPCE/IrOx/Tyr biosensor shows LOD = 0.08 μM and LOQ = 0.24 μM for catechol. The results of triplicate sets indicated by error bars reveal the in-day repeatability (Fig. 4B) of the measurements with a relative standard deviation (RSD) lower than 10%. Between-day repeatability was also obtained with a RSD value lower than 15%.

Pesticides are known to inhibit different enzymatic systems, tyrosinase being one of these.<sup>15</sup> To evaluate pesticide inhibition activity on the tyrosinase biosensor, the ‘percentage inhibition’ method was followed. The Tyr biosensor was immersed into a buffer solution under stirring and addition of catechol 5 μM was performed waiting until a steady state current response was achieved.

The stationary state current after each addition ( $I_{ss}$ ) is related to the enzyme activity of the biosensor when the inhibitor is not present. After that the same biosensor was incubated during a fixed interval of time (30 min) with chlorpyrifos pesticide. The pesticide incubated biosensor was measured again after the addition of the same concentration of catechol (5 μM). Lower steady-state currents ( $I_p$ ) were obtained due to inhibition by the pesticide. The Tyr biosensor inhibition percentage is calculated using the following equation:

$$I(\%) = \left[ \frac{(I_{ss} - I_p)}{I_{ss}} \right] \times 100 \quad (1)$$

In order to optimize the testing variables for pesticide detection using tyrosinase inhibition, catechol concentration and

incubation time were evaluated in the presence of 0.1 μM chlorpyrifos. Fig. 5A shows the optimum catechol concentration value to be used as the working substrate for Tyr inhibition experiments. Herein different concentrations of catechol (1, 2 and 5 μM) were used, and the best inhibition response was found to be achieved for a 5 μM substrate solution. The incubation time was also evaluated (see Fig. 5B) showing that when the incubation time increased the inhibition also increased. A 30 min incubation time (with stirring at 37.5 °C) was used for the following experiments.

A plot of the biosensor inhibition percentage as a function of pesticide concentration is shown in Fig. 6A. The proposed biosensor provides a linear range for chlorpyrifos concentrations from 0.01 to 0.1 μM with a correlation coefficient of 0.99 with a LOD = 0.003 μM and LOQ = 0.010 μM. As the pesticide irreversibly inhibits the enzyme, a new biosensor has to be used for each point of the calibration after being exposed to the pesticide. The results indicated by error bars reveal the in-day repeatability (Fig. 6A) of the measurements with a relative standard deviation (RSD) lower than 15%. Between-days repeatability was also obtained with a RSD value lower than 15%. These biosensors for CPF detection present high analytical performances in terms of sensitivity and LOD (Table 1 in ESI†).

To further demonstrate the applicability of the proposed biosensor, recovery tests by adding chlorpyrifos 0.1 μM into river and tap water were also performed. The results are presented in Fig. 6B. Recovery percentages of 113% ± 3.6 and 90%

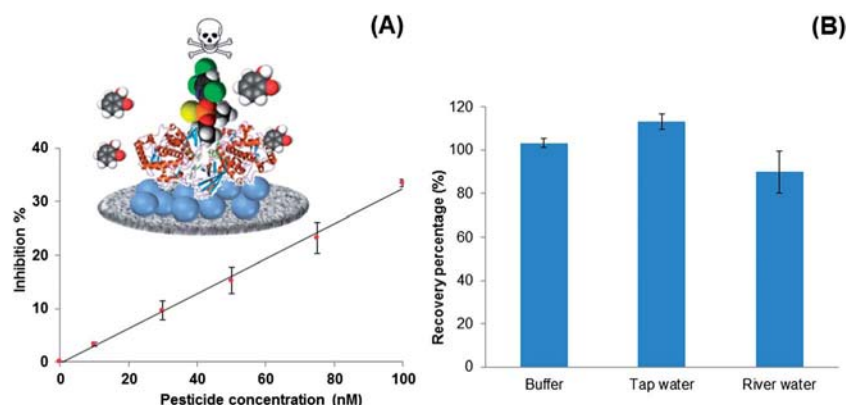


Fig. 6 Calibration curve of the biosensor as a function of the CPF concentration and the inhibition percentage (A). CPF recovery percentage from PBS, tap water and river water, using catechol biosensor (B).

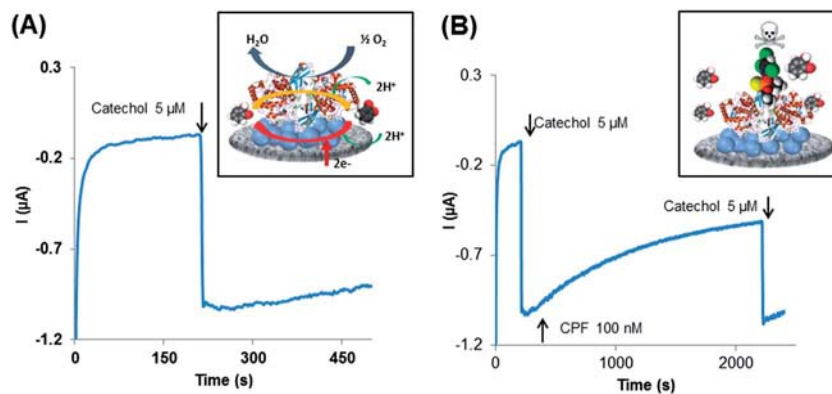


Fig. 7 IrOx nanoparticle induced dual catalytic/inhibition based detection of catechol (A) and CPF (B) using the same platform.

$\pm 9.6$  for tap and river water respectively with RSD lower than 10% ( $n = 3$ ) were found. Recovery percentages were calculated using eqn (2).

$$\text{recovery percentage} = \left( \frac{[\text{CPF}]_{\text{buffer}}}{[\text{CPF}]_{\text{real sample}}} \right) \times 100 \quad (2)$$

This indicates that the proposed biosensor can be used for trace level pesticide detection in real samples. In addition it is possible to detect catechol and CPF using the same platform given the fact that the catechol detection is almost instantaneous (10 s response time) and CPF detection requires a longer response (30 min) (see Fig. 7). It also can be extended to other kinds of enzyme and pollutant detection with interest for environmental monitoring.

## Conclusions

An IrOx NP based biosensing platform with effective tyrosinase immobilization properties and corresponding catalytic effect toward catechol is developed. Due to the high conductivity and the surface active area of the IrOx NPs, the proposed biosensor displays dramatic improvements of the analytical performance in terms of a wide linear range of response along with a good LOD and sensitivity for catechol detection. Moreover the chlorpyrifos pesticide is detected using the same biosensor through the enzyme inhibition mechanism. The LOD was found to be  $0.003 \mu\text{M}$  which is lower than the maximum contaminant level recommended by the European Environment Bureau.<sup>36</sup> In addition to the analytical performance the use of this biosensor for chlorpyrifos detection has advantages in comparison to other ones reported previously (Table 1 in ESI†) due to the fact that it is based on a simple cost-efficient screen-printed carbon electrode. In addition it is possible to detect catechol and CPF using the same platform. A careful operation of this platform should be versatile and efficient enough for dual detection applications. This dual phenol/pesticide detection biosensing system can be extended to other enzymes and consequently to other pollutants combining direct (catalytic) and indirect (inhibition) detection in the same platform.

## Acknowledgements

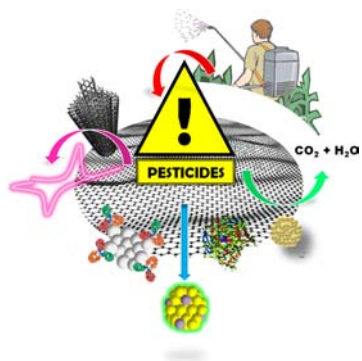
This work was supported by a grant from MICINN through MAT2011-25870 project. S. Kurbanoglu acknowledges Ankara University's BEYOD program.

## Notes and references

- 1 G. Aragay, F. Pino and A. Merkoçi, *Chem. Rev.*, 2012, **112**, 5317–5338.
- 2 C. W. Heath, *Cancer*, 1997, **80**, 1887–1888.
- 3 M. E. Ridano, A. C. Racca, J. Flores-Martín, S. A. Camolotto, G. Magnarelli de Potas, S. Genti-Raimondi and G. M. Panzetta-Dutari, *Reprod. Toxicol.*, 2012, **33**, 331–338.
- 4 A. Bódalo, E. Gómez, A. M. Hidalgo, M. Gómez, M. D. Murcia and I. López, *Desalination*, 2009, **245**, 680–686.
- 5 S. Viswanathan, H. Radecka and J. Radecki, *Biosens. Bioelectron.*, 2009, **24**, 2772–2777.
- 6 W. Zhong, D. Wang and X. Xu, *J. Hazard. Mater.*, 2012, **217–218**, 286–292.
- 7 A. Vermeulen, K. Welvaert and J. Vercammen, *J. Chromatogr., A*, 2005, **1071**, 41–46.
- 8 J. Gundel and J. Angerer, *J. Chromatogr., Biomed. Appl.*, 2000, **738**, 47–55.
- 9 J. Sherma, *Anal. Chem.*, 1993, **65**, 40R–54R.
- 10 I. Valenzuela, R. Lorenzini, M. J. Redondo and G. Font, *J. Chromatogr., A*, 1999, **839**, 101–107.
- 11 H. Wang, J. Wang, C. Timchalk and Y. Lin, *Anal. Chem.*, 2008, **80**, 8477–8484.
- 12 D. Du, W. Chen, W. Zhang, D. Liu, H. Li and Y. Lin, *Biosens. Bioelectron.*, 2010, **25**, 1370–1375.
- 13 J. Gong, Z. Guan and D. Song, *Biosens. Bioelectron.*, 2013, **39**, 320–323.
- 14 F. Arduini, S. Guidone, A. Amine, G. Paleschi and D. Moscone, *Sens. Actuators, B*, 2013, **179**, 201–208.
- 15 T. Liu, M. Xu, H. Yin, S. Ai, X. Qu and S. Zong, *Microchim. Acta*, 2011, **175**, 129–135.
- 16 S. Solé, A. Merkoçi and S. Alegret, *Crit. Rev. Anal. Chem.*, 2003, **33**, 89–126.
- 17 Y. D. Tanimoto de Albuquerque and L. F. Ferreira, *Anal. Chim. Acta*, 2007, **596**, 210–221.

- 18 C. C. Mayorga-Martinez, M. Cadevall, M. Guix, J. Ros and A. Merkoçi, *Biosens. Bioelectron.*, 2013, **40**, 57–62.
- 19 B. Pérez-López and A. Merkoçi, *Adv. Funct. Mater.*, 2011, **21**, 255–260.
- 20 C. Zhai, X. Sun, W. Zhao, Z. Gong and X. Wang, *Biosens. Bioelectron.*, 2013, **42**, 124–130.
- 21 S. Andrescu, L. Barthelmebs and J. L. Marty, *Anal. Chim. Acta*, 2002, **464**, 171–180.
- 22 J. P. Hart and S. A. Wring, *TrAC, Trends Anal. Chem.*, 1997, **16**, 89–103.
- 23 L.-G. Zamfir, L. Rotariu and C. Bala, *Biosens. Bioelectron.*, 2011, **26**, 3692–3695.
- 24 Y. Lin, F. Lu and J. Wang, *Electroanalysis*, 2004, **16**, 145–149.
- 25 S. Taufik, N. A. T. Yusof, T. W. Tee and I. Ramli, *Int. J. Electrochem.*, 2011, **6**, 1880–1891.
- 26 E. Katz and I. Willner, *Angew. Chem., Int. Ed.*, 2004, **43**, 6042–6108.
- 27 C. C. Mayorga Martinez, R. E. Madrid and C. J. Felice, *Sens. Actuators, B*, 2008, **133**, 682–686.
- 28 J. Tang, D. Tang, R. Niessner and D. Knopp, *Anal. Bioanal. Chem.*, 2011, **400**, 2041–2051.
- 29 T. Kuwabara, E. Tomita, S. Sakita, D. Hasegawa, K. Sone and M. Yagi, *J. Phys. Chem. C*, 2008, **112**, 3774–3779.
- 30 R. Meyer, S. Cogan, T. Nguyen and R. Rauh, *IEEE Trans. Neural Syst. Rehabil. Eng.*, 2001, **9**, 2–11.
- 31 C. M. Riley and T. M. Rosanske, *Development and validation of analytical methods*, Elsevier, New York, 1996.
- 32 M. E. Swartz and I. S. Krull, *Analytical method development and validation*, Marcel Dekker, New York, 1997.
- 33 J. Ermer and M. JHMcB, *Method validation in pharmaceutical analysis*, Wiley VCH, Weinheim, 2005.
- 34 P. De Bièvre and H. Günzler, *Validation in chemical measurements*, Springer, Berlin, 2005.
- 35 S. A. Ozkan, *Electroanalytical Methods in Pharmaceutical Analysis and Their Validation*, HNB Publishing, New York, 2012.
- 36 Council Directive 98/83/EC 1998 on the quality of water intended for human consumption, *Official Journal of the European Communities*, <http://eurlex.europa.eu/LexUriServ/LexUriServ.do?uri=OJ:L:1998:330:0032:0054:EN:PDF>.

## Nanomaterials for Sensing and Destroying Pesticides

Gemma Aragay,<sup>†</sup> Flavio Pino,<sup>†</sup> and Arben Merkoçi<sup>\*,†,‡</sup><sup>†</sup>Nanobioelectronics and Biosensors Group, Catalan Institute of Nanotechnology, UAB Campus, 08193 Bellaterra, Barcelona, Spain<sup>‡</sup>ICREA, Barcelona, Spain

## CONTENTS

1. Introduction	5317
2. Optical Sensing	5318
2.1. Optical-Based Immunosensors	5319
2.2. Enzyme-Based Optical Strategies	5321
2.3. MIPs and Other Host–Guest-Like Systems	5323
2.4. Alternative Optical Strategies	5324
3. Electrochemical Sensing	5325
3.1. Electrochemical-Based Immunosensors	5325
3.2. Enzyme-Based Electrochemical Systems	5327
3.3. MIPs and Other Host–Guest-Like Systems	5329
3.4. Other Electrochemical Strategies	5329
4. Degradation and Removal of Pesticides	5331
4.1. Degradation of Pesticides	5332
4.2. Pesticides Removal	5334
5. Conclusions and Future Prospects	5334
Author Information	5335
Corresponding Author	5335
Notes	5335
Biographies	5335
Acknowledgments	5335
References	5336

## 1. INTRODUCTION

The term *pesticide* is generally used for chemicals used to control and/or eliminate plant or animal pests and diseases. Pesticides can be classified as *herbicides*, *insecticides*, *fungicides*, or other types according to their purpose, and they involve different chemical compounds, the most common of which are arsenic, carbamates, organophosphates, pyrethroids, and nitrophenol derivatives. Pesticides can be classified by biological target, chemical structure, or safety profile. Table 1 gives an overview of pesticides (classified chemically), including their chemical formula, commercial name, and safety risks with their corresponding symptoms that manifest in humans.<sup>1</sup>

As revealed by Table 1, the most hazardous pesticides are carbamates, coumarin, organochlorides, organophosphates, and arsenic and mercury derivatives, all of which can be highly toxic to humans, chiefly by affecting the central nervous system (CNS). Because of the high toxicity of pesticides, environmental agencies have set maximum values for their contamination levels in drinking and surface water.<sup>2,3</sup>

Depending on their aqueous solubility, pesticides either remain in the soil or enter surface waters and groundwaters. The compounds that result from pesticide degradation can remain in animals, vegetables, and water sources, and they can become more concentrated as they move up the food chain. Because of the toxicity of these compounds—even at trace levels—there is increasing interest in the development of systems to sense, monitor, break down, and/or remove them.

Pesticides have traditionally been detected using high-performance liquid chromatography (HPLC) and GC/MS, which offer powerful trace analysis with high reproducibility and very low detection limits. However, these techniques involve extraction of large volumes of water, require extensive purification, often including derivatization, and demand qualified personnel and expensive equipment.<sup>4–6</sup> Thus, for many years efforts have been devoted to the development of cheap, user-friendly biosensing systems for pesticides and their derivatives, based mainly on electrochemical and optical techniques.<sup>7</sup> Albeit biosensing methods do not always offer the extremely low detection limits of the aforementioned conventional techniques, they do enable in situ analysis, which is in high demand for pesticide detection.

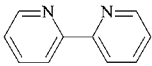
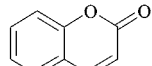
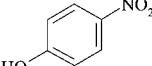
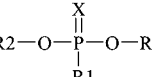
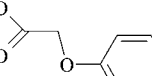
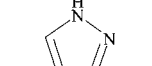
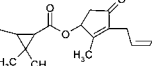
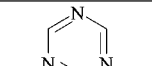
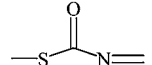
Great progress has recently been made in applying nanomaterials to sensor and biosensor development.<sup>8–11</sup> Owing to the properties afforded by the small size of nanomaterials—their large surface-to-volume ratios; their physicochemical properties, composition, and shape; and their unusual target binding characteristics—these sensors can markedly improve the sensitivity and specificity of analyte detection. Said properties, together with the overall structural robustness of nanomaterials, make these materials highly amenable for use in various detection schemes based on diverse transduction modes. An explosion of research in this field has yielded myriad approaches to pesticide detection and degradation systems employing various kinds of nanomaterials, including metal nanoparticles (MNPs), carbon nanotubes (CNTs), graphene, magnetic nanoparticles, and/or quantum dots.<sup>12,13</sup>

Beyond sensing systems, nanomaterials are also being harnessed to destroy pesticides. The unique surface area and the surface activity of the nanoparticles play a critical role in the

Received: January 18, 2012

Published: August 16, 2012

Table 1. Overview of Major Pesticide Classes<sup>a</sup>

Chemical class	Code	Chemical formula	Commercial group	Human hazardous risk	Symptoms of exposure
Arsenic compounds	AS	AsO <sub>4</sub> <sup>3-</sup>	Fungicide Insecticide Herbicide	Ia, Ib	Stomachache, nausea, vomiting, and diarrhea
Bipyridylum derivatives	BP		Herbicide	II	Neurologic effects, irritation
Carbamates	C	(-OCONHCH <sub>3</sub> )	Acaricide Fungicide	Ia, Ib, II, U	Central nervous system effects
Coumarin derivatives	CO		Rodenticide	Ia, Ib	Internal hemorrhage
Copper compounds	CU	CuO, CuS, Cu(OH) <sub>2</sub>	Algaecide Fungicide Insecticide	U	Skin and respiratory irritation
Mercury compounds	HG	Inorganic and Organic mercury	Fungicide	Ia, Ib, II	Neurological effects
Nitrophenol derivatives	NP		Acaricide Fungicide Herbicide Insecticide	Ib, II	Nausea, vomiting, and diarrhea
Organochlorine compounds	OC	-CH <sub>2</sub> Cl	Fungicide Insecticide	Ia, U	Gastrointestinal and neurological effects
Organophosphorous compounds	OP		Acaricide Fungicide Rodenticide	Ia, Ib, II, III	Central nervous system effects
Organotin compounds	OT	R <sub>4</sub> Sn, R <sub>3</sub> SnX, R <sub>2</sub> SnX <sub>2</sub> , RSnX <sub>3</sub>	Fungicide Herbicide	II	Gastrointestinal irritation
Phenoxyacetic acid derivatives	PAA		Herbicide	II, U	Skin and eye irritation
Pyrazole derivatives	PZ		Insecticide	U	Cytotoxic and mutagenic effects
Pyrethroids	PY		Acaricide Insecticide	Ib, II, III, U	Respiratory irritation
Triazine derivatives	T		Herbicide	II, U	Nausea, vomiting, diarrhea and abdominal pain
Thiocarbamates	TC		Acaricide Fungicide	III, U	Irritation

<sup>a</sup>Ia, extremely hazardous; Ib, highly hazardous; II, moderately hazardous; III, slightly hazardous; U, unlikely to present acute hazard.

catalytic reactions used to degrade pesticides with the formation of benign products.

This review presents novel advances in pesticide detection strategies that involve optical and/or electrochemical detection in tandem with nanomaterials, either as transducing platforms or as labels. It also covers different nanomaterials-based strategies for pesticide removal and/or destruction.

## 2. OPTICAL SENSING

The optical properties of nanomaterials are closely related to their size and to the surface-induced changes in their electronic structure. These properties have been exploited in pesticide-detection systems, which are most often based on colorimetric techniques or fluorescence (see Table 2).

Table 2. Optical Strategies for Pesticide Detection<sup>a</sup>

recognition principle	pesticide	(nano)material	recognition element	D.L.	detection technique	sample matrix	ref
immunoassay	2,4-dichloro phenoxyacetic acid	CdTe QDs	anti-2,4-D-IgG Ab	1.1 nM	FIA		22
	chlorpyrifos	CdTe QDs	anti-CPF Ab	11 nM	FIA	drinking water samples	23
	pyrethroid	QDs	anti-PBA Ab anti-AM Ab	0.5 nM	multiplexed competitive LFIA		25
	atrazine	polystyrene-Eu(III) chelate NP	anti-atrazine Ab	0.4 nM	competitive FIA		27
	atrazine	Eu <sub>2</sub> O <sub>3</sub> NP	anti-atrazine Ab	2 nM	competitive FIA		28
	pyrethroid/ endosulfan	AuNP's	anti-pyrethroid Ab anti-endosulfan Ab	800/4 nM	colorimetric competitive LFIA		34
	carbofuran/ triazophos	AuNP's	anti-carbofuran Ab anti-triazophos Ab	0.14/0.012 μM	colorimetric competitive LFIA	spiked, tap, surface, and groundwater	35
	methiocarb	carbon NPs	anti-methiocarbAb	0.6 nM	colorimetric competitive LFIA	surface water	39
	chlorpyrifos	CdS@ZnS QDs	anti-TCPAb	2.9 nM	fluorescence competitive LFIA	rat plasma samples	41
	enzyme inhibition	carbamate/ organophosphate	IPA	AChE	1–10 nM	colorimetric paper based assay	beverages and food samples
paraoxon		TNB	AChE	100 nM	Ellman's colorimetric paper-based assay		44
paraoxon		AuNP's	AChE	10 nM	growth of AuNP–colorimetric		47
BW284c51		CdS QDs	AChE	50 nM	growth of QDs–fluorescence		48
paraoxon/ parathion		CdTe QDs	AChE	0.01 nM/0.005 nM	fluorescence quenching	vegetables and fruit	49
paraoxon		AuNP's	AChE	0.9 nM	LSPR		51
host–guest		atrazine	label-free	atrazine-imprinted photonic polymer	0.001 nM	colorimetric	phosphate buffer
atrazine	molecular imprinted SiNPs	MIP of zinc protoporphyrin and MAA	1.8 μM	fluorescence	lake water	55	
parathion	AuNP's	mono-6-thio-β-cyclodextrin	1 × 10 <sup>-12</sup> M	SERS		57	
atrazine	AuNP's	molecularly imprinted nanocomposite	5 pM	SPR	acetonitrile	58	
fenamithion/ acetamiprid	CdTe QDs	<i>p</i> -sulfonatocalix [4] arene	1.2 × 10 <sup>-8</sup> M/3.4 × 10 <sup>-8</sup> M	fluorescence	garlic samples	63	
other methods	β-endosulfan	AgNPs	lucigerine dication	50 μM	SERS		65
	organophosphate	AuNP's-Eu <sup>3+</sup>	Eu <sup>3+</sup>	1 μM	NSEF		68
	parathion	Au/SiO <sub>2</sub> NPs			SHINERS	citrus fruits	71

<sup>a</sup>Ab, antibody; AChE, acetylcholinesterase; LFIA, lateral flow immunoassay; FIA, fluoroimmunoassay; TCP, trichloropyridinol; PBA, phenoxybenzoic acid; AM, atrazine mercapturic acid; SPR, surface plasmon resonance; TNB, 5-thio-2-nitrobenzoate; IPA, indophenyl acetate; MIP, molecular imprinted polymer; MAA, methacrylic acid; SERS, surface-enhanced Raman scattering; SHINERS, shell-isolated nanoparticle-enhanced Raman scattering; NSEF, normalized scattering electric field.

## 2.1. Optical-Based Immunosensors

Immunoassays have been used for many years in clinical chemistry as reliable and sensitive strategies to determine low concentrations of analytes in different matrices.<sup>14</sup> The use of immunoassays for sensing is advantageous in terms of speed, simplicity, reliability, cost-effectiveness, and other factors.

Immunoassays for various targets, including pesticides, have been adapted for field measurements. Indeed, reports indicate an increasing number of successful studies on immunoassay systems for pesticide monitoring.<sup>15–19</sup>

Immunoassays exploit the strong, specific interaction between an antibody (Ab) and its corresponding specific antigen (Ag). Antibodies are specifically generated by the immune system to defend against foreign substances (antigens). Substances with molecular weights lower than 1 000 Da (e.g., most pesticides) do not provoke an

immunogenic reaction alone but can do so upon binding to larger molecules (e.g., albumin). Such low-molecular-weight substances are called *haptens*. Although the production of haptens and their corresponding antibodies is fairly tedious, many kinds of immunoassay formats have been developed. Competitive immunoassays are the most frequently used type for pesticide sensing using optical detection. A schematic of a conventional competitive immunoassay for pesticide detection is shown in Figure 1. These immunoassays typically take one of two formats: they feature an immobilized antibody coupled to an antigen (hapten) label (Figure 1A) or vice versa (Figure 1B). Nonetheless, novel formats are being designed to avoid nonspecific reactions.

Different types of nanomaterials, including metal nanoparticles (e.g., gold nanoparticles (AuNP's)) and semiconductor nanoparticles (e.g., quantum dots (QDs)), have

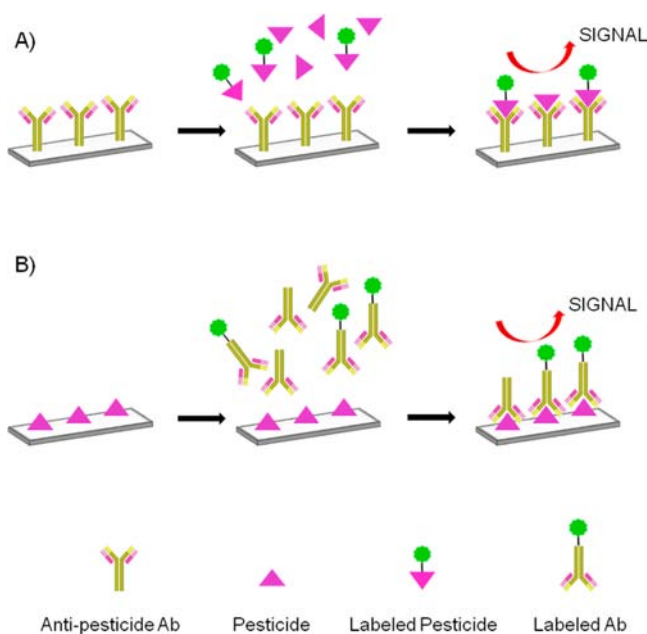


**Figure 1.** Schematic of traditional competitive immunoassay formats for pesticide detection. The concentration of analyte to be monitored is correlated with the amount of labeled antigen (A) or antibody (B) to the corresponding ligand coated on the transducer surface.

been widely used as versatile labels in immunoassays and enable superior signal amplification compared to traditional labels (e.g., organic dyes). Fluorescence-based immunoassays have become the most widely reported methods, probably due to the higher sensitivity of fluorescence techniques compared to colorimetric ones. Quantum dots have been the most widely used fluorescent labels, owing to their small size, high photostability, and size-tunable emission properties.<sup>20</sup> They are superior to conventional organic labels in many areas, including brightness (high extinction coefficient) and photostability (less photobleaching).<sup>21</sup>

Vinayaka et al. detected the common herbicide 2,4-dichlorophenoxyacetic acid (2,4-D) by exploiting the fluorescence properties of cadmium telluride (CdTe) QDs.<sup>22</sup> 2,4-D was first conjugated with alkaline phosphatase enzyme (ALP) to afford a 2,4-D–ALP conjugate, which was then reacted with mercaptopropionic acid (MPA)-coated QDs. Anti-2,4-D antibodies were immobilized in a glass capillary column. The assay is based on a competitive immunoassay between free 2,4-D and the 2,4-D–ALP–CdTe QDs conjugates, which were passed through the capillary column. Given the high concentration of free 2,4-D in the sample, less conjugate is immobilized in the column, and therefore, the collected sample will have a higher fluorescence. Using this strategy, Vinayaka et al. achieved a detection limit of 1.1 nM, a far lower threshold than they had previously obtained using an enzyme-linked immunosorbent assay (ELISA) test (4.4 nM). However, despite its low detection limits, in our opinion their system is limited by the fact that it is relatively complicated and is not robust.

Chen et al. described another QD-based immunoassay, used to detect the pesticide chlorpyrifos (CPF) in drinking water.<sup>23</sup> They treated CPF with 3-MPA and then added bovine serum albumin (BSA) to the resulting mixture to obtain a CPF–BSA conjugate, which they immobilized onto a microwell plate by simple adsorption. A specific anti-CPF biotin was modified with biotin, mixed with QDs that had previously been modified with

streptavidin, and then mixed together with the sample in the plate. As the amount of CPF present increases, the amount of Ab–QDs immobilized in the plate decreases, which translates into a diminishing fluorescence output signal. The system exhibits excellent accuracy and low variability, even in analysis of real (drinking water) samples. The authors reported an impressively low detection limit of 10 nM of CPF. However, the assay remains limited to lab use, because an integrated system has not been yet developed for practical use.

Among the advantages of using QDs there is the possibility to use different types of QDs as distinct labels to simultaneously analyze different analytes in the same (multiplex) device, based on the fact that each type of QD generates a unique fluorescence signal.<sup>24</sup> Nichkova et al. exploited this approach to develop a microarray system that can simultaneously detect 3-phenoxybenzoic acid (PBA) and atrazine mercapturate (AM).<sup>25</sup> Two different kinds of QDs with different spectral emissions (at 580 and 620 nm, respectively) were used for their simultaneous detection.

Quantum dots are not the only type of fluorescent label for pesticide immunoassays: nanoparticles, such as europium-based NPs, have also been used. With europium-based labels, the background emission is reduced due to their large Stokes shift and narrow emission bands, as well as the lack of quenching when multiple labeling is used. Unlike semiconductor QDs, the emission wavelength of lanthanide oxide nanoparticles is independent of particle size; hence, sample homogeneity is less crucial, enabling cheaper synthesis.<sup>26–28</sup> In this context, Nichkova et al. reported a microarray immunoassay for phenoxybenzoic acid (PBA) detection using Eu:Gd<sub>2</sub>O<sub>3</sub> nanoparticles labels tracked by confocal fluorescence microscopy.<sup>29</sup> Phenoxybenzoic acid is a generic biomarker of human exposure to pyrethroid insecticides. Although the detection limit in their system is even lower than the limit suggested by the U.S. Environmental Protection Agency (EPA; 6.5 nM PBA), confocal fluorescence microscopy is not amenable to field measurements.

The combination of fluorescence and magnetism is a new and powerful strategy that offers the high sensitivity of fluorescence labels plus the advantages of magnetic field manipulation (for mixing, temperature control, separation, and even preconcentration steps).<sup>30</sup> Particles combining these properties, such as lanthanide Tb core–shell NPs, have been used in detection of pyrethroid insecticide metabolites<sup>31</sup> not as reporter labels but rather as internal immunoassay standards that have enabled improved reproducibility.

Most of the previously described systems require expensive equipment and trained personnel for operations. Given the demand for overall speed and simplicity, lateral-flow immunoassays (LFIAs) have arisen as a suitable alternative,<sup>32</sup> as they are user-friendly, fast, and cost-effective, making them well-suited for on-site pesticide screening. Several LFIAs for pesticide detection have been reported over the past few years.<sup>33</sup>

In a typical NP-based LFIA (Figure 2A), the sample (“a” in Figure 2A) and the specific antibody–NP conjugate (“b” in Figure 2A) migrate along the reagent-coated membrane strip (“c” in Figure 2A). The detection takes place depending on the corresponding affinity interactions in the test and control lines (“c.1” and “c.2”, respectively, in Figure 2A).

Several authors have reported immunochromatographic test strips for different pesticides using gold nanoparticle (AuNP) labels.<sup>34–37</sup> The broad application of AuNP’s in LFIA is related



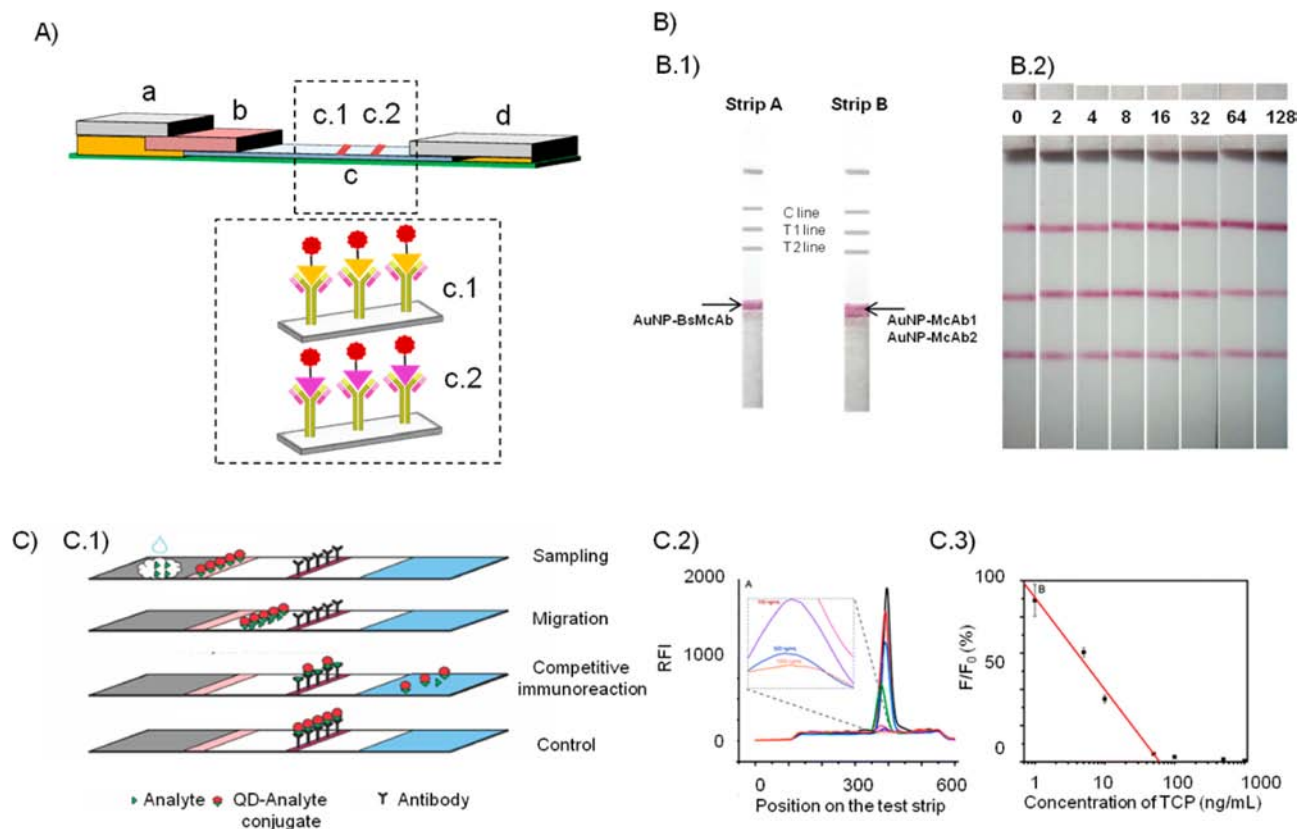


**Figure 2.** (A) Basic schematic of a lateral flow immunoassay. (a, sample pad; b, conjugation pad; c, nitrocellulose pad; c.1, test line; c.2, control line; d, adsorbent pad). (B) Colorimetric immunochromatographic test for triazophos and carbofuran. (B.1) Schematic diagram of one-step multiplex strips. Strip A has gold-labeled, bispecific monoclonal Ab (BsMcAb), and strip B has two conjugate pads with gold labeled anticarbofuran monoclonal Ab (McAb1) and antitriazophos (McAb2). (B.2) Dual pesticide immunoassay using strip format B. Mixed standard solutions of carbofuran and triazophos at each final concentration of 0, 2, 4, 8, 16, 32, 64, and 128  $\mu\text{g/L}$ . Reprinted with permission from ref 35. Copyright 2009 Elsevier. (C) Fluoroimmunoassay for trichloropyridinol. (C.1) Schematic illustration of the principle of fluorescence LFIA; (C.2) typical fluorescent responses of the immunosensor with increasing concentration of trichloropyridinol used as target; (C.3) corresponding calibration curve. Reprinted with permission from ref 41. Copyright 2010 American Chemical Society.

to the fact that these NPs can be easily obtained and conjugated and that the final test result is observable by the naked eye.

By combining AuNP's with different antibodies for different pesticides, one can achieve multiplex detection in a single strip (see Figure 2B). Guo et al. reported two AuNP-based LFIA formats (strips A and B in Figure 2B.1) for simultaneous detection of carbofuran and triazophos.<sup>35</sup> Strip A is based on a bispecific monoclonal antibody (BsMcAbs) against both pesticides, which, when combined with AuNP's, gives visual detection limits of 0.3  $\mu\text{M}$  for carbofuran and 0.03  $\mu\text{M}$  for triazophos. Strip B is based on two AuNP-labeled monospecific Abs (McAbs), separately immobilized onto the conjugation pad, offering detection limits of 150 nM for carbofuran and 12 nM for triazophos, with no cross-reactivity. Owing to the better performance of strip B, the authors decided to use this format for analysis of real samples (spiked tap water, surface water, and groundwater samples).<sup>35</sup>

Colorimetric LFIA's incorporating alternative labels, such as carbon nanoparticles<sup>38,39</sup> or  $\text{Fe}_3\text{O}_4$  nanoparticles,<sup>40</sup> have also been developed for pesticide detection. In addition to colorimetric techniques, fluorescence techniques are also used in LFIA's, in which the most commonly applied labels are semiconductor QDs, as happens in solution analysis. Table 2 summarizes the performance of various LFIA's involving either QDs or AuNP's for detection of distinct pesticide targets. As clearly indicated by the table, QDs enable much greater

sensitivity (on the order of ng/mL) than do AuNP's (on the order of  $\mu\text{g/mL}$ ).

In this context, Zou et al. recently reported the use of a QD-based LFIA for biomonitoring of trichloropyridinol (TCP), a biomarker of chlorpyrifos (CPF) exposure.<sup>41</sup> It is based on a competitive immunoreaction between the sample analyte (TCP) and QD-TCP conjugates. As illustrated in Figure 2C.1, an aqueous sample containing the target analyte is applied to the sample zone; it then migrates via capillary action toward the other end of the strip, together with the QD-TCP conjugate immobilized on the conjugation pad. If no analyte is present in the sample, then the QD-TCP conjugates fully bind to the Ab's in the test zone (Figure 2C.1). As the amount of analyte in the sample increases, the fluorescence signal (measured with a strip reader) decreases. Typical fluorescent responses of the immunosensor upon increasing concentration of TCP are shown in Figure 2C.2, together with the resulting calibration curve (Figure 2C.3). The authors estimated a detection limit of 5 nM TCP. However, they affirm that the reliability of the measurements could be improved by using a control line in addition to the test line.

## 2.2. Enzyme-Based Optical Strategies

Many pesticides are inhibitors of cholinesterases (ChE's), enzymes that are critical in neurobiology, toxicology, pharmacology, and other areas. Hence, efficient assay methods

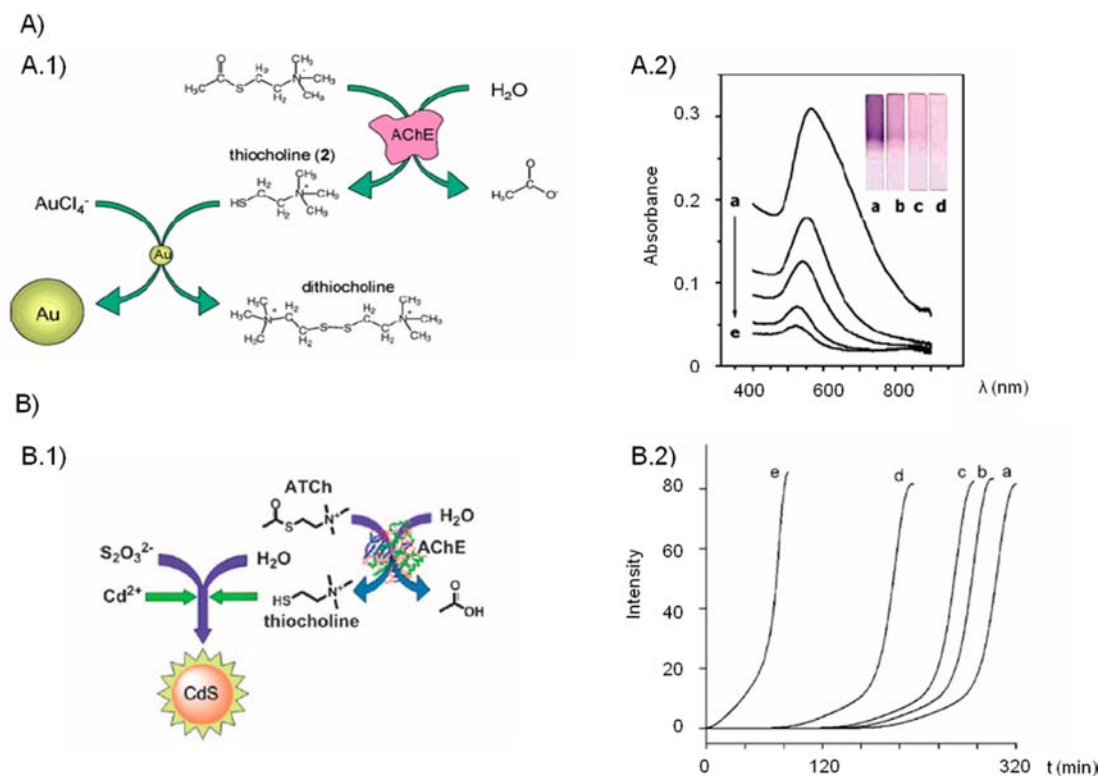
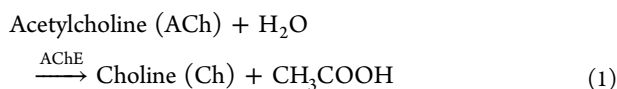


**Figure 3.** (A) (A.1) Detection of acetylcholinesterase activity by growth of Au nanoparticles; (A.2) absorbance spectra corresponding to the inhibition of AuNP growth on glass support, recorded in the presence of AChE, 0.13 units/mL, HAuCl<sub>4</sub>, 1.1 × 10<sup>-3</sup> M, 1.4 × 10<sup>-4</sup> M, and different concentrations of inhibitor: (a) 0; (b) 5.9 × 10<sup>-7</sup>; (c) 1.2 × 10<sup>-6</sup>; (d) 2.4 × 10<sup>-6</sup>; and (e) 5.9 × 10<sup>-6</sup> M. Inset: Images of glass slides formed in the presence of the respective concentrations of the inhibitor (left, no inhibitor; right, 2.410<sup>-6</sup> M inhibitor). Reprinted with permission from ref 47. Copyright 2005 American Chemical Society. (B) (B.1) Principle of enzymatic generation of CdS QDs for the detection of AChE activity. (B.2) Evolution of the fluorescence intensity of the CdS QDs formed in the presence of ATCh (10 mM) and different concentrations of AChE: (a) 0; (b) 25; (c) 50; (d) 100; and (e) 250 mU mL<sup>-1</sup>. In all experiments, the system included sodium thiosulfate (0.3 M) and CdSO<sub>4</sub> (1 mM). Reprinted with permission from ref 48. Copyright 2010 Wiley-VCH.

for ChE activities can be harnessed for pesticide detection.<sup>42</sup> Acetylcholinesterase (AChE) is a cholinesterase that hydrolyzes acetyl esters such as acetylcholine (see eq 1).



Acetylcholinesterase is crucial to human and animal health. Numerous methods have been reported for determination of AChE activity and inhibition. Typical methods in these assays include Ellman's colorimetric method<sup>43,44</sup> or the detection of hydrogen peroxide produced by oxidation of choline.<sup>45</sup> An ultrasensitive method to determine pesticides in a glass lab-on-a-chip via enzymatic inhibition of AChE immobilized onto magnetic microbeads was developed.<sup>46</sup> Extremely low limits of detection (nanomolar level for carbofuran) are achieved by enzymatic inhibition and amperometric detection in a glass lab-on-a-chip device by controlling the amount of magnetic beads, which leads to a high and controlled inhibited/noninhibited enzyme ratio.<sup>46</sup> Incorporation of nanomaterials into sensing systems has greatly facilitated development of alternative assays for determining the activity and inhibition of ChE's, and consequently, for indirectly detecting different kinds of pesticides, mainly carbamates and organophosphorous compounds (see Table 2).

Pavlov et al. developed a proof-of-concept method for indirect pesticide detection based on the growth of AuNP

stimulated by the presence of thiocholine.<sup>47</sup> The AChE mediates hydrolysis of acetylthiocholine, which yields a reducing agent, thiocholine, which in turn can catalyze the growth of AuNP seeds in the presence of AuCl<sub>4</sub><sup>-</sup> (see Figure 3A.1). If AChE activity is inhibited by any pesticides present, then the hydrolysis does not occur, and consequently, less AuNP's are formed. A detection limit of 10 nM (for paraoxon) was achieved using this system. Figure 3A.2 shows absorbance spectra corresponding to the inhibition of AuNP growth on glass supports recorded in the presence of AChE. In the absence of pesticide, the glass surface is blue; however, as the concentration of paraoxon increases, the surface loses its blue color as the plasmon band is blue-shifted and its intensity decreases.

The same group proposed a similar system for the enzymatic growth of CdS QDs instead of AuNP's (See Figure 3B.1).<sup>48</sup> Thiol-containing molecules (in this case, thiocholine) promote the decomposition of S<sub>2</sub>O<sub>3</sub><sup>2-</sup> to H<sub>2</sub>S, which, in the presence of Cd<sup>2+</sup> ions, forms fluorescent nanocrystals of CdS. Formation of these fluorescent nanoparticles is monitored by fluorescence spectroscopy. Figure 3B.2 depicts the change in fluorescence in response to a fixed level of acetylthiocholine (ATCh) and varying levels of AChE. As the concentration of AChE increases, so does the rate of CdS QDs generation.

More recently, Zheng et al. reported an organophosphorous pesticide (OP) biosensor based on quenching, upon thiocholine production, of the fluorescence from CdTe QDs that are

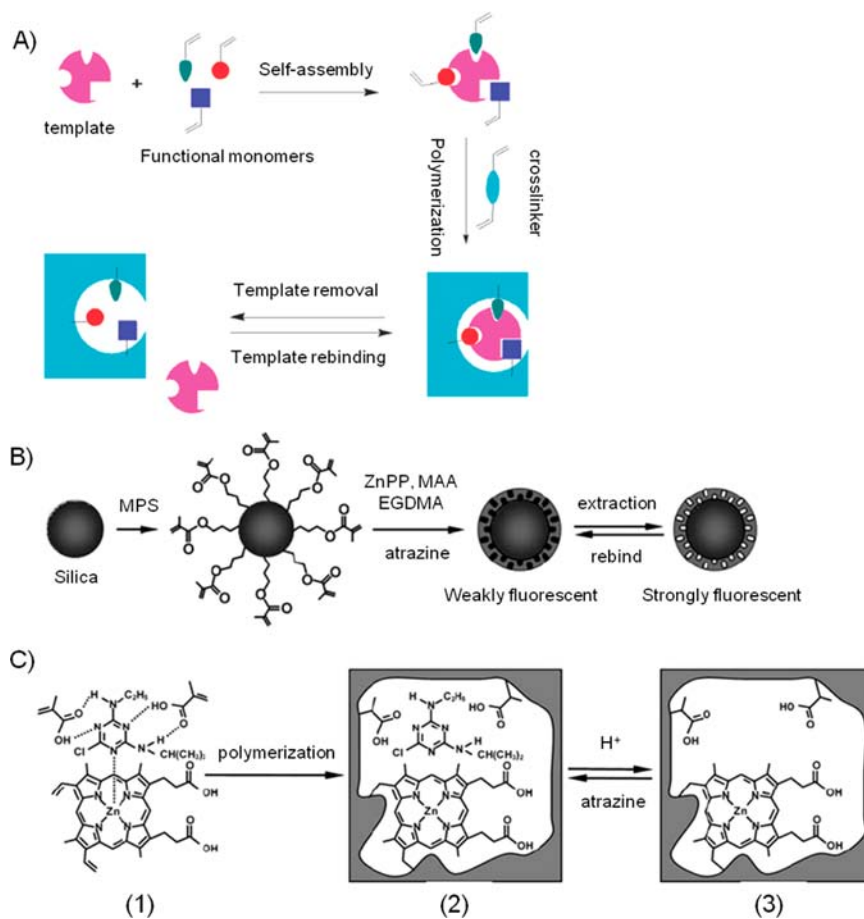


**Figure 4.** (A) General scheme of MIP preparation. Reprinted with permission from ref 53. Copyright 2007 Springer. (B) The mechanism of formation of atrazine-imprinted core-shell nanoparticles. (C) Schematic representation of molecular imprinting of atrazine using both ZnPP (Zn(II) protoporphyrin) and methacrylic acid (MAA) as functional monomers. Reprinted with permission from ref 55. Copyright 2011 RSC.

embedded in a multilayer platform of AChE.<sup>49</sup> When OPs are introduced into the solution, they interact with the active centers of AChE, causing its activity to decrease. This leads to a decrease in thiocholine production and, consequently, to a decrease in the quenching rate of the QDs. The authors also analyzed real fruit and vegetable samples containing picomolar concentrations of paraoxon and/or parathion, using a facile sample pretreatment method. However, the sensor responds differently to different pesticides, meaning that measurement may not be accurate for samples containing pesticide mixtures.

Similar to this work, Zheng et al. designed a multilayer film based on CdTe QDs, AChE, and choline oxidase for choline degradation that produces H<sub>2</sub>O<sub>2</sub>.<sup>50</sup> The authors discuss the possible surface etching of the QDs by H<sub>2</sub>O<sub>2</sub>, leading to production of more surface defects and a gradual decrease of QD sizes with the consequent decrease on the fluorescence.

Acetylcholinesterase inhibition has also been monitored using a localized surface plasmon resonance (LSPR) fiber optic biosensor.<sup>51</sup> The enzyme is immobilized onto a AuNP layer; its inhibition by pesticides (e.g., paraoxon) alters the light attenuation. The correlation between inhibition and light attenuation enables quantification of the pesticide concentration.

### 2.3. MIPs and Other Host–Guest-Like Systems

Production of high-affinity specific antibodies for immunoassays (section 3.1) is among the most complicated challenges in the development of such sensing systems, especially given

the difficulty of obtaining antibodies that are specific to a particular pesticide. In addition, natural antibodies are highly expensive and may undergo mutation, thus varying the interaction capacity of the recognition sites. Molecular imprinted polymers (MIPs) have attracted considerable attention as an alternative for preparing molecular recognition systems mimicking the specific binding events of antibodies.<sup>52,53</sup>

Generally, MIPs are prepared via polymerization of the appropriate monomer(s) in the presence of the target molecule or template (e.g., pesticide). After polymerization, the target is chemically removed, leaving behind nanocavities with the exact size, shape, and corresponding functional groups capable of rebinding the target with a high degree of selectivity. A general scheme of MIP preparation is shown in Figure 4A.

Wu and co-workers have developed a label-free colorimetric method for detecting trace levels of atrazine, based on a molecularly imprinted photonic polymer.<sup>54</sup> The photonic properties of the platform come from its 3D highly ordered macroporous structure, which gives rise to a readable optical signal via changes in diffraction properties of the macroporous arrays. The detection limit is very low (0.001 nM of atrazine), and the changes can even be observed by the naked eye. Such systems do not require any additional transduction element, making them highly interesting for future development of smart devices for sensor applications.

Although label-free systems are desired, the combination of specific molecular recognition nanocavities with other nanostructures that can act as recognition labels to provide moderate enhancements to sensitivity and, consequently, enable lower detection limits. For example, a combination of MIPs with fluorescent silica nanoparticle (SiNP) cores has been reported for use in pesticide detection in the field.<sup>55,56</sup> Direct imprinting polymerization at the surface of SiNPs enables integration and coupling of the recognition and transducing elements. Figure 4B shows the surface of SiNPs functionalized with vinyl groups that enable polymerization of MIPs onto the nanoparticle surface.<sup>55</sup> The researchers employed fluorescent Zn(II) protoporphyrin (ZnPP) as the reporter of atrazine binding, harnessing its fluorescence properties, which are tunable via coordination of one of the nitrogen atoms from the target toward the metal (Zn(II)). Figure 4C shows the monomer template (1), the molecular imprinting polymerization (2), and the extraction and rebinding of template molecules of the chemosensor (3).<sup>55</sup>

Gold nanoparticles also have been applied for atrazine detection.<sup>57,58</sup> A selective atrazine MIP was placed onto a gold surface combined with AuNP's, and the angle-shift upon atrazine binding was studied.<sup>58</sup> The main role of AuNP's is to provide an enhancement of the local electromagnetic field by a coupling effect with the gold film. In this way, very low detection limits (picomolar level) were achieved using surface plasmon resonance (SPR).

Recently, Zhao et al. reported quantum dot-based molecularly imprinted polymer (QD-MIP) composite nanospheres for quantification of the pesticide diazinon via quenching of the system's fluorescence.<sup>59</sup> They demonstrated overlapping of the QD excitation band and the diazinon absorption band, which results in energy transfer from the QDs to the pesticide, thereby leading to quenching of the QD fluorescence. Furthermore, the authors introduced other pesticides into the system to evaluate any possible interference effects, without any affect on the system's fluorescence.

Similarly to the work above, Li et al. reported silica nanosphere-embedded CdSe quantum dots modified with an MIP layer (CdSe@SiO<sub>2</sub>@MIP) for detection of the pyrethroid pesticide lambda-cyhalothrin.<sup>60</sup> They attributed the sensing signal to the fact that lambda-cyhalothrin can act as an efficient hole or electron acceptor, thereby introducing new, non-radiative decay pathways for the excitation. As such, quenching of the system fluorescence indicates the presence of the analyte.

In addition to the host-guest-like chemistry of MIPs, researchers have also employed combinations of macromolecules and nanomaterials for pesticide detection using optical techniques. Calixarene-based molecules are a good example of macrocyclic compounds that can accommodate other molecules in their cavities with fairly good selectivity.<sup>61</sup> Their supramolecular chemistry, along with their ability to be involved in self-assembly processes for the construction of new nanomaterials, has recently been reported.<sup>62</sup>

Qu et al. reported a simple, rapid, and sensitive detection system for fenamithion and acetamiprid based on *p*-sulfonatocalix[4]arene and CdTe QDs.<sup>63</sup> The authors reported that interaction of free QDs and fenamithion leads to a selective decrease in QD fluorescence. They also described the ability of acetamiprid to enter the cavity of the calixarene unit to form a complex that alters the emission wavelength of the QDs such that they exhibit a blue-shift and even an increase in fluorescence emission intensity. They attributed this blue-shift

to the physical deformation of the QDs when they were near the acetamiprid/*p*-sulfonatocalix[4]arene inclusion complex, which may change the emission wavelength of the CdTe QDs.

Cyclodextrins are also good receptors for host-guest interactions.<sup>64</sup> In this context, Wang et al. recently reported the use of a mono-6-thio- $\beta$ -cyclodextrin combination with AuNP's to efficiently capture methyl parathion at picomolar levels via surface-enhanced Raman scattering (SERS),<sup>57</sup> a powerful analytical technique for rapid and sensitive detection of chemical and structural data at the microscopic scale. Compared with the other methods appearing in Table 2, this method has drastically higher detection levels ( $1 \times 10^{-12}$  M for parathion). However, the system is complex and must be operated by specialized personnel.

Although MIPs and other host-guest receptors present many significant advantages over biological receptors, such as greater stability, lower cost, and more engineering options, they are also associated with many problems, including template leakage, incompatibility in aqueous media, low binding capacity, and slow mass transfer.

#### 2.4. Alternative Optical Strategies

Recent advances have greatly improved the sensitivity of optical pesticide sensors based on nanomaterials that do not require immunoassays, host-guest chemistry, or enzyme-inhibition strategies. In this context, AgNPs have been used in combination with lucigenine dication (LG) for detection of the organochlorine pesticide endosulfan (ES).<sup>65</sup> In the presence of halides, LG can be strongly attached to a metal surface.<sup>66</sup> Thus, in a sensor based on metallic nanostructures LG can act simultaneously as a recognition element for ES and for metallic nanostructures: interaction between the two compounds leads to an enhancement of the Raman spectrum. The analyte is detected by SERS, which offers a detection limit of 20 ppb.

Gold nanoparticles have also been used by Li et al., in combination with SiNPs.<sup>67</sup> Their sensing mechanism is based on the strong hydrogen-bond interactions between the amine groups of Ag@SiO<sub>2</sub>-NH<sub>2</sub> NPs and the trifluoromethylfluoroyl group of the pyrethroid pesticide lambda-cyhalothrin (LC). The output signal comes from the color change (from yellow to pink) of Ag@SiO<sub>2</sub>-NH<sub>2</sub> NPs, immediately upon the introduction of LC; for other pyrethroids, the signal is considered negligible. Although the mechanism proposed by the authors seems logical, the high selectivity of the system for LC over other pyrethroid pesticides remains to be explained.

Dasary et al. reported described gold nanoparticle-based surface-enhanced fluorescence (NSEF) spectroscopy for the screening of organophosphorous agents.<sup>68</sup> Surface-enhanced fluorescence (SEF) is one of the enhanced optical phenomena prompted by large local electromagnetic fields on the surfaces of metal nanostructures, particularly those of silver or gold.<sup>69,70</sup> The system described in this work is based on the use of AuNP's modified with Eu<sup>3+</sup> ions. Because the binding constant of Eu<sup>3+</sup> with organophosphorus compounds is much higher than that with AuNP's, in the presence of pesticides Eu<sup>3+</sup> ions are released from the gold surface; this causes a very distinct fluorescence signal change to be observed. For typical organophosphorous agents, this system has a linear response range from 1 to 25  $\mu$ M; this range is not sufficiently high, and therefore, the system lacks of specificity. Thus, tests with other phosphorus-based molecules and molecules able to chelate Eu<sup>3+</sup>

ions should be performed in order to better improve the selectivity.

Li et al. recently published novel work on in situ detection of pesticide residues in fruits using a technique that they named *shell-isolated nanoparticle-enhanced Raman spectroscopy* (SHINERS).<sup>71</sup> In this system, the Raman signal amplification is provided by AuNP's covered by an ultrathin silica or alumina shell (Figure 5A). A monolayer of these nanoparticles is spread

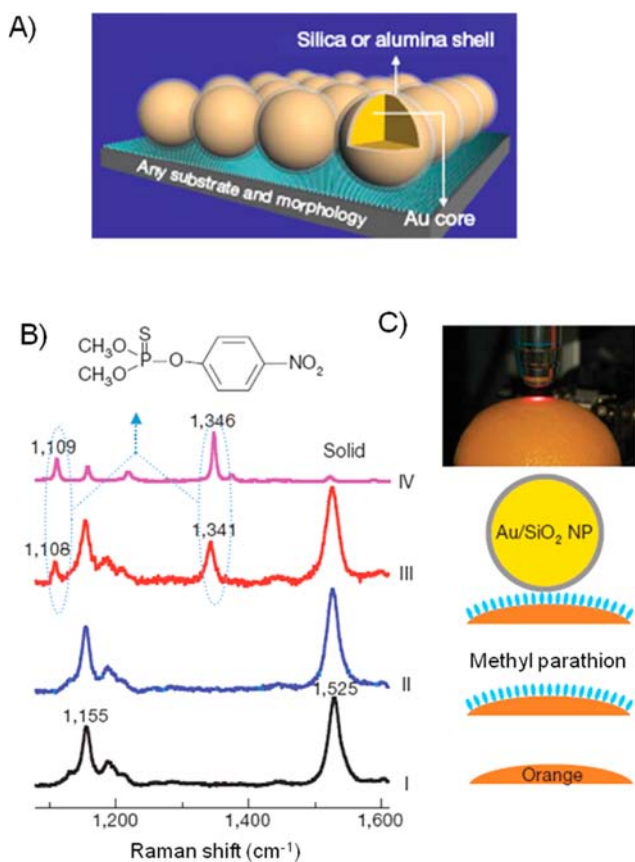


**Figure 5.** (A) AuNP's covered by an ultrathin silica or alumina shell used in shell-isolated nanoparticle-enhanced Raman spectroscopy (SHINERS). (B) In situ SERS inspection of pesticide residues in food/fruit. Normal Raman spectra of fresh citrus fruit samples. Curve I, with clean pericarps; curve II, contaminated by parathion; curve III, SHINERS spectrum of contaminated orange modified with Au/SiO<sub>2</sub> nanoparticles; curve IV, Raman spectrum of solid methyl parathion. Laser power on the sample was 0.5 mW, and the collected times were 30 s. (C) Schematic of the SHINERS experiment. Reprinted with permission from ref 71. Copyright 2010 Nature Publishing Group.

over the surface to be tested (e.g., a fruit sample). The authors pointed out that the ultrathin silica or alumina coating prevents the AuNP's from agglomerating, separates them from direct contact with the test material, and enables them to conform to different substrates. Figure 5B shows that normal Raman spectra recorded on a fresh orange without (I) and with (II) parathion do not show parathion-related peaks. However, by spreading shell-isolated AuNP's on the same surface, one can clearly detect the pesticide-related peaks (III). Additionally, the authors achieved similar results using a portable Raman spectrometer. Although these results are very promising and demonstrate the many advantages of SHINERS analyzer (ease of use, portability for field use, and cost-effectiveness), more

studies are required to achieve reliable analytical performance of the system.

A very simple strategy has been proposed by Zhang et al. based on inducing *fluorescence resonance-enhanced transfer* (FRET) upon ligand replacement from the QDs surface.<sup>72</sup> First, CdTe QDs were synthesized; these showed green emission fluorescence (520 nm). When dithizone (a bidentate metal chelating agent) ethanol solution was added to a QD suspension, the system's fluorescence was quenched by a FRET mechanism. Afterward, upon the addition of pesticide chlorpyrifos (CPF) in a basic medium, diethylphosphorothioate (the hydrolysis product of CPF) replaced dithizone from the QD surfaces, thereby enhancing the system's fluorescence. Real apple samples were tested and gave good responses. The main advantages of this system are that it does not involve the use of antibodies, enzymes, or a complicated surface modification, and it is very simple and inexpensive. However, problems related to the reproducibility of the developed system for work with real samples (error values not reported) must still be carefully considered.

### 3. ELECTROCHEMICAL SENSING

The main parameters that must be considered for development of electrochemical sensors—especially those for pesticide detection—are reproducibility, selectivity, sensitivity, long-term stability, portability, ease of use, and cost-effectiveness. Driven by these needs, great efforts have been made in the design, fabrication, and application of nanomaterials for electrochemical sensing devices. Table 3 provides an overview of technological and analytical performance data for the nanomaterial-based electrochemical pesticide sensors reported in the literature.

#### 3.1. Electrochemical-Based Immunosensors

Electrochemical immunosensors have attracted considerable interest for many years because of their high sensitivity, low cost, and inherent miniaturization.<sup>8,73</sup> Emerging nanomaterials, ranging from nanoparticles to graphene, are opening new doors for electrochemical immunoassays, in terms of improved electrochemical properties of the transducers and better conjugation with biological compounds and acting in some cases as electrochemical labels.

In this field, colloidal gold has been extensively used in pesticide electrochemical immunoassays because of its intrinsic electrochemical characteristics.<sup>74</sup> Tang et al. described a system based on a chitosan/AuNP composite membrane for the electrochemical detection of picloram, a widely used chlorinated herbicide.<sup>75</sup> The antipicloram antibody was embedded in the composite membrane, to which horseradish peroxidase (HRP)-labeled secondary antibody was then attached; pesticide quantification was tracked using this secondary antibody. Enzymatic electrocatalytic hydrolysis of quinone (by HRP) was used for the electrochemical response. In this work, nanoparticles shuttle the electron transfer between the HRP and the electrode surface. A detection limit of 21 nM of picloram was achieved using cyclic voltammetry with good precision and storage stability.

Chen et al. recently published a similar picloram-detection system to that previously described.<sup>76</sup> Their system deals with ordered three-dimensional (3D) gold (Au) nanoclusters. Enzymatic electrocatalytic hydrolysis of quinone (by HRP) was used here also. The authors highlight that compared to the chitosan/AuNP composite system devised by Tang et al.<sup>75</sup> (see

Table 3. Electrochemical Strategies for Pesticide Detection<sup>a</sup>

recognition principle	pesticide	electrochemical platform/label	recognition element	D.L.	detection technique	sample matrix	ref
immunoassay	picloram	chitosan-AuNP's membrane	anti-picloram Ab	20 nM	chronoamperometry	rice, lettuce, and paddy field water	75
	picloram	3D-Au nanoclusters	anti-picloram Ab	2 nM	chronoamperometry	peach samples	76
	atrazine	AuNP's labeled Ab	anti-atrazine Ab	0.16 $\mu$ M	conductivity	red wine samples	77
	diuron	PB-AuNP's film	alkaline phosphatase rabbit anti-IgGAb	4 pM	SWV		78
	paraoxon	CdS@ZnS QDs labeled Ab	anti-phospherine Ab	0.5 nM	SWV	plasma samples	79
enzymatic	paraoxon	ZrO <sub>2</sub> NPs-coated SPE/QDs labeled Ab	ZrO <sub>2</sub> NPs	8.0 pM	SWV	spiked human plasma samples	80
	paraoxon	AChE-AuNP's into scaffolds gel	AChE inhibition	6 pM	chronoamperometry	river water samples	81
	carbofuran	MWCNT-AChE/PB/MWCNT	AChE inhibition	0.4 $\mu$ M	amperometry	spiked beverage samples	83
	paraoxon	AuNP's-MWCNTs-based electrode	AChE inhibition	0.1 nM	amperometry		84
	methyl parathion	AuNP's-MWCNTs-CdTeQDs-MPDE	MPDE hydrolysis	3.4 nM	amperometry	spiked garlic samples	85
	methyl parathion	AuNP-SP-MWCNT-MPDE	MPDE catalytic hydrolysis	1 nM	SWV	spiked garlic samples	86
	paraoxon	AuNP's/cr-Gs hybrid	AChE inhibition	0.1 pM	chronoamperometry		89
	paraoxon	AChE-Fe <sub>3</sub> O <sub>4</sub> NPs- silica shell SPE	AChE inhibition	5.0 $\times 10^{-9}$ M	chronoamperometry		96
immunoassay/enzymatic	organophosphates	CdS@ZnS QDs labeled Ab	anti-BChEAb/BChE inhibition	0.5 nM	SWV	spiked human plasma samples	97
host-guest	chlorpyrifos	PATP-AuNP's-GCE	molecular imprinted PATP	3.3 $\times 10^{-7}$ M	CV	spiked tap water samples	98
	dimethoate	AgNPs-PoPD	molecular imprinted PoPD	2.2 nM	CV		99
other methods	paraoxon	RGON hybrid-based electrodes		1.37 $\times 10^{-7}$ M	chronoamperometry		92
	dichlofenthion	TiO <sub>2</sub> NPs SPE		2.0 nM	DPASV	green vegetable samples	100
	cypermethrin/permethrin	chitosan-Fe <sub>3</sub> O <sub>4</sub> nanobiocomposite	binding of pesticides to ssCT-DNA	8 nM/2.5 $\mu$ M	DPV		101
	methyl parathion	CNT-web-based electrode		1.0 nM	DPV		102

<sup>a</sup>PB, Prussian blue; CV, cyclic voltammetry; SWV, square-wave voltammetry; DPV, differential pulse voltammetry; DPASV, differential pulse anode stripping voltammetry; GO, graphene oxide; ssCT-DNA, single standard calf thymus deoxyribose nucleic acid; cr-Gs, chemically-reduced graphene nanosheets; SPE, screen-printed electrode; SP, silica particles; MWCNT, multiwalled carbon nanotubes; MPDE, methyl parathion degradation enzyme; PATP, electropolymerized polyaminothiophenol; GCE, glassy carbon electrode; PoPD, poly-*o*-phenylenediamine; RGON, reduced graphene oxide/Nafion; AChE, acetylcholinesterase; BChE, butylcholinesterase.

above), their AuNP 3D network offers significantly greater specific surface area for molecular bioconjugation and better electron-exchange capability, thereby enabling lower detection limits.

Although the aforementioned systems have good responses and low detection limits, the fact that they require additional substrates (in these two cases, HRP) to generate the analytical response is not very desirable. Around the same time as the Chen group reported its work, Valera et al. reported the use of interdigitated  $\mu$ -electrodes (ID $\mu$ Es) combined with AuNP's and specific antibodies to detect atrazine in wine samples by conductometric measurements.<sup>77</sup> The detection principle is based on the conductometric change, which occurs when secondary antibodies labeled with AuNP's are deposited onto the electrode gaps after the immunoassay. Gold nanoparticle inclusions reduce the gap between ID $\mu$ Es and increase the electric field between them, generating an analytical readout signal. Among the main advantages of the ID $\mu$ E system is the potential for relatively high throughput (48 samples in 5 h) without the need for sample pretreatment.

Sharma et al. recently reported an electrochemical immunosensor for diuron herbicide involving the use of laser-ablated gold electrodes modified with a Prussian Blue-gold nanoparticle (PB-AuNP) film.<sup>78</sup> The available antipesticide antibodies were bound to the PB-AuNP film using alkaline phosphatase rabbit anti-IgGAb and 1-naphthyl phosphate substrate for the electrochemical analytical response by square wave voltammetry (SWV). The authors of the work state that PB-AuNP film has the advantage of a large surface-to-volume ratio, strong adhesion, and high surface activity, all of which give the assay greater sensitivity relative to the case of unmodified electrodes. The system is highly specific for diuron, with a sensitivity of 4 pM to 0.4  $\mu$ M.

In addition to AuNP's, other nanomaterials, such as QDs or ZrO<sub>2</sub> nanoparticles, have been used for electrochemical pesticide immunoassays. Wang et al. employed QDs in a new tool for biomonitoring exposure to organophosphates (OPs) by direct detection of organophosphorylated acetylcholinesterase.<sup>79</sup> The system combines magnetic separation for preconcentration purpose and the sensitive square wave voltammetric technique for QD label detection. Antiphospho-

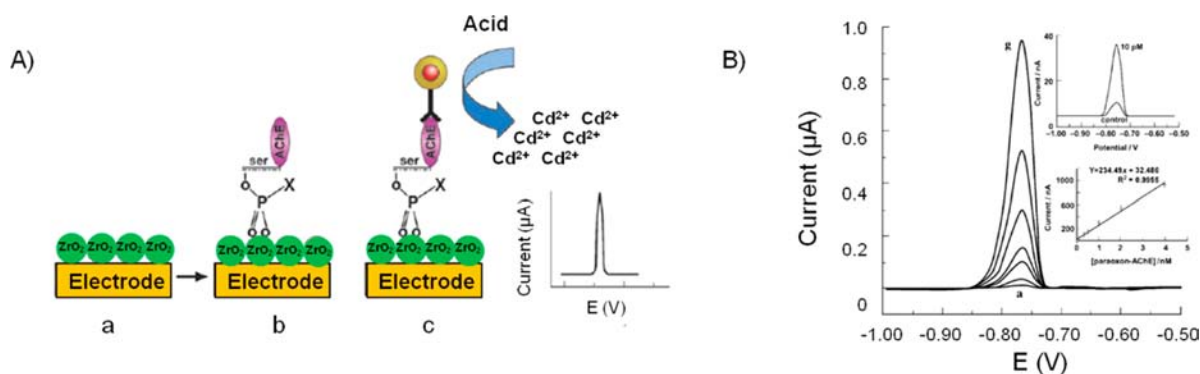


**Figure 6.** (A) (A.1) Principle of electrochemical immunosensing of phosphorylated AChE, (a)  $\text{ZrO}_2$  nanoparticle-modified SPE; (b) selective capturing phosphorylated AChE adducts; (c) immunoreaction between bound phosphorylated AChE adducts and QD-labeled anti-AChE antibody; (d) dissolution of nanoparticles with acid following electrochemical stripping analysis. AChE, purple;  $\text{ZnO}_2$ , green; electrode, yellow. (A.2) Typical electrochemical responses of the immunosensor upon increasing phosphorylated AChE concentration (from (a) to (g)): 0.01, 0.05, 0.3, 0.5, 1.0, 2.0, and 4.0 nM). The insets show the resulting calibration plot (bottom) and the electrochemical responses to 10 pM and 0 pM paraoxon-AChE. Reprinted with permission from ref 80. Copyright 2008 Wiley–VCH.

serine polyclonal antibodies were immobilized onto magnetic nanoparticles (MNPs) to capture phosphorylated acetylcholinesterase (AChE-OP).<sup>79</sup> In addition, antihuman AChE monoclonal antibodies were labeled with  $\text{CdS@ZnS}$  QDs to selectively recognize the captured AChE-OP. The group was able to quantify organophosphorous compounds based on  $\text{CdS@ZnS}$  QDs stripping signals in square-wave voltammetry.

Phosphorylated AChE has been used in other works. For example, Liu et al. reported an electrochemical immunoassay based on the use of zirconia nanoparticles, for the selective binding of OP-AChE adduct, and QDs, as tags for labeling anti-AChE-Ab to quantify the immunorecognition event (see Figure 6A).<sup>80</sup> Typical electrochemical responses for increasing amounts of phosphorylated AChE (coming from increasing amounts of paraoxon) are shown in Figure 6B. Well-defined stripping peaks are observed across the concentration range. The resulting calibration plot of current versus known concentration of AChE-OP (inset Figure 6B) is linear from 10 pM to 4 nM, which is suitable for the quantitative working range.

The main advantage of these two last presented works is that they provide a general response to OPs, an entire pesticide chemical group, rather than to one single pesticide, thus providing a broader response of interest for real sample analysis. In terms of electrochemical immunosensor systems for pesticide monitoring, efforts must be focused on the development of multiple electrochemical detection systems for different pesticides, as most of the developments in this field involve single detection only. One potentially interesting alternative would be the use of different QDs with different electrochemical fingerprints coated with antibodies specific for different pesticides. However, generation of antibodies against small molecules is a very tedious and expensive task; therefore, other recognition molecules are desirable.

### 3.2. Enzyme-Based Electrochemical Systems

Different inhibition biosensor systems based on the use of AChE immobilized onto different nanostructured electrochemical transducers have been proposed for pesticide screening. The most widely applied nanomaterials in this field have been AuNP's and carbon nanostructure-based platforms, including combinations of these two materials.

Lu et al. recently reported a work involving immobilization of AuNP-AChE conjugates for paraoxon electrochemical biosens-

ing.<sup>81</sup> The authors highlight the use of gel scaffolds to provide essentially the same local aqueous microenvironment as in biological medium, giving rise to a favorable host matrix that isolates the AuNP-AChE conjugates, thereby protecting them from aggregation and leaching. The system enables direct measurements of OPs in real environmental samples, with impressive detection limits (6 pM for paraoxon).

Regarding carbon nanomaterials, multiwalled carbon nanotubes (MWCNTs) have attracted much attention not only due to their unique electronic properties but also due to the high surface area that they offer when used as electrodes and to their ability to enhance enzymatic activity.<sup>82</sup> In this field, Chen et al. reported a system comprising MWCNTs coupled to Prussian blue (as redox mediator for the electrochemical oxidation of the enzymatic product thiocholine) and AChE, whereby inhibition of AChE by pesticides generates an electrochemical signal that is amplified by the MWCNTs.<sup>83</sup>

The combination of MWCNTs and AuNP's has also been studied for pesticide-monitoring systems. For example, Jha et al.<sup>84</sup> modified a glassy carbon electrode (GCE) with AuNP's and MWCNTs to achieve strong electron transfer and large immobilization sites for the bioenzyme (AChE), exploiting the strong electrocatalytic activity of the MWCNTs. Without using any redox mediator, they reached a very high sensitivity of 0.1 nM for the model analyte paraoxon.

Du et al. performed similar work,<sup>85</sup> combining AuNP-MWCNT-based electrodes with CdTe QDs as carriers to load a large amount of enzyme. Their use of methyl parathion degrading enzyme (MPDE) further set their work apart from that of Jha et al.<sup>84</sup> The authors highlight that, unlike cholinesterase-based biosensors, the MPDE-based biosensor can be potentially reused and is suitable for continuous monitoring. They reported the system to be selective toward pesticides containing P–S bonds, which obviates any interference coming from carbamates or OP pesticides.

Methyl parathion hydrolase (MPDE) was also used by Chen et al. to develop a nanocomposite biosensor based on the mixture of silica particles  $\text{SP@AuNP}$  and MWCNTs placed on the surface of a glassy carbon electrode (GCE).<sup>86</sup> The biosensor is selective for methyl parathion over its analogues. The authors used SWV to obtain the analytical signal. The response for this specific system comes from the electrochemical activity of 4-nitrophenol, which is provided by the

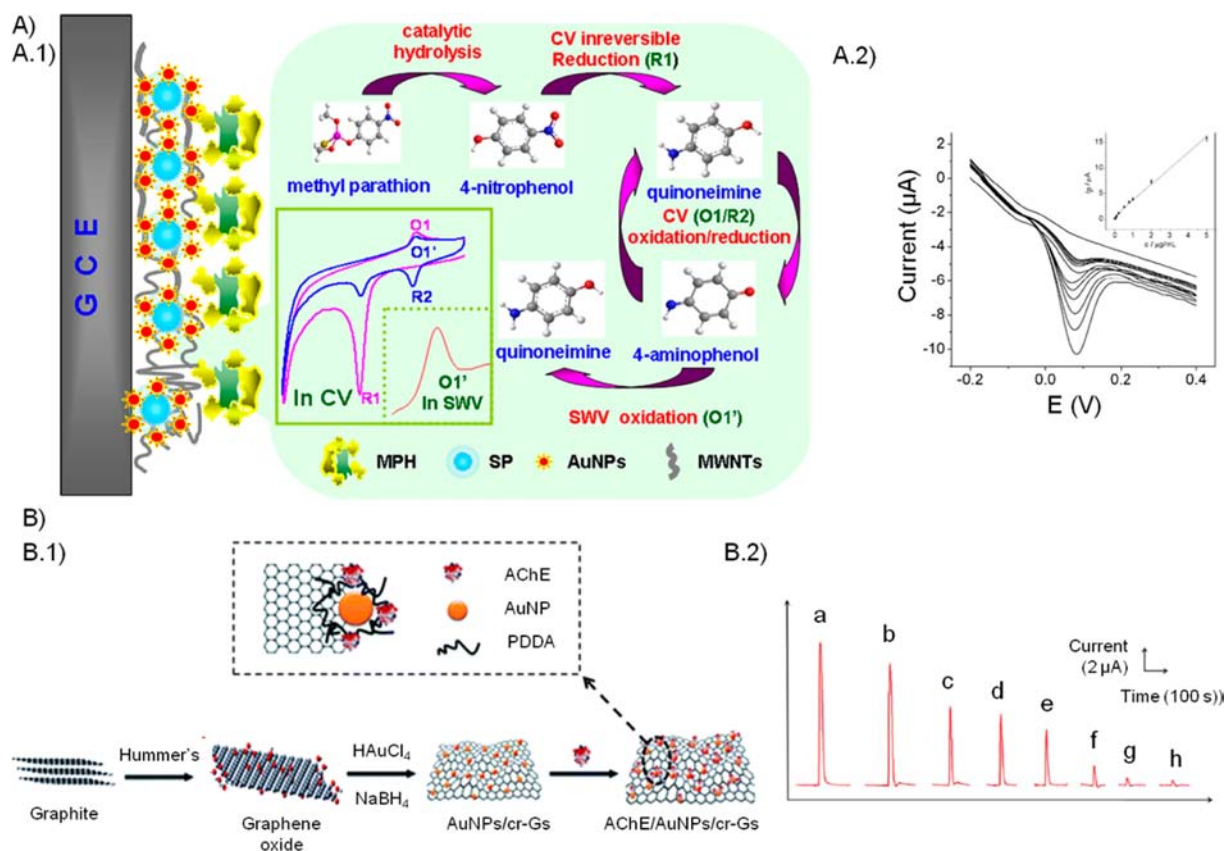


**Figure 7.** (A) Working principle of MPH biosensor for determination of methyl parathion. (B) Square wave voltammetric responses of the MPH/SP@AuNP's/MWNTs/GCE biosensor toward methyl parathion with varying concentrations. Inset: linear relationship between peak currents and methyl parathion concentrations. Reprinted with permission from ref 81. Copyright 2011 Elsevier B.V. (B) (B.1) Schematic illustration of Au NP/cr-Gs hybrid synthesis and AChE/Au NP/cr-Gs nanoassembly generation by using poly(diallyldimethylammonium chloride) (PDDA); (B.2) typical amperometric responses of AChE/Au NP/cr-Gs-based SPEs to paraoxon using a flow-injection analysis system. Signal (a) is from 2 mM ATCh, signals from (b–h) are from 2 mM ATCh after the AChE/Au NP/cr-Gs-based SPEs were incubated with paraoxon for 15 min at concentrations of 0.1 pM, 0.25 pM, 2.5 pM, 25 pM, 0.25 nM, 2.5 nM, and 5 nM, respectively. Reprinted with permission from ref 89. Copyright 2011 Roayl Society of Chemistry.

hydrolysis of methyl parathion (MP). Figure 7A.1 depicts the working principle of the MPDE biosensor for the determination of MP, as proposed by the authors. Figure 7A.2 displays the SWV responses for the designed MPDE/SP@AuNP's/MWCNT/GCE biosensor to different concentrations of methyl parathion as well as the linear relationship between peak currents and MP concentration (inset Figure 7A.2).

Beyond MWCNTs, other carbon nanomaterials are being employed for pesticide sensors. For example, owing to its remarkable electrochemical properties, graphene shows fascinating advantages in electrochemical biosensors. Compared to CNTs, graphene—which was experimentally discovered only 7 years ago<sup>87</sup>—is reported to offer more advanced properties and is likely to exhibit fewer weakness.<sup>88</sup> Graphene is an excellent electrical conductor. Heterogeneous electron transfer occurs at the edges of the graphene or at defects in the basal plane. Thus, the high surface area of graphene translates to numerous defects and, consequently, to many electroactive sites.

Wang et al. described a strategy for depositing AuNP's and AChE onto chemically reduced graphene nanosheets (cr-Gs) with a long-chain polyelectrolyte (poly(diallyldimethylammonium chloride), PDDA), which acts as a stabilizer and dispersible medium for the other materials (see Figure 7B.1).<sup>89</sup> Figure 7B.2 shows typical amperometric responses of the AChE/Au NP/cr-Gs-based screen-printed

electrodes (SPEs) to paraoxon, obtained using a flow-injection analysis system. The novel device gave lower detection limits compared to other systems for paraoxon detection.<sup>90,91</sup> Despite having been designed for pesticide detection, the nanoassembly could be outfitted with other immobilized materials, such as antibodies or even host–guest recognition molecules, for analysis of other compounds (e.g., toxins or nerve agents). The optical properties of graphene are also being studied extensively; simultaneously exploiting its electrochemical and optical properties may yield interesting applications.

Choi et al. have demonstrated a proof-of-concept system using graphene-based electrodes for pesticide detection.<sup>92</sup> They used free-standing, conductive, reduced graphene oxide/Nafion (RGON) nanohybrids to create an electrochemical biosensor platform that contains organophosphorus hydrolase as an enzyme for the hydrolysis of OPs. Functionalization by Nafion provided highly stable dispersibility of RGOs and mechanical integrity of the hybrid material, due to its intrinsic molecular structures and functionality. A detection limit of  $1.37 \times 10^{-7}$  M of paraoxon was obtained.

Liu et al. have described a nanocomposite modified electrode system based on RGO, AuNP's, and AChE, which they used to detect organophosphorous and carbamate pesticides via enzyme inhibition.<sup>93</sup> Other nanostructures besides AuNP's and carbon nanomaterials have been applied in electrochemical



pesticide-detection tools involving inhibition of AChE.<sup>94,95</sup> For instance, Won et al.<sup>96</sup> devised a model system for nanomolar detection of paraoxon incorporating biomagnetic glass platforms based on Fe<sub>3</sub>O<sub>4</sub>-silica NPs and AChE. They immobilized the core-shell NPs by simple physical adsorption onto a carbon-SPE that they used as a working electrode for the amperometric measurements, which could imply problems with stability. The authors did not exploit the magnetism of the Fe<sub>3</sub>O<sub>4</sub>-silica NPs to preconcentrate the sample on the working electrode, which would have enabled a stronger response.

Enzyme activity assays and immunoassay strategies based on electrochemical detection of pesticides can be combined for further improvements. Du et al. recently reported a system involving both strategies for biomonitoring of exposure to OPs.<sup>97</sup> As shown in Figure 8A, they used antibodies to

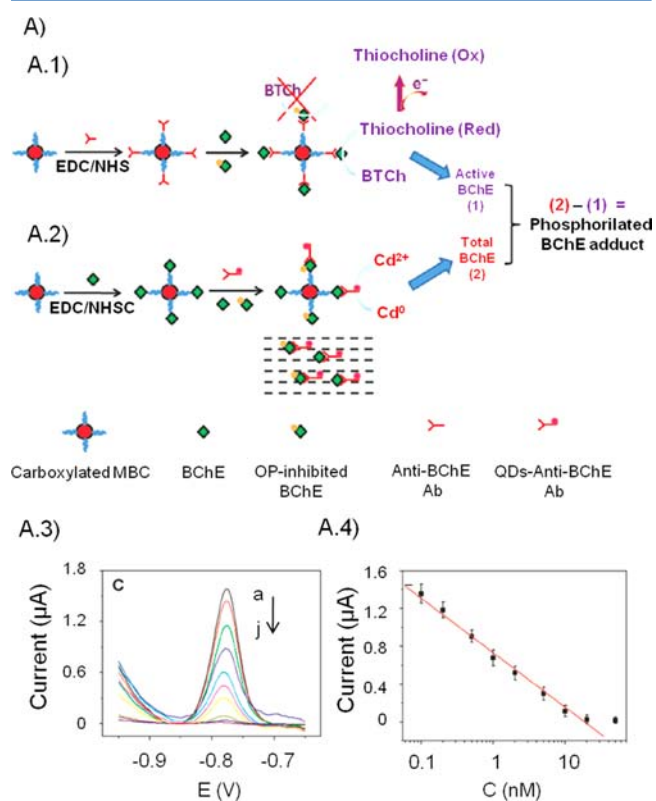


**Figure 8.** (A) Schematic of the immunosensing platform based on (A.1) immunodetection of enzyme activity and (A.2) immunoassay of total amount of enzyme simultaneously for biomonitoring of OP exposure; (A.3) SWV responses for MB BChE incubated with different concentrations of BChE: (a) 0; (b) 0.1; (c) 0.2; (d) 0.5; (e) 1.0; (f) 2.0; (g) 5.0; (h) 10; (i) 20; and (j) 50 nM; (A.4) calibration plot for SWV response and BChE concentration. Reprinted with permission from ref 97. Copyright 2011 American Chemical Society.

selectively capture enzyme for the enzyme activity assay (Figure 8A.1), while simultaneously using an immunoassay to quantify total enzyme levels (Figure 8A.2). The values obtained from the difference between the total amount and the active butylcholinesterase (BChE) are used to estimate the amount of OP-BChE adducts in serum. Additionally, magnetic beads are used to capture the analyte from the biological matrix. The analytical signal comes from thiocholine oxidation (for the immunodetection of enzyme activity) and from antibodies labeled with CdS@ZnS QDs (for the total BChE determination). Square wave voltammetry responses for MB BChE

incubated with different concentrations of BChE and the calibration plot of SWV response against BChE concentration are shown in Figure 8A.3 and A.4, respectively.

### 3.3. MIPs and Other Host-Guest-Like Systems

As mentioned for the optical sensing strategies, despite the high sensitivity of antibody- and enzyme-based pesticide detection systems, they suffer from poor chemical/physical stability, which prevents their use in harsh environments (e.g., acidic or basic media, organic solvents, high temperatures, etc.). Thus, replacement of biological receptors with synthetic counterparts such as recognition elements also is extremely important for electrochemical-based systems. To this end, MIPs represent a good alternative, as described above for the optical sensing strategies.

A nice example of an MIP-based system recently published by Xie et al. can be seen in Figure 9.<sup>98</sup> The authors report a surface molecular self-assembly strategy for molecular imprinting in electropolymerized polyaminothiophenol (PATP) membranes at the surface of AuNP-modified glassy carbon electrodes (GCEs) for the electrochemical detection of chlorpyrifos (CPF). Figure 9A and B depicts the procedure for preparing the imprinted PATP-AuNP's-GCE electrodes: electrodeposition of AuNP's of the GCE surface; followed by electrodeposition of ATP on the surface of GCE; and finally, removal of the imprinting CPF molecules (Figure 9A). Figure 9C displays the cyclic voltammetric responses of the system to different amounts of CPF. Well-defined peaks are shown, with the current increasing as CPF concentration increases. A linear relationship in the range from 0.5 to 10 μM CPF was obtained with a detection limit of 0.33 μM of CPF. The AuNP's not only enhance the signal but also increase the mass transport, which is a normal drawback for these sensing methods.

Du and collaborators reported a similar system, which involves use of imprinted poly(*o*-phenylenediamine) and AgNP's instead of AuNP's and cyclic voltammetry as the detection technique.<sup>99</sup> They achieved detection limits of 2.2 nM for the pesticide dimethoate detection.

### 3.4. Other Electrochemical Strategies

In addition to the aforementioned methodologies described for pesticide detection, there are other analytical methods being evaluated to develop new, simple, low-cost, portable, and sensitive devices that do not require biological or synthetic receptors. For example, Li et al. recently reported a novel photoelectrochemical sensor for electrochemical detection of dichlofenthion.<sup>100</sup> They harnessed nanosized titania to obtain electroactive compounds by photocatalytic degradation of dichlofenthion, which they then readily detected using differential pulse anodic stripping voltammetry (DPASV). For dichlofenthion, the detection limit appears to be in the nanomolar range. In the future, this strategy could be applied for other nonelectroactive compounds.

Kaushik et al. used Fe<sub>3</sub>O<sub>4</sub> NPs for electrochemical detection of pyrethroids.<sup>101</sup> Their system is not based on AChE inhibition but rather on the binding of pesticides to single-stranded calf thymus DNA (ssCT-DNA). The ssCT-DNA is immobilized onto a chitosan (CH)-Fe<sub>3</sub>O<sub>4</sub> NPs/ITO electrode. When pesticides are recognized by the DNA strand, the current intensity decreases, and this change is detected by DPV.

Musameh et al. recently reported on the use of CNT-webs for methyl parathion detection.<sup>102</sup> They define CNT-webs as "a novel form of CNT(s) produced by drawing CNT(s) away from the front face of specially grown 'forests' of aligned

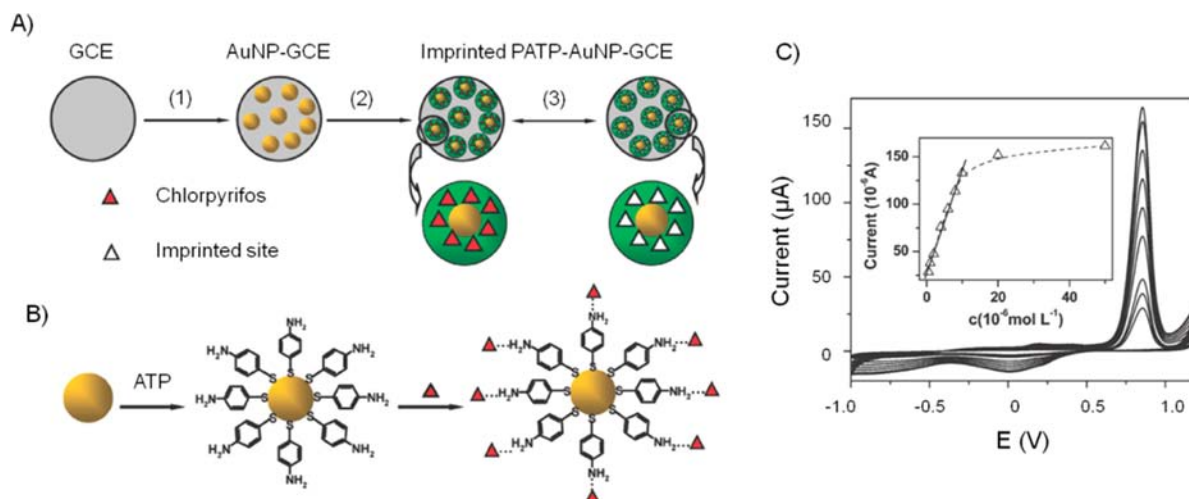


**Figure 9.** (A) Procedures for preparing the imprinted PATP–AuNP–gc electrode: (1) electrodeposition of AuNP's on the surface of the glassy carbon electrode (GCE); (2) electropolymerization of ATP on the surface of the AuNP–gc electrode; (3) removal/rebinding of chlorpyrifos on the imprinted sites of the imprinted PATP–AuNP–GCE. (B) Schematic of adsorption of the ATP molecule onto the AuNP surface and subsequent self-assembly of CPF at ATP-modified AuNP–GCE. (C) Cyclic voltammograms of increasing CPF concentration in 0.05 M PBS (pH 6.86) containing 0.1 M KCl. The inset shows the calibration curve of CPF. CPF concentration was 0.5, 1, 2, 4, 6, 8, 10, 20, and 50  $\mu\text{M}$  (from bottom to top), respectively. Reprinted with permission from ref 98. Copyright 2010 American Chemical Society.

**Table 4. Degradation or Removal of Pesticides<sup>a</sup>**

application	pesticide	nanomaterial	strategy	max. degradation or recovery (%)	sample matrix	ref
degradation	Alachlor/Fenitrothion	TiO <sub>2</sub> NPs	photocatalysis	100		114
	atrazine	TiO <sub>2</sub> NWs	photocatalysis			115
	atrazine	TiO <sub>2</sub> NPs coated MWCNTs	microwave-assisted photocatalysis	100		116
	methyl parathion/2,4-D	AuNP's-coated TiO <sub>2</sub> NT array	photocatalysis	100		117
	Malathion	Au–Pd–TiO <sub>2</sub> NT film	photocatalysis	>96		118
	Propachlor	TiO <sub>2</sub> NPs/ $\gamma$ -Fe <sub>2</sub> O <sub>3</sub>	photocatalysis		water samples	120
	PCP	nanoporous Ti-doped $\beta$ -Bi <sub>2</sub> O <sub>3</sub>	photocatalysis			121
	2-CP/DCP/TCP	Ag–AgBr NP/MAP	photocatalysis	71–80		122
	4-CP	ZnO/Au NRs	photocatalysis	91	water samples	123
	phenol	MNPs	Fenton-like catalysis	85	water samples	125
	Metalaxyl	bidoped goethite-hematite NS	photo-Fenton-like catalysis	99		126
	atrazine	NZVI/CTMA-Bent	chemical reduction	64		127
	lindane	Pd NPs	catalytic dechlorination	75	groundwater samples	128
	methyl parathion/Lindane/dichlorvos	Nano-TiO <sub>2</sub> immobilized on Pyrex glass	photocatalysis	100		129
	removal	diuron	Mag-PCMA	magnetic separation	>95	water and soil samples
TCP		MHNTs composites	magnetic separation	83.3–96.3	tap and river water samples	134
DNOC		nanomagnetite	magnetic separation and cathodic fenton degradation			136
phenol		FePtNPs@C	magnetic separation			137
atrazine/dimethoate		nanoporous membrane	nanofiltration	95/90	water samples	142
atrazine		nanoporous membranes	nanofiltration	94	water samples	143

<sup>a</sup>CP, chlorophenol; DCP, 2,4-dichlorophenol; TCP, 2,4,6-trichlorophenol; MAP, ordered mesoporous  $\gamma$ -Al<sub>2</sub>O<sub>3</sub>; NR, nanorods; PCP, pentachlorophenol; NS, nanostructures; NT, nanotube; CTMA-Bent, cetyltrimethylammonium bromide–bentonite; ZVI, zero-valent iron; NW, nanowires; MHNTs, magnetic halloysite nanotubes; FePtNPs@C, magnetic mesoporous carbon with FePt nanoparticles; DNOC, 4,6-dinitro-*o*-cresol; Mag-PCMA, magnetically permanently confined micelle arrays; MNPs, magnetic nanoparticles.

CNT(s)), a method which generates high porosity surfaces. Because of this large surface area and good electrochemical properties, CNT-webs represent great surfaces for the adsorption of molecules and their subsequent electrochemical

detection. Using DPV, they achieved detection limits of 1.0 nM for methyl parathion. Furthermore, they demonstrated that their new system outperforms a system based on a bare GCE. The main aim of such technologies is to provide a nonanalyte

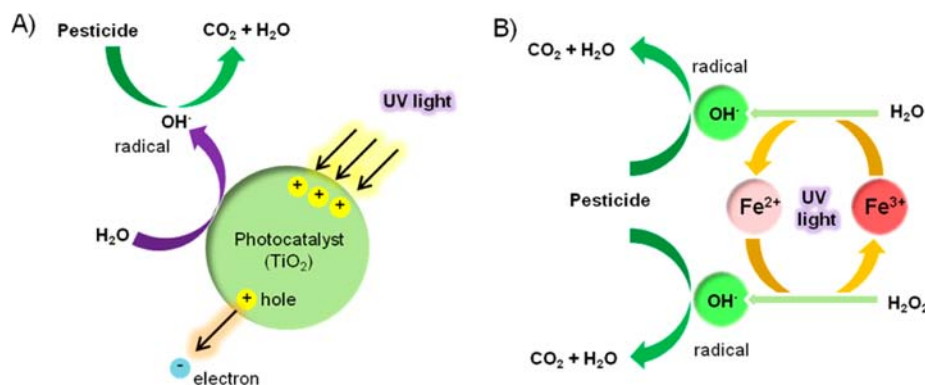


**Figure 10.** Schematic of pesticide degradation mechanisms: (A) photocatalytic oxidation and (B) photo-Fenton degradation.

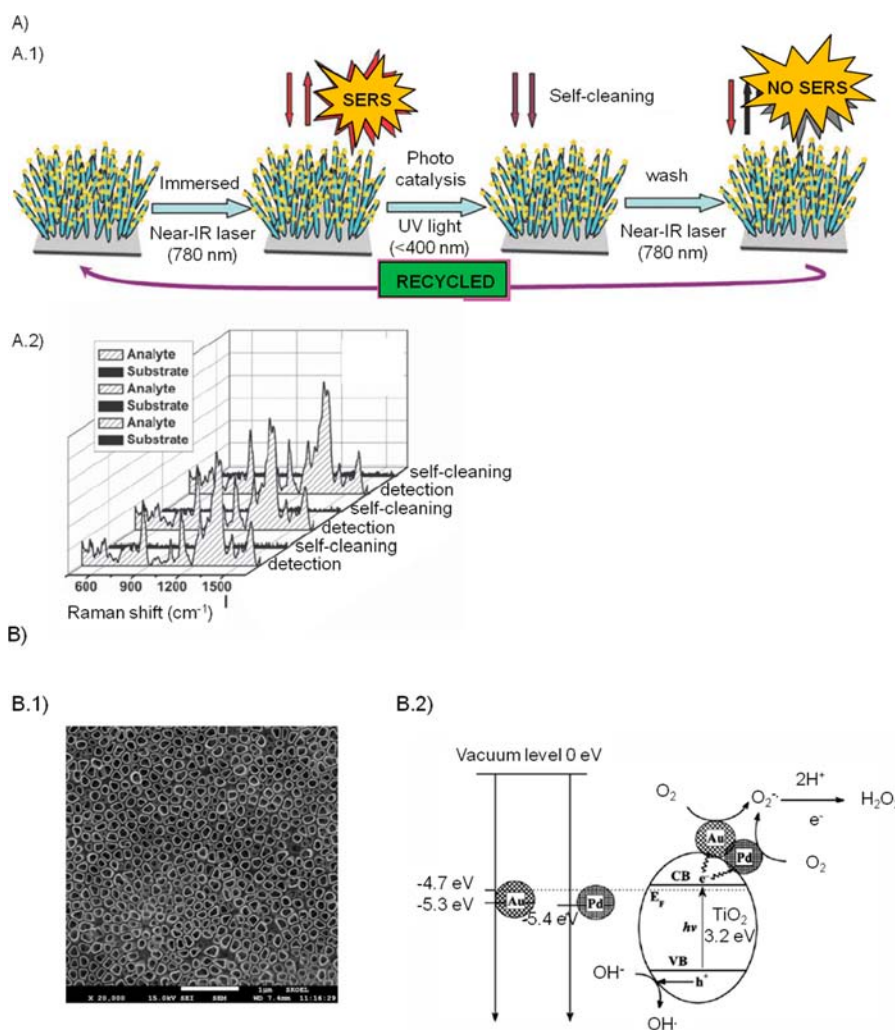


**Figure 11.** (A) (A.1) Scheme of reversible SERS behavior of the multifunctional SERS substrate; (A.2) Raman spectrum of solid 2,4-D. Reversible SERS behavior of gold-coated TiO<sub>2</sub> nanotube arrays (Au/TTA-4) with three cycles of MP 10<sup>-4</sup> M. Reprinted with permission from ref 117. Copyright 2010 Wiley-VCH. (B) (B.1) SEM images of the bare TiO<sub>2</sub> nanotube film and schematic diagram; (B.2) representing the charge-carrier transfer on Au-Pd-TiO<sub>2</sub> and its interaction with the adsorbed O<sub>2</sub>. Reprinted with permission from ref 118. Copyright 2010 Elsevier B.V.

restricted system with the purpose of general pesticides analysis using electrochemical techniques.

#### 4. DEGRADATION AND REMOVAL OF PESTICIDES

Once pesticides are introduced into the environment, whether through direct agricultural use or from waste or accidental spillage, they can undergo various changes. Biological effects

will ultimately determine the persistence and final fate of a pesticide. Some microorganisms (e.g., fungi or bacteria) use certain pesticides as a food source and can metabolize them in the soil. Albeit this can compromise the efficacy of the pesticide, it can also help with pesticide degradation, by breaking down toxic compounds into nontoxic ones. However, some pesticides are resistant to this type of biodegradation (or

partial degradation) and instead generate other toxic compounds that remain in the environment for a long time, ultimately entering into the food chain. Thus, there is a pressing need for methods to remove pesticides and their derivatives from the environment.

Nanostructured materials with unique physical and chemical properties are not only useful for pesticide detection but are also promising tools for pesticide removal and degradation strategies to remediate environmental pollution. Some of the strategies in this area reported for real samples are summarized in Table 4, which includes data such as degradation percentages.

#### 4.1. Degradation of Pesticides

Besides typical chemical degradation,<sup>103</sup> a promising method for mineralization of pesticides is application of advanced oxidation processes (AOPs).<sup>104</sup> Various AOPs can be employed, depending on the oxidants added to accelerate the photodegradation process, such as hydrogen peroxide and/or ozone, metallic salts, or semiconductors (e.g., TiO<sub>2</sub>).<sup>105–108</sup> The most-widely used AOPs for pesticide degradation are photocatalytic oxidation (e.g., TiO<sub>2</sub>/UV) and photo-Fenton and Fenton-like systems (H<sub>2</sub>O<sub>2</sub>/UV/Fe<sup>3+</sup>) (see Figure 10).

Photocatalytic oxidation is based on the use of UV irradiation of semiconductors (usually TiO<sub>2</sub>). When TiO<sub>2</sub> is irradiated with photons (e.g., at  $\lambda = 390$  nm) whose energy is equal to or greater than its band gap energy ( $E_G = 3.2$  eV), electron–hole pairs are created. In aqueous system, these holes react with H<sub>2</sub>O or OH<sup>−</sup> adsorbed at the surface of the semiconductor to produce OH· radicals, which are the strongest oxidants in this process (Figure 10A).<sup>109,110</sup> In photo-Fenton and Fenton-like systems, Fe<sup>3+</sup> ions are added to acidic H<sub>2</sub>O<sub>2</sub> medium to form the complex Fe(OH)<sup>2+</sup>, which, upon UV irradiation, decomposes to generate Fe<sup>2+</sup> ions and OH· radicals, the latter of which act as oxidant (Figure 10B).<sup>111</sup>

Interestingly, use of nanomaterials in either of these above processes enables enhanced efficiency due to multiple factors involving the greater specific surface area or greater surface energy of these materials. The most widely studied nanoparticles for the pesticide degradation are TiO<sub>2</sub> and ZnO NPs, as they function at room temperature and pressure with low-energy photons and do not require any chemical reagents except the oxygen in the air.

Much research using TiO<sub>2</sub> NPs as nanostructures for photocatalytic degradation of either a single pesticide or mixed pesticides has been reported.<sup>112–114</sup> The catalytic reaction involves the adsorption of pollutant molecules onto the surface of titania nanoparticles, the breakage of the chemical bonds, and the formation and subsequent release of the degradation product molecules. The unique surface area and surface activity of nanoparticles are crucial for catalytic reactions.

Hu et al. ascertained TiO<sub>2</sub> nanowires for their ability to simultaneously provide mechanical filtration and photocatalytic degradation of organic pollutants (e.g., atrazine) under UV irradiation.<sup>115</sup> More recently, Chen et al. reported the combination of titania nanoparticles with multiwalled carbon nanotubes (MWCNTs) for photocatalytic degradation of atrazine.<sup>116</sup> The authors employed microwave irradiation for degradation rather than UV light. Compared to TiO<sub>2</sub> alone, their TiO<sub>2</sub>/MWCNT system showed higher efficiency (20–30% higher) for degradation of atrazine, a difference that they

attribute mainly to the strong capacity of the material to absorb microwaves, which is not observed under UV irradiation.

In another study, Li et al. found that Au-coated TiO<sub>2</sub> nanotube arrays can serve as recyclable surface-enhanced Raman spectroscopy (SERS) substrates.<sup>117</sup> Although their primary objective was to detect organic pollutants (e.g., 2,4-D, methylparathion, and 4-chlorophenol) by SERS, they discovered that the system cleans itself by photocatalytic degradation under UV light, a phenomenon made possible by the catalytic functions of the substrate (see Figure 11A.1). Figure 11A.2 shows the results of recyclable detection of methyl parathion. Interestingly, the characteristic vibrational pattern can be identified when analyte is present but disappears completely after UV irradiation (ca. 30 min) and water washing. Among the main advantages of this system are the possibility to detect numerous analytes (e.g., 2,4-D, methylparathion, and 4-chlorophenol) and the unique recycling properties of the substrate, which prevents the single-use problem of traditional SERS substrates. However, the recycling time is quite long (30 min), and SERS can only be performed by highly trained personnel. Furthermore, in our opinion, problems related to industrial or large-scale applications should be considered.

Researchers have fabricated TiO<sub>2</sub> nanotubes with diverse surface modifications for various functions. For example, metallic inclusions can trap photoinduced charge carriers to improve charge separation and enhance light absorption in semiconductor oxides. In this context, Yu et al. designed a Au–Pd comodified TiO<sub>2</sub>(Au–Pd–TiO<sub>2</sub>) nanotube film photocatalyst for degradation of malathion and proposed a corresponding photocatalytic mechanism (see Figure 11B).<sup>118</sup> Figure 11B.1 shows the morphology of the prepared nanotube films after Au–Pd alloy deposition. Compared to the naked TiO<sub>2</sub> film, malathion could be more efficiently degraded by using Au–Pd–TiO<sub>2</sub>, probably due to the effective separation of photogenerated charge carriers and to the faster synthesis of H<sub>2</sub>O<sub>2</sub>. As shown in Figure 11B.2, the excited electrons effectively migrated to gold and palladium, as the work functions of both noble metals were larger than that of TiO<sub>2</sub>.

Certain doping agents in TiO<sub>2</sub> nanomaterials can provoke negative effects. Direct contact between TiO<sub>2</sub> and Fe<sub>2</sub>O<sub>3</sub> compromises photocatalytic activity, due to the fact that Fe<sub>2</sub>O<sub>3</sub> acts as recombination center for electrons and positive holes.<sup>119</sup> To overcome this effect, Belessi et al. used polyelectrolyte insulators.<sup>120</sup> Their system is stable and does not suffer from photodissolution, degrading chloroacetamide herbicides in good yields.

Another doping agent used in nanostructured TiO<sub>2</sub> is Bi<sub>2</sub>O<sub>3</sub>, as reported by Yin et al. for destroying chlorophenols.<sup>121</sup> Chlorophenols cannot be degraded by O<sub>2</sub><sup>−</sup> or H<sub>2</sub>O<sub>2</sub>, as in a typical system. Exploiting the fact that the higher number of surface atoms in a material at the nanoscale enables reactions that cannot be achieved in the corresponding bulk material, the authors described the possibility of degrading chlorophenols using nanoporous TiO<sub>2</sub> doped with  $\beta$ -Bi<sub>2</sub>O<sub>3</sub>.

In addition to TiO<sub>2</sub> and doped-TiO<sub>2</sub>, other metal nanostructures, such as AgNPs<sup>122</sup> and ZnO/Au nanorods,<sup>123</sup> have been harnessed for photocatalytic destruction of pesticides. Fenton-like processes have been reported for pesticide degradation, although they have not been used as often as photocatalytic reactions. The Fenton reaction was first described 100 years ago by Fenton<sup>124</sup> and is based on the production of hydroxyl radicals from Fe<sup>2+</sup> (see eqs 2 and 3):

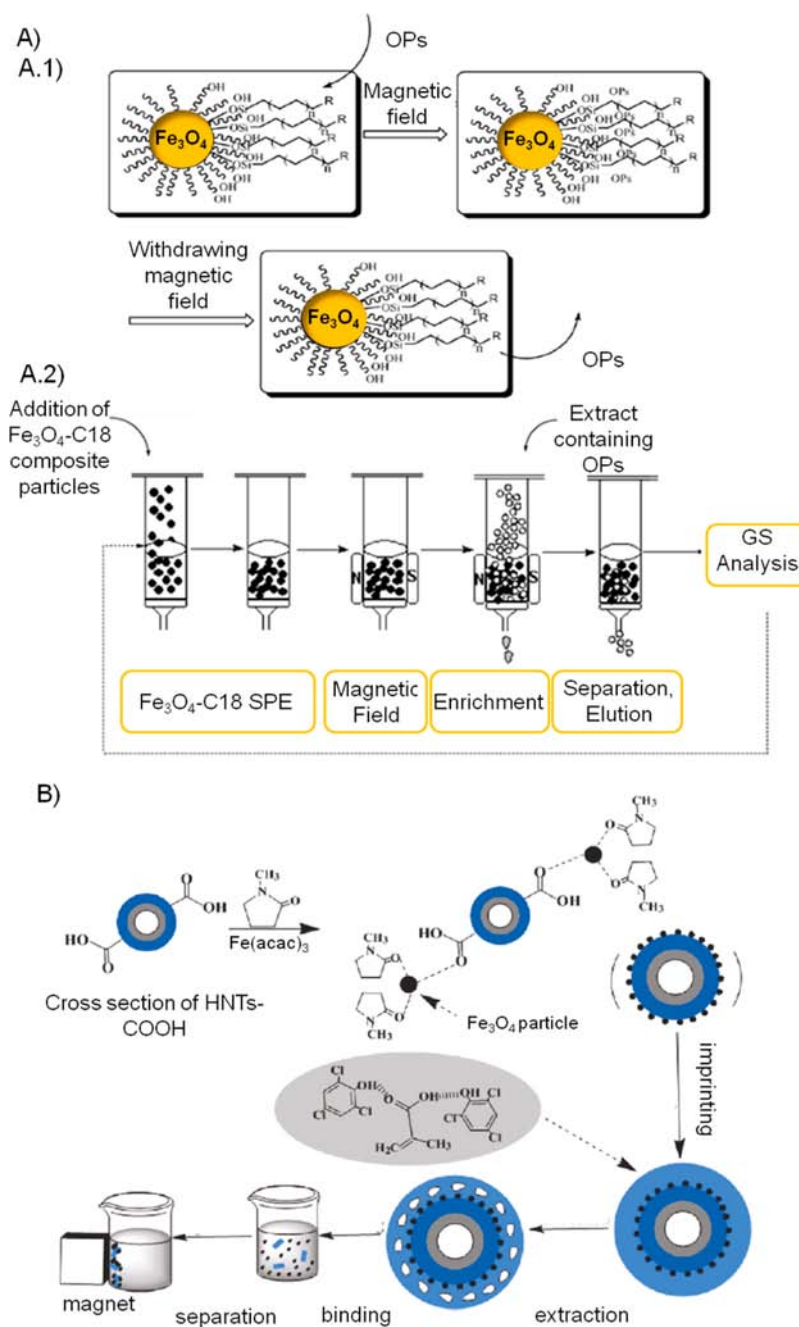
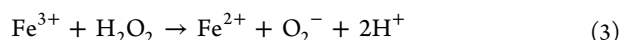
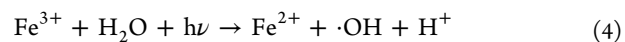


**Figure 12.** (A) Proposed mechanism for the adhesion of OPs to  $\text{Fe}_3\text{O}_4\text{-C}_{18}$  magnetic nanoparticles. Reprinted with permission from ref 133. Copyright 2007 Springer. (B) Synthesis route of MIPs and their application for removal of 2,4,6-TCP with the help of an applied magnetic field. Reprinted with permission from ref 134. Copyright 2011 American Chemical Society.



Although this chemistry is an attractive option for oxidizing organic compounds; it requires large amounts of iron and generates large amounts of iron waste that require subsequent treatment. Nanomaterials such as ferromagnetic nanoparticles can overcome the problems of the homogeneous Fenton reaction due to their high stability, cheap and easy preparation, environmental soundness, and potential for reuse (based on magnetic separation, as reported by Zhang et al. among others).<sup>125</sup> In this work, over 85% of phenol is believed to be removed at the optimal reaction conditions.

Efficiency of the Fenton reaction can be enhanced by using UV/vis irradiation, in what is known as *photo-Fenton-like processes*. The main advantage of UV/vis irradiation is that  $\text{Fe}^{2+}$  species can be regenerated more quickly than in the standard Fenton process, giving one more hydroxyl radical ready for the organic pollutants degradation:



Gajovic et al. extensively investigated a photo-Fenton-like process for metalaxyl decomposition, using bismuth-doped goethite-hematite nanostructures.<sup>126</sup> The authors affirmed that the addition of bismuth affects the morphology of iron nanostructures. Moreover, they demonstrated that catalytic

activity is closely related to the phase composition and morphology: the highest activity was shown by a homogeneous mixture of hematite and bismuth ferrite nanoparticles, which had the largest surface area of all the materials they tested. In addition to the works described above, other reports on the use of iron and nanomaterials for degrading pesticides have been described.<sup>127–130</sup>

#### 4.2. Pesticides Removal

Activated carbon has been the standard sorbent for organic pollutants in water for many years.<sup>131</sup> However, its small particle size, high regeneration temperatures (up to 800 °C), and decreasing sorption capacity influences its performance. Thus, magnetic sorbents have emerged as a new class of materials for environmental decontamination.<sup>132</sup> The combination of magnetic separation and nanoparticles for pollutant removal provides very large surface areas and greater surface reactivity.

Among the most relevant pesticide cleanup methods is the use of magnetic Fe<sub>3</sub>O<sub>4</sub> nanoparticles. Surface-modified MNPs are commonly used to selectively extract and adsorb the desired target compounds.

Shen et al. described the potential of magnetic nanoparticles modified with a C18 composite for cleanup of OPs.<sup>133</sup> Figure 12A.1 depicts their proposed mechanism for adhesion of the OPs to the Fe<sub>3</sub>O<sub>4</sub>-C<sub>18</sub> NPs, and Figure 12A.2 shows their cleanup procedure using a solid-phase extraction column. The authors describe an enrichment phenomenon whereby, under a magnetic field, OPs are easily captured while the remaining components in the sample are eluted. Withdrawal of the magnetic field and addition of the appropriate eluent releases the OPs from the magnetic nanoparticles for subsequent detection.

Pan et al. devised an interesting pesticide-removal strategy.<sup>134</sup> They employed magnetic halloysite nanotube (MHNT) composites modified with molecularly imprinted polymers (MIPs) to selectively recognize 2,4,6-trichlorophenol (TCP). Halloysite nanotubes (HNTs) are two-layered, hollow nanotubes of the aluminosilicate clay mineral halloysite that are organized in the submicrometer range and offer a large specific surface area. In contrast to nanotubes of other materials (e.g., carbon, SiO<sub>2</sub>, and TiO<sub>2</sub>), HNTs are readily obtainable and much cheaper. The Pan group's synthesis of MHNTs coated with TCP-specific MIPs is shown in Figure 12B. They obtained the MHNTs by thermal decomposition of organic iron precursors and subsequent coating with an MIP film, previously obtained by using TCP as template. The authors reported that the MHNTs specifically recognize TCP and can be reused and regenerated five times with good adsorption capacities.

Liu et al. used a similar strategy, based on core-shell Fe<sub>3</sub>O<sub>4</sub>@MIP NPs for rapid enrichment and separation of herbicides in water (e.g., 2,4-dichlorophenoxyacetic acid).<sup>135</sup> Some researchers have reported the combination of magnetic separation of Fe<sub>2</sub>O<sub>3</sub> NPs and the Fenton catalytic abilities of iron that are described in the previous section.<sup>136</sup> In this context, the catalytic and magnetic properties of superparamagnetic FePt NPs have also been combined, for phenol removal.<sup>137</sup>

Apart from magnetic separation, nanofiltration membranes also have been ascertained over the past few years for pesticide removal, owing to their retention properties and to the fact that most pesticides weigh more than 200 Da.<sup>138,139</sup> Nanofiltration has been successfully applied in many drinking water treatment

plants.<sup>140,141</sup> For instance, Ahmad et al. have studied the parameters of different commercial nanofiltration membranes (e.g., NF90 from Dow/Filmtec (U.S.A.), with 0.55 nm average pore size) for the pesticides dimethoate and atrazine, such as the retention quality, the permeate flux, and the robustness.<sup>142</sup> They found that, by increasing the transmembrane pressure, pesticides retention and permeate flux were improved. Removal of other pesticides (e.g., atrazine) using similar strategies has also been reported.<sup>143</sup>

Finally, other nanostructures, such as gold nanoparticles, have also been used for pesticide removal. Das et al. demonstrated that AuNP's biomodified with fungal mycelia (a fungal strain) strongly adsorb different OPs.<sup>144</sup>

#### 5. CONCLUSIONS AND FUTURE PROSPECTS

In the past few decades, development of novel methods for pesticide detection with high accuracy, precision, and reproducibility and low detection limits has proven challenging for the scientific community. The use of nanomaterials in sensing strategies may not always guarantee high sensitivity for pesticide analysis, but it definitively enables low-cost and user-friendly devices of interest for field use, which is far more desirable than traditional, tedious laboratory analysis.

The attractive physicochemical properties of nanomaterials (e.g., metal nanoparticles, quantum dots, magnetic nanoparticles, carbon nanotubes, and graphene), including strong absorption, excellent electron transfer and a large ratio of surface area to volume, make them particularly attractive for use in labels or transducing platforms for optical or electrochemical sensors and biosensors.<sup>145–147</sup> The large surface area of nanoparticles provides features that enable lower detection limits—namely, good optical properties, which are highly dependent on environmental changes, and attractive catalytic properties.

Gold nanoparticles have been the nanoparticles of choice for most nanomaterial-based optical detection systems, owing to their small size, sensitivity, robust manufacturing methods, and ready functionalization and the fact that they can be seen even with the naked eye. Fluorescence detection systems based on nanomaterials mainly exploit the great properties of quantum dots (QDs) as labels, as these materials offer greater brightness and photostability than do traditional organic dyes.

Carbon nanomaterials (e.g., carbon nanotubes and graphene) are the most widely used materials in electrochemical transducing platforms for pesticide detection, as they offer dramatically high levels of sensitivity made possible by their large specific surface area and high surface free energy. The use of nanomaterials as immobilization matrices in the pesticide detection provides greater system sensitivity than do traditional materials, due to the excellent response on storage of the recognition/degradation elements.

In addition to transducing platforms, nanomaterials can also be used as electrochemical labels for immunosensing systems. For example, QDs are very well-known as electrochemical labels, owing to their ease of use and to their low detection limits, which are made possible by electrochemical stripping techniques. Moreover, QDs are amenable to barcode generation, based on their unique, composition-dependent (e.g., Cd(II), Zn(II), Pb(II), etc.) voltammetric stripping signatures.

Recognition elements (e.g., antibodies and host-guest systems) are another fundamental factor to the selectivity and sensitivity of pesticide-detection systems. When choosing the

recognition element for a given system, a compromise among selectivity, sensitivity, and stability must be sought. In addition to recognition elements, enzymatic inhibition based on cholinesterases also has been extensively used for pesticide detection. Such inhibition is subsequently detected using different strategies (e.g., optical and electrochemical).

In this regard, pesticide-monitoring systems based on many of the aforementioned nanomaterials look promising; however, most have not yet been studied in real-world applications. Thus, research efforts must be focused on the final aim: to create cost-efficient devices for rapid in-field pesticide detection/screening in polluted areas. In this context, development of lateral-flow devices that incorporate nanoparticles as labels or other nanomaterials may prove to be excellent alternatives.

Biopolymers also can be used, as they not only represent a “friendly” matrix that offers better structural features than do nanomaterials but also act as functional materials for pesticide detection and enable high stability and sensitivity in biosensors.<sup>148,149</sup> Nanomaterials can also be used for pesticide degradation and/or removal. For example, use of metal nanoparticles for catalytic degradation is an exciting and rapidly growing area. Compared to the conventional catalysis technologies applied to chemical degradation or removal, use of nanomaterials offers crucial advantages. First, they offer high surface area, which is critical for ensuring high catalytic performance and enables novel nanoscale reactions that are not possible with analogous bulk material. Additionally, nanomaterial adsorbents offer more adsorbent atoms per unit mass than do conventional materials, thereby enabling greater or faster removal of the target chemical.

## AUTHOR INFORMATION

### Corresponding Author

\*Fax: (+)34935868020. E-mail: arben.merkoci@icn.cat. Website: www.icn.cat; www.nanobiosensors.org/.

### Notes

The authors declare no competing financial interest.

### Biographies



Gemma Aragay holds a master's (2007) degree in Chemistry from the Universitat Autònoma de Barcelona (UAB). She completed a Ph.D. in Chemistry at the Catalan Institute of Nanotechnology (ICN), in Barcelona, and UAB in 2011. Her Ph.D. research focused on development of nano- and macrostructured materials and devices of interest for pollutant detection. She studied pyrazole receptors in combination with nanomaterials (e.g., gold nanoparticles) to be used in optical detection of heavy metals in tandem with screen-printing

electrodes and anodic stripping voltammetry for trace metal detection. She is currently working as a postdoctoral researcher at ICN. Her research is focused on the design of new strategies using micro- and nanomaterials for pollutants detection.



Flavio Pino earned a master's degree in Analytical Chemistry from the University of Rome Tor Vergata in 2006. He obtained a Marie Curie Early Stage Research Grant in 2007 to work in microfabrication at the Research Center of Finland. He is currently a doctoral student at Catalan Institute of Nanotechnology, in the Nanobioelectronics and Biosensors Group, where he is researching electrochemical biosensors and printing technology.



Arben Merkoçi is ICREA Research Professor and head of the Nanobioelectronics and Biosensors Group at Catalan Institute of Nanotechnology, in Barcelona. He studied industrial chemistry at University of Tirana (Albania), where he obtained a Ph.D. in Chemistry, working in the field of ion-selective electrodes. In 1992 began work as a postdoctoral fellow and latter, as a research professor, at Polytechnic University of Budapest (Hungary), University of Ioannina (Greece), Università degli Studi di Padua (Italy), Universitat Politècnica de Catalunya (Spain), Universitat Autònoma de Barcelona (Spain), and New Mexico State University (U.S.A.). His research is focused on the integration of biological molecules (DNA, antibodies, cells, and enzymes) and other receptors with micro- and nanostructures of interest for the design of novel sensors and biosensors.

## ACKNOWLEDGMENTS

The authors would like to acknowledge MICINN for PIB2010JP-00278 and MAT2011-25870 projects and NATO for FP 983807 project. G.A. thanks Generalitat de Catalunya for a predoctoral fellowship (FI 2009). The authors thank Mr. G. Qushair from ICN for the very helpful revision of the manuscript.

## REFERENCES

- (1) (a) www.who.int; (b) www.eco-usa.net; (c) www.panna.org; (d) <http://www.epa.gov>; (e) www.atsdr.cdc.gov.
- (2) U.S. Environmental Protection Agency (EPA); Risk assessment, management and communication of drinking water contamination; US EPA 625/4-89/024; Environmental Protection Agency: Washington, DC, 1989.
- (3) Richardson, S. D.; Ternes, T. A. *Anal. Chem.* **2011**, *83*, 4614.
- (4) Alder, L.; Greulich, K.; Kempe, G.; Vieth, B. *Mass Spectrom. Rev.* **2006**, *25*, 838.
- (5) Stan, H. *Compr. Anal. Chem.* **2005**, *43*, 269.
- (6) Culea, M.; Gocan, S. *Food Sci. Tech. (Handbook of Water Analysis)*; Nollet, L. M. L.; Marcel Dekker: New York, 2000; Vol. 102, p 571.
- (7) Llorent-Martínez, E. J.; Ortega-Barrales, P.; Fernández-de Córdova, M. L.; Ruiz-Medina, A. *Anal. Chim. Acta* **2011**, *684*, 30.
- (8) Liu, G.; Lin, Y. *Talanta* **2007**, *74*, 308.
- (9) Aragay, G.; Pons, J.; Merkoçi, A. *Chem. Rev.* **2011**, *111*, 3433.
- (10) Pérez-López, B.; Merkoçi, A. *Anal. Bioanal. Chem.* **2011**, *399*, 1577.
- (11) Zhang, X.; Guo, Q.; Cui, D. *Sensors* **2009**, *9*, 1033.
- (12) Liu, S.; Yuan, L.; Yue, X.; Zheng, Z.; Tang, Z. *Adv. Powder Technol.* **2008**, *19*, 419.
- (13) Zhang, L.; Fang, M. *Nano Today* **2010**, *5*, 128.
- (14) De la Escosura-Muñiz, A.; Parolo, C.; Merkoçi, A. *Mater. Today* **2010**, *13*, 24.
- (15) Suri, C. R.; Boro, R.; Nangia, Y.; Gandhi, S.; Sharma, P.; Wangoo, N.; Rajesh, K.; Shekhawat, G. S. *TrAC, Trends Anal. Chem.* **2009**, *28*, 29.
- (16) Ahn, K. C.; Kim, H.; McCoy, M. R.; Gee, S. J.; Hammock, B. D. *J. Agric. Food Chem.* **2011**, *59*, 2792.
- (17) Yuan, M.; Liu, B.; Liu, E.; Sheng, W.; Zhang, Y.; Crossan, A.; Kennedy, I.; Wang, S. *Anal. Chem.* **2011**, *83*, 4767.
- (18) Xu, Z.; Shen, Y.; Zheng, W.; Beier, R. C.; Xie, G.; Dong, J.; Yang, J.; Wang, H.; Lei, H.; She, Z.; Sun, Y. *Anal. Chem.* **2010**, *82*, 9314.
- (19) Boro, R. C.; Kaushal, J.; Nangia, Y.; Wangoo, N.; Bhasin, A.; Suri, C. R. *Analyst* **2011**, *136*, 2125.
- (20) Vinayaka, A. C.; Thakur, M. S. *Anal. Bioanal. Chem.* **2010**, *397*, 1445.
- (21) Reiss, P.; Protière, M.; Li, L. *Small* **2009**, *19*, 154.
- (22) Vinayaka, A. C.; Basheer, S.; Thakur, M. S. *Biosens. Bioelectron.* **2009**, *24*, 1615.
- (23) Chen, Y.; Ren, H. L.; Sai, N.; Liu, X.; Liu, Z.; Gao, Z.; Ning, B. *J. Agric. Food Chem.* **2010**, *58*, 8895.
- (24) Rosenthal, S. J. *Nat. Biotechnol.* **2001**, *19*, 621.
- (25) Nichkova, M.; Dosev, D.; Davies, A. E.; Gee, S. J.; Kennedy, I. M.; Hammock, B. D. *Anal. Lett.* **2007**, *40*, 1423.
- (26) Wang, G.; Peng, Q.; Li, Y. *Acc. Chem. Res.* **2011**, *44*, 322.
- (27) Cummins, C. M.; Koivunen, M. E.; Stephanian, A.; Gee, S. J.; Hammock, B. D.; Kennedy, I. M. *Biosens. Bioelectron.* **2006**, *21*, 1077.
- (28) Feng, J.; Shan, G.; Maquieira, A.; Koivunen, M. E.; Guo, B.; Hammock, B. D.; Kennedy, I. M. *Anal. Chem.* **2003**, *75*, 5282.
- (29) Nichkova, M.; Dosev, D.; Gee, S. J.; Hammock, B. D.; Kennedy, I. M. *Anal. Chem.* **2005**, *77*, 6864.
- (30) Ma, Z.; Dosev, D.; Nichkova, M.; Dumas, R. K.; Gee, S. J.; Hammock, B. D.; Liu, K.; Kennedy, I. M. *J. Magn. Magn. Mater.* **2009**, *321*, 1368.
- (31) Ahn, K. C.; Kim, H.; McCoy, M. R.; Gee, S. J.; Hammock, B. D. *J. Agric. Food Chem.* **2011**, *59*, 2792.
- (32) Posthuma-Trumpie, G. A.; Korf, J.; Van Amerongen, A. *Anal. Bioanal. Chem.* **2009**, *393*, 569.
- (33) Ngom, B.; Guo, Y.; Wang, X.; Bi, D. *Anal. Bioanal. Chem.* **2010**, *397*, 1113.
- (34) Kranthi, K. R.; Davis, M.; Mayerr, C. D.; Russell, D. A.; Shukla, R. M.; Satija, U.; Kshirsagar, M.; Shiware, D.; Kranthi, S. *Crop Prot.* **2009**, *28*, 428.
- (35) Guo, Y.; Liu, S.; Gui, W.; Zhu, G. *Anal. Biochem.* **2009**, *389*, 32.
- (36) Hua, X.; Qian, G.; Yang, J.; Hu, B.; Fan, J.; Qin, N.; Li, G.; Wang, Y.; Liu, F. *Biosens. Bioelectron.* **2010**, *26*, 189.
- (37) Kim, Y. A.; Lee, E.; Kim, K.; Lee, Y. T.; Hammock, B. D.; Lee, H. *Anal. Chim. Acta* **2011**, *693*, 106.
- (38) Blazková, M.; Rauch, P.; Fukal, L. *Biosens. Bioelectron.* **2010**, *25*, 2122.
- (39) Blazková, M.; Micková-Holubová, B.; Rauch, P.; Fukal, L. *Biosens. Bioelectron.* **2009**, *25*, 753.
- (40) Liu, C.; Jia, Q.; Yang, C.; Qiao, R.; Jing, L.; Wang, L.; Xu, C.; Gao, M. *Anal. Chem.* **2011**, *83*, 6778.
- (41) Zou, Z.; Du, D.; Wang, J.; Smith, J. N.; Timchalk, C.; Li, Y.; Lin, Y. *Anal. Chem.* **2010**, *82*, 5125.
- (42) Periasamy, A. P.; Umasankar, Y.; Chen, S. *Sensors* **2009**, *9*, 4034.
- (43) Hossain, S. M. Z.; Luckham, R. E.; McFadden, M. J.; Brennan, J. D. *Anal. Chem.* **2009**, *81*, 9055.
- (44) Hossain, S. M. Z.; Luckham, R. E.; Smith, A. M.; Lebert, J. M.; Davies, L. M.; Pelton, R. H.; Filipe, C. D. M.; Brennan, J. D. *Anal. Chem.* **2009**, *81*, 5474.
- (45) Miao, Y.; He, N.; Zhu, J. *Chem. Rev.* **2010**, *110*, 5216.
- (46) Llopis, X.; Pumera, M.; Alegret, S.; Merkoçi, A. *Lab Chip* **2009**, *9*, 213.
- (47) Pavlov, V.; Xiao, Y.; Willner, I. *Nano Lett.* **2005**, *5*, 649.
- (48) Saa, L.; Virel, A.; Sanchez-Lopez, J.; Pavlov, V. *Chem.—Eur. J.* **2010**, *16*, 6187.
- (49) Zheng, Z.; Zhou, Y.; Li, X.; Liu, S.; Tang, Z. *Biosens. Bioelectron.* **2011**, *26*, 3081.
- (50) Zheng, Z.; Li, X.; Dai, Z.; Liu, S.; Tang, Z. *J. Mater. Chem.* **2011**, *21*, 16955.
- (51) Lin, T.; Huang, K.; Liu, C. *Biosens. Bioelectron.* **2006**, *22*, 513.
- (52) Vasapollo, G.; Del Sole, R.; Mergola, L.; Lazzoi, M. R.; Scardino, A.; Scorrano, S.; Mele, G. *Int. J. Mol. Sci.* **2011**, *12*, 5908.
- (53) Jiang, X.; Jiang, N.; Zhang, H.; Liu, M. *Anal. Bioanal. Chem.* **2007**, *389*, 355.
- (54) Wu, Z.; Tao, C.; Lin, C.; Shen, D.; Li, G. *Chem.—Eur. J.* **2008**, *14*, 11358.
- (55) Liu, R.; Guan, G.; Wang, S.; Zhang, Z. *Analyst* **2011**, *136*, 184.
- (56) Xu, S.; Li, J.; Chen, L. *J. Mater. Chem.* **2011**, *21*, 4346.
- (57) Wang, J.; Kong, L.; Guo, Z.; Xu, J. Y.; Liu, J. *Chem. Mater.* **2010**, *20*, 5271.
- (58) Matsui, J.; Takayose, M.; Akamatsu, K.; Nawafune, H.; Tamaki, K.; Sugimoto, N. *Analyst* **2009**, *134*, 80.
- (59) Zhao, Y.; Ma, Y.; Li, H.; Wang, L. *Anal. Chem.* **2012**, *84*, 386.
- (60) Li, H.; Li, Y.; Cheng, J. *Chem. Mater.* **2010**, *22*, 2451.
- (61) Kim, H. J.; Lee, M. H.; Muthiac, L.; Vicens, J.; Kim, J. S. *Chem. Soc. Rev.* **2012**, *41*, 1173.
- (62) Muthiac, L.; Lee, J. H.; Kim, J. S.; Vicens, J. *Chem. Soc. Rev.* **2011**, *40*, 2777.
- (63) Qu, F.; Zhou, X.; Xu, J.; Li, H.; Xie, G. *Talanta* **2009**, *78*, 1359.
- (64) Coscarello, E. N.; Barbiric, D. A.; Castro, E. A.; Vico, R. V.; Bujánm, E. I.; De Rossi, R. H. *J. Struct. Chem.* **2009**, *50*, 671.
- (65) Guerrini, L.; Aliaga, A. E.; Cárcamo, J.; Gómez-Jeria, J. S.; Sanchez-Cortes, S.; Campos-Vallette, M. M.; García-Ramos, J. V. *Anal. Chim. Acta* **2008**, *624*, 286.
- (66) Millan, J. I.; Garcia-Ramos, J. V.; Sanchez-Cortes, S. *J. Electroanal. Chem.* **2003**, *556*, 83.
- (67) Li, Y.; Cui, Z.; Li, D.; Li, H. *Sens. Actuators, B* **2011**, *155*, 878.
- (68) Dasary, S. S. R.; Rai, U. S.; Yu, H.; Anjaneyulu, Y.; Dubey, M.; Ray, P. C. *Chem. Phys. Lett.* **2008**, *460*, 187.
- (69) Guerrero, A. R.; Aroca, R. F. *Angew. Chem., Int. Ed.* **2011**, *50*, 665.
- (70) Fort, E.; Gresillon, S. *J. Phys. D: Appl. Phys.* **2008**, *41*, 013001.
- (71) Li, J. F.; Huang, Y. F.; Ding, Y.; Yang, Z. L.; Li, S. B.; Zhou, X. S.; Fan, F. R.; Zhang, W.; Zhou, Z. Y.; Wu, D. Y.; Ren, B.; Wang, Z. L.; Tian, Z. Q. *Nature* **2010**, *464*, 392.
- (72) Zhang, K.; Mei, Q.; Guan, G.; Liu, B.; Wang, S.; Zhang, Z. *Anal. Chem.* **2010**, *82*, 9579.
- (73) Kimmel, D. W.; LeBlanc, G.; Meschievitz, M. E.; Cliffe, D. E. *Anal. Chem.* **2012**, *84*, 685.
- (74) Cao, X.; Ye, Y.; Liu, S. *Anal. Biochem.* **2011**, *417*, 1.



- (75) Tang, L.; Zeng, G.; Shen, G.; Li, Y.; Zhang, Y.; Huang, D. *Environ. Sci. Technol.* **2008**, *42*, 1207.
- (76) Chen, L.; Zeng, G.; Zhang, Y.; Tang, L.; Huang, D.; Liu, C.; Pang, Y.; Luo, J. *Anal. Biochem.* **2010**, *407*, 172.
- (77) Valera, E.; Azcon, J. R.; Barranco, A.; Alfaro, B.; Baeza, F. S.; Marco, M. P.; Rodriguez, A. *Food Chem.* **2010**, *122*, 888.
- (78) Sharma, P.; Sablok, K.; Bhalla, V.; Suri, C. R. *Biosens. Bioelectron.* **2011**, *26*, 4209.
- (79) Wang, H.; Wang, J.; Timchalk, C.; Lin, Y. *Anal. Chem.* **2008**, *80*, 8477.
- (80) Liu, G.; Wang, J.; Barry, R.; Petersen, C.; Timchalk, C.; Gassman, P. L.; Lin, Y. *Chem.—Eur. J.* **2008**, *14*, 9951.
- (81) Lu, D.; Shao, G.; Du, D.; Wang, J.; Wang, L.; Wang, W.; Lin, Y. *Lab Chip* **2011**, *11*, 381.
- (82) Zamfir, L.; Rotariu, L.; Bala, C. *Biosens. Bioelectron.* **2011**, *26*, 3692.
- (83) Chen, H.; Zuo, X.; Su, S.; Tang, Z.; Wu, A.; Song, S.; Zhang, D.; Fan, C. *Analyst* **2008**, *133*, 1182.
- (84) Jha, N.; Ramaprabhu, S. *Nanoscale* **2010**, *2*, 806.
- (85) Du, D.; Chen, W.; Zhang, W.; Liu, D.; Li, H.; Lin, Y. *Biosens. Bioelectron.* **2010**, *25*, 1370.
- (86) Chen, S.; Huang, J.; Du, D.; Li, J.; Tu, H.; Liu, D.; Zhang, A. *Biosens. Bioelectron.* **2011**, *26*, 4320.
- (87) Novoselov, K. S.; Geim, A. K.; Morozov, S. V.; Jiang, D.; Zhang, Y.; Dubonos, S. V. I.; Grigorieva, V.; Firsov, A. A. *Science* **2004**, *306*, 666.
- (88) Brownson, D. A. C.; Banks, C. E. *Analyst* **2010**, *135*, 2768.
- (89) Wang, Y.; Zhang, S.; Du, D.; Shao, Y.; Li, Z.; Wang, J.; Engelhard, M. H.; Li, J.; Lin, Y. *J. Mater. Chem.* **2011**, *21*, 5319.
- (90) Wang, H.; Wang, J.; Choi, D. W.; Tang, Z. W.; Wu, H.; Lin, Y. H. *Biosens. Bioelectron.* **2009**, *24*, 2377.
- (91) Viswanathan, S.; Radecka, H.; Radecki, J. *Biosens. Bioelectron.* **2009**, *24*, 2772.
- (92) Choi, B. G.; Park, H.; Park, T. J.; Yang, M. H.; Kim, J. S.; Jang, S.; Heo, N. S.; Lee, S. Y.; Kong, J.; Hong, W. H. *ACS Nano* **2010**, *4*, 2910.
- (93) Liu, T.; Su, H.; Qu, X.; Ju, P.; Cui, L.; Ai, S. *Sens. Actuators, B* **2011**, *160*, 1255.
- (94) Ganesana, M.; Istarboulie, G.; Marty, J.; Noguier, T.; Andreescu, S. *Biosens. Bioelectron.* **2011**, *30*, 43.
- (95) Chauhan, N.; Narang, J.; Pundir, C. S. *Biosens. Bioelectron.* **2011**, *29*, 82.
- (96) Won, Y. H.; Jang, H. S.; Kim, S. M.; Stach, E.; Ganesana, M.; Andreescu, S.; Stanciu, L. *Langmuir* **2010**, *26*, 4320.
- (97) Du, D.; Wang, J.; Wang, L.; Lu, D.; Smith, J. N.; Timchalk, C.; Lin, Y. *Anal. Chem.* **2011**, *83*, 3770.
- (98) Xie, C.; Li, H.; Li, S.; Wu, J.; Zhang, Z. *Anal. Chem.* **2010**, *82*, 241.
- (99) Du, D.; Chen, S.; Cai, J.; Tao, Y.; Tu, H.; Zhang, A. *Electrochim. Acta* **2008**, *53*, 6589.
- (100) Li, H.; Li, J.; Yang, Z.; Xu, Q.; Hu, X. *Anal. Chem.* **2011**, *83*, 5290.
- (101) Kaushik, A.; Solanki, P. R.; Ansari, A. A.; Malhotrab, B. D.; Ahmad, S. *Biochem. Eng. J.* **2009**, *46*, 132.
- (102) Musameh, M.; Notivoli, M. R.; Hickey, M.; Kyratzis, I. L.; Gao, Y.; Huynh, C.; Hawkins, S. C. *Adv. Mater.* **2011**, *23*, 906.
- (103) Hapeman-Somich, C. J. *Pest. Waste Manage.* **1992**, 157.
- (104) Von Sonntag, C. *Water Sci. Technol.* **2008**, *58*, 1015.
- (105) Liu, Y.; Su, G.; Zhang, B.; Jiang, G.; Yan, B. *Analyst* **2011**, *136*, 872.
- (106) Pradeep, A. T. *Thin Solid Films* **2009**, *517*, 6441.
- (107) Poyatos, J. M.; Muñoz, M. M.; Almecija, M. C.; Torres, J. C.; Hontoria, E.; Osorio, F. *Water Air Soil Pollut.* **2010**, *205*, 187.
- (108) Matilainen, A.; Sillanpää, M. *Chemosphere* **2010**, *80*, 351.
- (109) Ahmed, S.; Rasul, M. G.; Brown, R.; Hashi, M. A. *J. Environ. Manage.* **2011**, *92*, 311.
- (110) Devipriya, S.; Yesodharan, S. *Sol. Energy Mater. Sol. Cells* **2005**, *86*, 309.
- (111) Sun, C.; Chen, C.; Ma, W.; Zhao, J. *Phys. Chem. Chem. Phys.* **2011**, *13*, 1957.
- (112) Gupta, S. M.; Tripathi, M. *Chin. Sci. Bull.* **2011**, *56*, 1639.
- (113) Baruah, S.; Dutta, J. *Environ. Chem. Lett.* **2009**, *7*, 191.
- (114) Mahmoodia, N. M.; Arami, M. *J. Alloys Compd.* **2010**, *506*, 155.
- (115) Hu, A.; Zhang, X.; Oakes, K. D.; Peng, P.; Zhou, Y. N.; Servos, M. R. *J. Hazard. Mater.* **2011**, *189*, 278.
- (116) Chen, H.; Yang, S.; Yu, K.; Ju, Y.; Sun, C. *J. Phys. Chem. A* **2011**, *115*, 3034.
- (117) Li, X.; Chen, G.; Yang, L.; Jin, Z.; Liu, J. *Adv. Funct. Mater.* **2010**, *20*, 2815.
- (118) Yu, H.; Wang, X.; Sun, H.; Huo, M. *J. Hazard. Mater.* **2010**, *184*, 753.
- (119) Beydoun, D.; Amal, R.; Low, G. K. C.; McEvoy, S. *J. Phys. Chem. B* **2000**, *104*, 4387.
- (120) Belessi, V.; Lambropoulou, D.; Konstantinou, I.; Zboril, R.; Tucek, J.; Jancik, D.; Albanis, T.; Petridis, D. *Appl. Catal., B* **2009**, *87*, 181.
- (121) Yin, L.; Niu, J.; Shen, Z.; Chen, J. *Environ. Sci. Technol.* **2010**, *44*, 5581.
- (122) Zhou, X.; Hu, C.; Hu, X.; Peng, T.; Qu, J. *J. Phys. Chem. C* **2010**, *114*, 2746.
- (123) Wang, Q.; Geng, B.; Wang, S. *Environ. Sci. Technol.* **2009**, *43*, 8968.
- (124) Fenton, H. J. H. *J. Chem. Soc., Trans.* **1894**, 65, 899.
- (125) Zhang, J.; Zhuang, J.; Gao, L.; Zhang, Y.; Gu, N.; Feng, J.; Yang, D. *Chemosphere* **2008**, *73*, 1524.
- (126) Gajovic, A.; Silva, A. M. T.; Segundo, R. A.; Sturm, S.; Jancar, B.; Ceh, M. *Appl. Catal., B* **2011**, *103*, 351.
- (127) Zhang, Y.; Li, Y.; Zheng, X. *Sci. Total Environ.* **2011**, *409*, 625.
- (128) Hennebel, T.; Simoen, H.; Verhagen, P.; Windt, W. D.; Dick, J.; Weise, C.; Pietschner, F.; Boon, N.; Verstraete, W. *Environ. Chem. Lett.* **2011**, *9*, 417.
- (129) Senthilnathan, J.; Philip, L. *Water Air Soil Pollut.* **2010**, *210*, 143.
- (130) Mahmoodi, N. M.; Arami, M. *J. Alloys Compd.* **2010**, *506*, 155.
- (131) Rivera-Utrilla, J.; Sanchez-Polo, M.; Gomez-Serrano, V.; Alvarez, P. M.; Alvim-Ferraz, M. C. M.; Dias, J. M. *J. Hazard. Mater.* **2011**, *187*, 1.
- (132) Wang, P.; Shi, Q.; Shi, Y.; Clark, K. K.; Stucky, G. D.; Keller, A. A. *J. Am. Chem. Soc.* **2009**, *131*, 182.
- (133) Shen, H.; Zhu, Y.; Wen, X.; Zhuang, Y. *Anal. Bioanal. Chem.* **2007**, *387*, 2227.
- (134) Pan, J.; Yao, H.; Xu, L.; Ou, H.; Huo, P.; Li, X.; Yan, Y. *J. Phys. Chem. C* **2011**, *115*, 5440.
- (135) Liu, B.; Han, M.; Guan, G.; Wang, S.; Liu, R.; Zhang, Z. *J. Phys. Chem. C* **2011**, *115*, 17320.
- (136) Zeng, X.; Hanna, K.; Lemley, A. T. *J. Mol. Catal. A: Chem.* **2011**, *339*, 1.
- (137) Zhu, Y.; Kockrick, E.; Kaskel, S.; Ikoma, T.; Hanagata, N. *J. Phys. Chem. C* **2009**, *113*, 5998.
- (138) Plakas, K. V.; Karabelas, A. J.; Wintgens, T.; Melin, T. *J. Membr. Sci.* **2006**, *284*, 291.
- (139) Chen, S. S.; James, S. T.; Mulford, L. A.; Norris, C. D. *Desalination* **2004**, *160*, 103.
- (140) Cyna, B.; Chagneaub, Bablon, G.; Tanghe, N. *Desalination* **2002**, *147*, 69.
- (141) Bonne, P. A. C.; Beerendonk, E. F.; Van der Hoek, J. P.; Hofman, J. A. M. H. *Desalination* **2000**, *132*, 189.
- (142) Ahmad, A. L.; Tan, L. S.; Shukor, S. R. A. *J. Hazard. Mater.* **2008**, *151*, 71.
- (143) Tepus, B.; Simonic, M.; Petrinic, I. *J. Hazard. Mater.* **2009**, *170*, 1210.
- (144) Das, S. K.; Das, A. R.; Guha, A. K. *Langmuir* **2009**, *25*, 8192.
- (145) Daniel, M. C.; Astruc, D. *Chem. Rev.* **2004**, *104*, 293.
- (146) Chaudhuri, R. G.; Paria, S. *Chem. Rev.* **2012**, *112*, 2373.
- (147) Pumera, M. *Chem. Soc. Rev.* **2010**, *39*, 4146.
- (148) Ghormade, V.; Deshpande, M. V.; Paknikar, K. M. *Biotechnol. Adv.* **2011**, *29*, 792.

(149) Ruiz-Hitzky, E.; Aranda, P.; Darder, M.; Rytwo, G. *J. Mater. Chem.* **2010**, *20*, 9306.